Western Australia School of Mines

Department of Exploration Geophysics

Cooperative Inversion of Magnetotelluric and Seismic Data

Le Van Anh Cuong

This thesis is presented for the Degree of

Doctor of Philosophy

of

Curtin University

March 2017

DECLARATION OF ACADEMIC INTEGRITY

To the best of my knowledge and belief this thesis contains no material previously published by any other person except where due acknowledgment has been made.

This thesis contains no material which has been accepted for the award of any other degree or diploma in any university.

Signature: 

Date: 06 March 2017

The path to greatness is along with others.

~ Baltasar Gracian

ACKNOWLEDGEMENTS

I, from the bottom of my heart, would like to thank to my main supervisor, Associate Professor, Brett D. Harris for his tireless and constant support in my PhD years at Curtin University. His passion for geophysics as well as geoscience has inspired me and enriched my geophysics views. I would also like to thank Dr. Eric M. Takam Takougang for his technical and academic support and Professor Anton Kepic for his theoretical input.

I would also like to express my special thanks to Dr. Andrew M. Pethick. He has helped and provided me with the beauty of computing science in geophysics. I am thankful to Dr. Ralf Schaa for his great academic support.

I highly appreciate the Australian Government for the Australian Awards Scholarship they have provided to me. I would also like to thank the DETCRC project and the companies which have generously provided data.

I would give my big thank to Pawsey Supercomputing Centre, Perth and to the Curtin Geophysics Research Cluster for access to CPU time on their systems.

I would sincerely thank to the staffs and colleagues of the Curtin University's Department of Exploration Geophysics for their supports. I am thankful to Mr. Robert Verstandig for his valuable technical support.

Finally, I would appreciate the support of my parents, brother, sister and friends. This work would not be achievable without their support.

PUBLICATIONS

During my PhD research, I have been first author on a major extended research article in a high rank Journal, and three conference expanded abstracts. I have been co-author on a second journal paper and a conference abstract. All these works are listed below.

Journals

i. **Le, Cuong V.A.**, B.D. Harris, and A.M. Pethick, 2017, Seismic texture for rock volume classification and cooperative inversion. Submitted to Nature: Scientific Reports (currently under review). This paper is the basis of chapter 3 in this thesis.

ii. **Le, Cuong V.A.**, B.D. Harris, and A.M. Pethick, E.M. Takam Takougang, B. Howe, 2016, Semiautomatic and automatic cooperative inversion of Seismic and magnetotelluric data Surveys in Geophysics **37**: 845-896. doi:10.1007/s10712-016-9377-z. (The major journal paper published in 2016 is chapter 2)

iii. Takam Takougang E., B. Harris, A. Kepic, **C. V.A. Le,** 2015, Cooperative joint inversion of 3D seismic and magnetotelluric data: With application in a mineral province Geophysics **80**:1-13 doi:10.1190/GEO2014-0252.1

Expanded Abstracts

iv. **Le, Cuong V. A.,** B.D. Harris, and A.M. Pethick, 2016, Unconstrained 2D and 3D Magnetotelluric Inversion-Detection of a Ni-Cu-PGE Ore Zone and Carbonaceous Phyllites-Kevitsa: Near Surface Geoscience 2016 - First Conference on Geophysics for Mineral Exploration and Mining.

v. **Le, Cuong V.A.,** B.D. Harris, and A.M. Pethick. 2016. "Magnetotelluric inversion, carbonaceous phyllites and an ore zone: Kevitsa; Finland: ASEG-PESA 2016, Adelaide, Australia. (The work published in 2016 is the appendix A)

vi. Kieu, D.T., A. Kepic, and, **C. V.A. Le,** 2016, Fuzzy Clustering Constrained Magnetelluric Inversion-Case Study over the Kevitsa Ultramafic Intrusion, Northern Finland: Near Surface Geoscience 2016 - First Conference on Geophysics for Mineral Exploration and Mining.

vii. **Le, Cuong V.A.,** B.D. Harris, E.M. Takam Takougang, and A.M. Pethick, 2015, Application of seismic attributes for constraining Magnetotelluric Inversion: ASEG Extended Abstracts 2015: 24th International Geophysical Conference and Exhibition.

ABSTRACT

Seismic and natural source electromagnetic methods are fundamental geophysical technologies used to investigate the subsurface. Human endeavors where these techniques are known to have value include: deep crustal research, mineral exploration, groundwater resource delineation, hydrocarbon resource exploration and geothermal exploration. The depth range of investigation for seismic and electromagnetic methods can extend to tens or even hundreds of kilometers below the surface.

Seismic reflectivity methods can provide high-resolution images of the subsurface, while the magnetotelluric method provides a much-lower resolution impression of the subsurface electrical conductivity distribution. Stand-alone inversion of magnetotelluric data to subsurface conductivity is known to suffer from non-uniqueness and a dramatic reduction in resolution with depth. This low resolution and non-uniqueness present a major challenge for application of the magnetotelluric method, especially in three dimensional geo-electrically complex settings or for investigations below deep conductive cover. Cooperative inversion of seismic and magnetotelluric data has the potential to significantly improve subsurface imaging.

Cooperative inversion is the beneficial transference of information from one geophysical technique to another to improve the recovery of subsurface rock properties. The main focus of my research is the development and comparison of new strategies for cooperative inversion of seismic and magnetotelluric data that are intended to improve the recovery of subsurface conductivity.

Early in my research I also recognised that cooperative inversion has considerable potential for automation. Therefore, I have entertained possible pathways for this to be achieved. Additionally, I have assisted others with developing methods that enhance model-based post stack seismic inversion to recover the distribution of acoustic impedance.

Another key requirement for my research is that strategies must be demonstrated on industry-scale data sets. I have used data from two sites with large co-located seismic and MT surveys. These included data sets from Nevada, USA and Kevitsa, Finland.

These locations possess high-resolution 3D seismic data and conventional MT data. I have concentrated on the Nevada data set as it has complete 3D tipper MT records for over 200 stations spanning an area of more than 30 square kilometers. The area is also covered by high-resolution 3D seismic data and is intersected by several deep drill holes.

New and novel automatic cooperative inversion strategies have been developed. For one strategy, the distribution of geometrical seismic attributes is statistically analysed to build a model framework. The model framework is then populated with (i) electrical conductivity within subvolumes and (ii) inversion smoothness constraints across key boundaries. For this seismically guided large-scale model of conductivity, smoothness constraints are designed to be suitable for input of three dimensional magnetotelluric inversion. The full inversion was then run on a Cray XC30 Cascade supercomputer system to generate a detailed picture of the conductivity distribution for the Nevada data set. The resulting conductivity distribution is shown to be consistent with existing geophysical, geochemical and geological data sets and have an RMS misfit of less than 2%. This example is just one of many strategies developed. The benefits and limitations of the various strategies are assessed against a range of methods for establishing that model data fit all available data sets.

I believe an important outcome of my research into cooperative inversion was the development of new methods for recovering seismic texture. I initially intended to use seismic attributes to automatically build a framework for cooperative inversion. However, I realised that a set of grey level co-occurrence matrix textural attributes could be combined with k-means cluster analysis to build a detailed volumetric representation of seismic textures. I believe that seismic texture possesses considerable value for interpretation in its own right, but I also show that it can provide a framework that will guide inversion of MT data to a higher-resolution subsurface conductivity distribution.

I believe my work has made significant and practical contributions to the inversion of multiple geophysical data sets and when combined with modern cloud and supercomputing can make these methods viable. I hope I have inspired others to continue this work.

TABLE OF CONTENTS

LIST OF FIGURES AND TABLES

FIGURES

FIGURES IN APPENDIX

TABLES

SYMBOLS AND ABBREVIATIONS

Symbol	Meaning/Definition	Units (SI)
Constants		
π	3.1415926…	-
i	Imaginary unit $\sqrt{-1}$	-
Space Coordinates		
x, y, z	Cartesian coordinates	m
t	Time coordinates	s
Partial derivatives		
$\partial_x, \partial_y, \partial_z$	Spatial partial derivatives (Cartesian coordinates)	m^{-1}
Position vector		
i	Unit vector	
r	$\boldsymbol{i_x}x + \boldsymbol{i_y}y + \boldsymbol{i_z}z$	
Vector Nabla operator		
∇	$\boldsymbol{i_x}\partial_x + \boldsymbol{i_y}\partial_y + \boldsymbol{i_z}\partial_z$	
Electromagnetic field quantities		
E	Electric field	V/m
H	Magnetic field	A/m
T_x, T_y	Tipper, relationship between vertical and horizontal components of the magnetic field	
Frequency symbols		

f	Frequency	Hz
ω	Angular frequency	rad/s
Material parameters		
ε	Scalar electrical permittivity	F/m
ε_o	Electrical permittivity of a vacuum	F/m
μ	magnetic permeability	H/m
μ_o	magnetic permeability of a vacuum	H/m
σ	Conductivity	S/m
ρ	Resistivity	Ohm.m
$\hat{Z}$	Impedance tensor	
Other terms		
m	earth conductivity model parameters	
$\boldsymbol{d}$	Field data	
$\boldsymbol{C_d}$	covariance of data errors	
$\boldsymbol{f(m)}$	forward modelling operator	
$\boldsymbol{m_0}$	the initial model	
ν	Lagrange multiplier	
$P_{i,j}$	The ith row and jth column of the grey – level co – occurrence Matrix (GLCM)	
δ	Skin depth	

Abbreviations

AGC	Automatic Gain Control
CT	Computed Tomography
DC	Direct current
ERT	electrical resistivity tomography
EM	Electromagnetic
GLCM	grey – level co – occurrence Matrix
GPR	ground-penetrating radar
MRI	Magnetic resonance imaging
MT	Magnetotelluric
MI	Mutual Information
Ni-Cu-PGE	Nickel – Cooper – Platinum group elements
PCA	principal component analysis
QC	Quality control
RMS	Root mean square
TE	Transverse electric
TM	Transverse magnetic

CHAPTER 1. INTRODUCTION

My research focuses on combining seismic and MT methods for mitigating inversion problems associated with data coverage, resolution and non-uniqueness of the individual geophysical methods. I'll describe possible methods for integrating seismic attributes into MT inversion in Chapter 1. I also introduce the fundamentals of the MT inversion and provide a definition for cooperative inversion. Many novel and new methods for cooperative inversion of seismic and MT data are introduced in Chapter 2 and Chapter 3. In Chapter 2 I use seismic boundaries and geometric sub-volumes from interpretation of seismic attributes. In Chapter 3 I provide: (i) a method for assessing rock mass character with groups of textural seismic attributes, and (ii) a method for cooperative inversion using sub-volumes with statistically similar seismic texture for the prior model of MT inversion. Chapter 4 provides a summary of the research completed.

1.1 Objectives

The objective of this research is to design, develop and demonstrate a set of novel cooperative geophysical inversion strategies. Specific research objectives include:

i. To ascertain which seismic attributes have value and are practical for integration within cooperative inversion.
ii. To create new cooperative inversion strategies.
iii. To develop a workflow for analysis and extraction of seismic texture attributes from seismic reflectivity data. The textural attributes will then be assessed for application in rock mass characterization and for applications in cooperative inversion of seismic and MT data.
iv. To assess the new cooperative inversion workflows on large co-located 3D industry scale magnetotelluric and seismic data sets.

1.2 Thesis Structure

This thesis has three distinct technical components. These includes:

i. Chapter 2; titled "Semiautomatic and Automatic cooperative inversion of seismic and magnetotelluric data".
ii. Chapter 3; titled "Seismic texture for rock volume classification and cooperative inversion" and,

iii. Several appendixes including an expanded abstract and supplementary information.

Chapter 2 and 3 are extended Journal articles for which I am first author. In particular Chapter 2, which is published in the Journal "Surveys in Geophysics", provides a comprehensive review of joint and cooperative inversion in addition to original research outcomes. For this reason, I provide only a brief review of core background concepts, the MT methods, MT inversion, and seismic attributes in the introductory chapter. The appendixes also provide many research outcomes and these are used to support and enhance the content of the main chapters.

I hope my thesis has been constructed to be accessible to a broad range of geoscientists. These includes geoscience academics, mineral explorers, interpreting geologists and geophysicists with expertise in seismic and or electromagnetic methods. The thesis content assumes a basic understanding of seismic and magnetotelluric theory; however, below I also provide a primer for the main concepts that I later use in considerable more depth.

1.3 MT and MT Inversion

1.3.1 MT basics

Natural electromagnetic fields are caused by global lightning activity and by the interaction between solar generated charged particles with the earth's magnetosphere and ionosphere. These electromagnetic fields span a large range of frequencies which are utilised for magnetotelluric (MT) surveys. These randomly fluctuating electromagnetic fields diffuse through the earth and propagate within the earth's volume to great depths. The propagation of the signal is affected by both frequency and the distribution of electrical conductivity in the earth. The currents produced in the earth are called telluric currents (Naidu 2012, Berdichevsky and Dmitriev 2008).

Given a sufficient distance between an electromagnetic source and receiver, the sources can be approximated as a plane wave. For the MT method the source is considered to exist far from the receiver location, and the source EM fields can usually be regarded as plane waves. The electromagnetic fields recorded on the surface vary with subsurface electrical properties (Cagniard 1953, Meqbel 2009, Heinson and

White 2005) and can reveal the subsurface electrical conductivity distribution from meters to tens or even hundreds of kilometres below the surface.

The propagation of these electromagnetic fields is explained through Maxwell's equations as provided below in the frequency domain in terms of electric field intensity $\vec{E}$ and magnetic field intensity $\vec{H}$:

$$\nabla \times \vec{E} = -i\omega\mu\vec{H} \qquad (1.1)$$

$$\nabla \times \vec{H} = (\sigma + i\varepsilon\omega)\vec{E} \qquad (1.2)$$

$$\nabla \cdot \varepsilon\vec{E} = q_v \qquad (1.3)$$

$$\nabla \cdot \vec{H} = 0 \qquad (1.4)$$

where i is the imaginary unit, ω is the angular frequency, μ is the magnetic permeability and ε the electrical permittivity; σ is the electrical conductivity and q_v the electric charge density.

The magnetotelluric method requires processing the time series electromagnetic data into an impedance tensor in frequency domain form (Chave and Jones 2012). This leads to the well-known Tikhonov–Cagniard impedance, defined as the ratio of the electric to magnetic component as a function of frequency:

$$Z_{xy} = \frac{E_x}{H_y} \qquad Z_{yx} = \frac{E_y}{H_x} \qquad (1.5)$$

More general, the relationship between the electromagnetic fields and their impedance tensor is given by the following relationship (e.g., Vozoff 1991):

$$\begin{pmatrix} E_x \\ E_y \end{pmatrix} = \begin{pmatrix} Z_{xx} & Z_{xy} \\ Z_{yx} & Z_{yy} \end{pmatrix} \begin{pmatrix} H_x \\ H_y \end{pmatrix} \qquad (1.6)$$

For each frequency, the impedance tensor contains characteristics of the geoelectrical structure. Dimensionality and direction can be extracted from the impedance tensor, which has the following form for a 1D, 2D or a 3D earth (Simpson and Bahr 2005):

$$\text{1D: } \hat{Z} = \begin{pmatrix} 0 & Z \\ -Z & 0 \end{pmatrix} \qquad (1.7)$$

$$\text{2D: } \hat{Z} = \begin{pmatrix} 0 & Z_{xy} \\ Z_{yx} & 0 \end{pmatrix} \qquad (1.8)$$

$$\text{3D: } \hat{Z} = \begin{pmatrix} Z_{xx} & Z_{xy} \\ Z_{yx} & Z_{yy} \end{pmatrix} \qquad (1.9)$$

Chave and Jones (2012) provide a detailed discussion about various classical dimensionality tools, which are based on the magnitudes of the elements of the impedance tensor, such as polar diagrams, ellipticity and Swift skews. Also discussed are modern dimensionality tools, such as the WAL invariants, based on work by Weaver, Agarwal and Lilley (Weaver, Agarwal, and Lilley 2000).

The relationship between the measured vertical and horizontal components of the magnetic field only, is known as induction arrows or tipper, since they transform (tip) horizontal magnetic fields into the vertical plane. The tipper vectors point towards anomalous concentrations of current when adopting the Parkinson convention. The tipper is non-zero near lateral conductivity changes, where $\nabla \times \vec{E}$ has a vertical component and is defined as follows (Simpson and Bahr 2005):

$$H_z = \begin{pmatrix} T_x & T_y \end{pmatrix} \begin{pmatrix} H_x \\ H_y \end{pmatrix} \qquad (1.10)$$

1.3.2 MT Inversion Overview

The MT inversion recovers a subsurface conductivity distribution by iteratively updating a synthetic geo-electrical model that decreases the residual difference between the field and modelled data. There are two main processes: (i) modelling the synthetic data based on a given conductivity distribution (model parameters) and (ii) updating the model parameters, which results in a smaller residual difference of the measured and synthetic data.

The MT inversion process starts with solving Maxwell's equations (or their derived equations, see below) using an initial electrical conductivity model for a given band of frequencies (Chave and Jones, 2012):

$$\nabla \times \mu^{-1} \nabla \times \vec{E} + i\omega\hat{\sigma}\vec{E} = 0 \qquad (1.11)$$

$$\nabla \times \hat{\sigma}^{-1} \nabla \times \vec{H} + i\omega\mu\vec{H} = 0 \qquad (1.12)$$

with $\hat{\sigma}$ is the complex conductivity given as $\hat{\sigma} = \sigma + i\omega\epsilon$ (the term $i\omega\epsilon$ is often neglected). Finite difference modelling is a common technique to approximate equation (1.11) or (1.12). This technique defines the differential operators as the ratio of differences between field values at distinct points and the distances between the

points (Chave and Jones 2012, Egbert and Kelbert 2012, Meqbel 2009, Weaver 1998). In this approach, the electrical conductivity model is discretised using 2D cells or 3D cubes (for 2D or 3D models respectively). For the 3D case, the electric field components are approximated on cell edges, whereas the magnetic fields are evaluated on the cell faces, see Fig. 1-1 below.

The modelled data refers to impedance tensor or tipper components, which are calculated from the modelled fields. In this thesis I use the ModEM code developed by Egbert and Kelbert (2012) for my experiments**.** In the numerical approach of Egbert and Kelbert (2012), the computation of the electric or magnetic fields within the conductivity model evaluates to solving the linear equation system:

$$S_m e = b \tag{1.13}$$

where S_m is the complex, sparse coefficient matrix reflecting a discrete conductivity distribution, e is the unknown field such as the electric or magnetic field and b are the boundary values. The solution of the linear equation system, in turn, is used to compute the impedance tensor and the tipper.

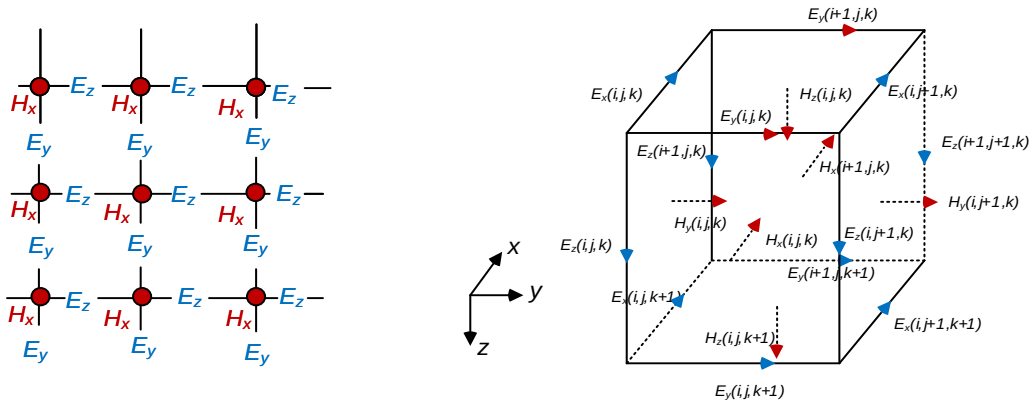

Fig. 1-1: ModEM finite difference grid setup for 2D (left) and 3D settings, the electric and magnetic field orientations are shown (reproduced from Egbert and Kelbert (2012))

The inversion proceeds by minimising an objective function, which must satisfy both, data misfit as well as smoothness constraints (e.g. prior model constraints). ModEM uses the nonlinear conjugate gradient approach for minimising the objective function:

$$\Phi(\mathbf{m}, \mathbf{d}) = \Phi_d + \nu\, \Phi_m \tag{1.14}$$

with

$$\Phi_d = \big(\mathbf{d} - f(\mathbf{m})\big)^T \boldsymbol{C}_d^{-1} \big(\mathbf{d} - f(\mathbf{m})\big)$$

$$\Phi_m = (\mathbf{m} - \mathbf{m}_0)^T C_m^{-1} (\mathbf{m} - \mathbf{m}_0)$$

and:

m – vector of earth conductivity model parameters

d – vector of field data

$\boldsymbol{C_d}$ – covariance matrix of data errors

***f*(m)** – forward modelling operator

$\mathbf{m}_0$ – parameter vector of prior model or first guess

ν – Lagrange multiplier

$\boldsymbol{C}_\mathrm{m}$ – model covariance (smoothing matrix)

The objective function $\Phi(\mathbf{m}, \mathbf{d})$ combines the two penalty functions Φ_d and Φ_m relating to data misfit and model roughness, respectively, where balance of the two functions is controlled via the regularisation parameter ν (Lagrange multiplier). A large value of the regularisation parameter ν emphasises the model roughness term whereas small values of ν accentuates the data misfit. An optimal value of ν would ensure that neither term is too influential. During inversion high damping factors are reduced automatically for improving the data misfit (Meqbel 2009).

The model roughness term Φ_m contains the model covariance matrix $\boldsymbol{C}_\mathrm{m}$ which acts as a model penalty term. By default, the elements of $\boldsymbol{C}_\mathrm{m}$ are constant across model boundary cells with (nearly) identical resistivity. In my strategy I define the elements of $\boldsymbol{C}_\mathrm{m}$ according to boundaries or structures inferred from seismic. Moreover, the prior resistivity model is also devised based on structure inferred from seismic. This is explained in detail in the next chapter.

At minimum, the calculated model defines a subsurface conductivity distribution that can explain the measured data. The difference between the measured and modelled data can be measured for example using the root mean square misfit (RMS) (Meju 1994). The normalised RMS is defined as follows:

$$rms = \frac{1}{n} \sum_{i=1}^{n} \frac{\left(d_i - f(m_i)\right)^2}{\sigma_i^2} \qquad (1.15)$$

d_i – field data

$f(m_i)$ – forward modelling operator

σ_i – data errors

1.4 Cooperative inversion of geophysical data

Combinations of different geophysical methods can reduce non-uniqueness that must exist when surface geophysical data is inverted to subsurface parameter distributions. Cooperative inversion can include a broad range of methods for combining geophysical data to improve subsurface imaging. These may include joint or sequential inversion (Lines, Schultz, and Treitel 1988, Treitel and Lines 2001).

For joint inversion, it's necessary to minimize an objective containing more than one type of geophysical data. The cross-gradient method is a good example of joint inversion. Here we must minimise difference in the vector directions of the spatial gradients of several earth properties such as velocity and conductivity (Gallardo and Meju 2004, Moorkamp et al. 2013, Doetsch, Linde, and Binley 2010, Linde et al. 2006). Multivariate geostatistics may also be used in the process. For example fuzzy logic can be used to create distinct groups with different membership (Paasche and Tronicke 2007, Kieu and Kepic 2015) within the cooperative inversion process.

For sequential inversion prior information of one geophysical method can constrain other inversion of other methods. For example well defined boundaries from seismic data can be used to constrain electromagnetic or gravity inversion (Le et al. 2016, Takam Takougang et al. 2015, Lines, Schultz, and Treitel 1988).

In my thesis I will focus on application of seismic attributes or combinations of attributes within cooperative inversion (Brown 2011, Chopra and Marfurt 2007, Taner et al. 1994). In particular I'll consider possible applications for seismic texture attributes. These were developed in the 1970's, refined in the 1980's and revived in the mid 2000's (Chopra and Marfurt 2007). Textural attributes were developed to "pick out zones of common signal character" (Chopra and Marfurt 2007). This statistical approach classifies seismic textures produced with the grey – level co – occurrence Matrix (GLCM) (Hall-Beyer 2007, Haralick, Shanmugam, and Dinstein 1973).

1.5 References

Berdichevsky, Mark N, and Vladimir I Dmitriev. 2008. *Models and methods of Magnetotellurics*: Springer.

Brown, Alistair R. 2011. *Interpretation of three-dimensional seismic data*: Society of Exploration Geophysicists and American Association of Petroleum Geologists.

Cagniard, Louis. 1953. "Basic theory of the magneto-telluric method of geophysical prospecting." *Geophysics* 18 (3):605-635.

Chave, Alan D, and Alan G Jones. 2012. *The magnetotelluric method: Theory and practice*: Cambridge University Press.

Chopra, Satinder, and Kurt J. Marfurt. 2007. *Seismic attributes for prospect identification and reservoir characteriztion*. Edited by Stephen J. Hill, *SEG Geophysical Development Series No. 11*. United States of America: Tulsa, Okla. (8801 South Yale St., Tulsa OK 74137-3175) : Society of Exploration Geophysicists

Doetsch, Joseph, Niklas Linde, and Andrew Binley. 2010. "Structural joint inversion of time-lapse crosshole ERT and GPR traveltime data." *Geophysical Research Letters* 37.

Egbert, Gary D., and Anna Kelbert. 2012. "Computational recipes for electromagnetic inverse problems." *Geophysical Journal International* 189 (1):251-267. doi: 10.1111/j.1365-246X.2011.05347.x.

Gallardo, Luis A., and Max A. Meju. 2004. "Joint two-dimensional DC resistivity and seismic travel time inversion with cross-gradients constraints." *Journal of Geophysical Research: Solid Earth* 109 (B3). doi: 10.1029/2003JB002716.

Hall-Beyer, M. 2007. "GLCM Texture Tutorial." http://www.fp.ucalgary.ca/mhallbey/tutorial.htm.

Haralick, R. M., K. Shanmugam, and I. Dinstein. 1973. "Textural Features for Image Classification." *IEEE Transactions on Systems, Man, and Cybernetics* SMC-3 (6):610-621. doi: 10.1109/TSMC.1973.4309314.

Heinson, Graham, and Antony White. 2005. "Electrical resistivity of the Northern Australian lithosphere: Crustal anisotropy or mantle heterogeneity?" *Earth and Planetary Science Letters* 232 (1):157-170.

Kieu, Duy Thong, and Anton Kepic. 2015. "Incorporating prior information into seismic impedance inversion using fuzzy clustering technique." SEG New Orleans Annual Meeting, USA.

Le, Cuong V. A., Brett D. Harris, Andrew M. Pethick, Eric M. Takam Takougang, and Brendan Howe. 2016. "Semiautomatic and Automatic Cooperative Inversion of Seismic and Magnetotelluric Data." *Surveys in Geophysics* 37 (5):845-896. doi: 10.1007/s10712-016-9377-z.

Linde, Niklas, Andrew Binley, Ari Tryggvason, Laust B. Pedersen, and Andre´ Revil. 2006. "Improved hydrogeophysical characterization using joint inversion of cross-hole electrical resistance and ground-penetrating radar traveltime data." *Water Resources Research* 42.

Lines, Larry R, Alton K Schultz, and Sven Treitel. 1988. "Cooperative inversion of geophysical data." *Geophysics* 53 (1):8-20.

Meju, Max A. 1994. *Geophysical data analysis: Understanding inverse problem theory and practice*: Society of Exploration Geophysicists.

Meqbel, Naser Mohammad Meqbel. 2009. "The electrical conductivity structure of the Dead Sea Basin derived from 2D and 3D inversion of magnetotelluric data." Freie Universität Berlin.

Moorkamp, M., A. W. Roberts, M. Jegen, B. Heincke, and R. W. Hobbs. 2013. "Verification of velocity-resistivity relationships derived from structural joint inversion with borehole data." *Geophysical Research Letters* 40:3596-3601.

Naidu, G Dhanunjaya. 2012. "Magnetotellurics: Basic Theoretical Concepts." In *Deep Crustal Structure of the Son-Narmada-Tapti Lineament, Central India*, 13-35. Springer.

Paasche, Hendrik, and Jens Tronicke. 2007. "Cooperative inversion of 2D geophysical data sets: A zonal approach based on fuzzy c-means cluster analysis." *Geophysics* 72 (3):A35-A39.

Takam Takougang, Eric, Brett Harris, Anton Kepic, and Cuong V. A. Le. 2015. "Cooperative joint inversion of 3D seismic and magnetotelluric data: With application in a mineral province." *Geophysics* 80:1-13. doi: 10.1190/GEO2014-0252.1.

Taner, M Turhan, James S Schuelke, Ronen O'Doherty, and Edip Baysal. 1994. "Seismic attributes revisited." In *SEG Technical Program Expanded Abstracts 1994*, 1104-1106. Society of Exploration Geophysicists.

Treitel, Sven, and Larry Lines. 2001. "Past, present, and future of geophysical inversion—A new millennium analysis." *Geophysics* 66 (1):21-24.

Weaver, John T, Aman K Agarwal, and FEM Lilley. 2000. "Characterization of the magnetotelluric tensor in terms of its invariants." *Geophysical Journal International* 141 (2):321-336.

Weaver, JT. 1998. "Numerical modelling in electromagnetic induction." In *Deep Electromagnetic Exploration*, 299-363. Springer.

Without forgiveness, there can be no real freedom to act within a group.

~Max DePree

CHAPTER 2. SEMIAUTOMATIC AND AUTOMATIC COOPERATIVE INVERSION OF SEISMIC AND MAGNETOTELLURIC DATA

This chapter is currently published with Surveys in Geophysics (**Le, Cuong V.A.**, B.D. Harris, and A.M. Pethick, E.M. Takam Takougang, B. Howe, 2016, Semiautomatic and automatic cooperative inversion of Seismic and magnetotelluric data Surveys in Geophysics **37**: 845-896. doi:10.1007/s10712-016-9377-z). This article is Open access and has been reproduced without modification of content.

Key points:

- Define suitable seismic attributes for integrating their information within cooperative inversion
- To establish new cooperative inversion strategies that can automatically and semi-automatically create prior electrical conductivity and covariance models.
- To validate the cooperative inversion workflow and confirm its applicability to real-life commercial environments more advantageous than unconstrained inversion.

2.1 Abstract

Natural source electromagnetic methods have the potential to recover rock property distributions from the surface to great depths. Unfortunately, results in complex 3D geo-electrical settings can be disappointing especially where significant near-surface conductivity variations exist. In such settings, unconstrained inversion of magnetotelluric data is inexorably non-unique. We believe that: (i) correctly introduced information from seismic reflection can substantially improve MT inversion, (ii) a cooperative inversion approach can be automated and (iii) massively parallel computing can make such a process viable. Nine inversion strategies including baseline unconstrained inversion and new automated/semiautomated cooperative inversion approaches are applied to industry scale co-located 3D seismic and magnetotelluric datasets. These datasets were acquired in one of the Carlin gold deposit districts in North Central Nevada, USA. In our approach, seismic information feeds directly into the creation of sets of prior conductivity model and covariance coefficient distributions. We demonstrate how statistical analysis of the distribution of selected seismic attributes can be used to automatically extract subvolumes that form the framework for prior model 3D conductivity distribution. Our cooperative inversion strategies result in detailed subsurface conductivity distributions that are consistent with seismic, electrical logs and geochemical analysis of cores. Such 3D conductivity distributions would be expected to provide clues to 3D velocity structures that could feed back into full seismic inversion for an iterative practical and truly cooperative inversion process. We anticipate that, with the aid of parallel computing, cooperative inversion of seismic and magnetotelluric data can be fully automated and we hold confidence that significant and practical advances in this direction have been accomplished.

2.2 Introduction and Background

Co-location of seismic and magnetotelluric surveys is becoming increasing viable for shallow to mid depth exploration programs like those completed by the minerals, hydrocarbon, groundwater and hydrothermal industries. It is also increasingly routine for deeper crustal research. The challenge we identify and address is the creation and testing of practical cooperative inversion strategies intended to link information from seismic and magnetotelluric (MT) surveys to recover detailed subsurface rock property distributions.

The goal of the MT method is to recover subsurface electrical conductivity distributions from the measurement of naturally occurring electromagnetic fields. The information content residing within a co-located seismic dataset should be capable of improving outcomes from magnetotelluric inversion and vice-versa. To achieve mutual benefit, we should develop and if possible automate methods able to extract suitable and consequential information from the seismic data, which is a higher resolution than the MT data.

There are significant differences between the seismic reflection method and the MT method. First, high-frequency electromagnetic fields recorded by MT instruments are rapidly attenuated with depth. Consequentially, sharp geo-electrical boundaries in complex 3D settings are increasingly difficult to resolve with depth. Genuinely sharp 3D geo-electrical boundaries or high conductivity anomalies tend to appear as highly smoothed transitional zones after conventional MT processing. Seismic reflection methods do not suffer from the same loss in resolution with depth. If used correctly, this information can potentially improve MT inversion outcomes. In an example from the Red Sea, Colombo et al. (2013) demonstrate considerable improvement of subsurface resistivity distributions after integrating seismic and MT data.

We propose several cooperative inversion strategies that have the potential to improve MT inversion results. The strategies will be tested using large co-located 3D seismic reflection and tensor MT datasets. These strategies have the potential to be automated and integrate ideas from a range of areas including: 3D MT inversion, seismic attribute analysis and geo-statistics. An overview of these and other key ingredients, which may find value within cooperative or joint inversion strategies, is provided below.

2.2.1 An Overview of the Magnetotelluric Method

The MT method records naturally occurring electric and magnetic fields. These fields are then converted into electrical impedance and tipper values. The frequency-dependent impedance tensor **Z** (Simpson and Bahr 2005) expresses the ratio between electric and magnetic fields. The apparent effective resistivity, calculated from the effective invariant impedance, can then be used to visualise and validate the quality of MT data over a survey region (Berdichevsky and Dmitriev 2008). It is usually the MT derived transverse electric (TE) and transverse magnetic (TM) apparent resistivity modes that provide a first but exceedingly basic representation of subsurface electrical conductivity distribution.

Parameters derived from the "tipper" can also be exploited in both interpretation and full 3D MT inversion. The tipper values are derived from horizontal and vertical magnetic fields (Berdichevsky and Dmitriev 2008, Vozoff 1972). The Vozoff tipper points away from areas of higher conductivity and towards areas of lower conductivity. The tipper will be polarised linearly in 2D environments and elliptically in 3D environments. The tipper can also aid in the evaluation of complex conductivity distributions, as would be encountered across large fault systems (Berdichevsky and Dmitriev 2008). Divergence of the tipper can be explained by the Bio-Savart law (Berdichevsky and Dmitriev 2008). Both apparent resistivity and tipper value can be plotted against log frequency (z axis) or against a pseudo depth parameter for quality control (QC) purposes to provide a preliminary impression of subsurface geo-electrical structures. Beyond the basic assessment of MT apparent resistivity and tipper values, full inversion is required.

2.2.2 Seismic Processing and Seismic Attributes

Once a 3D seismic survey is acquired the objective of seismic processing is usually to generate a volume of "true" relatively amplitude reflections (Yilmaz 2001b). Preservation of true relative amplitudes during processing, can be challenging but is a critical element of modern seismic processing. It is needed for subsequent attempts to recover rock properties (e.g., acoustic impedance) from the seismic data (Takam Takougang et al. 2015, Virieux and Operto 2009). True relative amplitude processing is also highly desirable for the computation of seismic attributes and for optimal use of seismic information within cooperative or joint inversion strategies.

Of particular interest for our research are seismic attributes or multi-attributes that are able to identify broad subvolumes with common geological or physical characteristics that may be linked to electrical conductivity distributions**.** Seismic attributes can be designed to reveal or enhance structural, stratigraphic and/or reservoir characteristics that may not otherwise be apparent in the seismic reflectivity image (Onajite 2013). They can be computed from: (i) real and quadrature components of seismic data (Taner, Koehler, and Sheriff 1979) and (ii) the temporal or geometric relationships within seismic data (Chopra and Marfurt 2007). Attributes derived from the complex trace, such as instantaneous phase and instantaneous frequency, are routinely applied to assist seismic interpretation (Taner 2001, Taner, Koehler, and Sheriff 1979).

Computation of geometric seismic attributes such as polar dip, dip angle, azimuth and curvature typically use similarity and geometric relationships between neighbouring seismic traces within a sliding window to recover estimates of the distribution of geological dip and azimuth throughout a volume (Chopra and Marfurt 2007, Tingdahl and Groot 2003). Other attributes such as semblance-based coherence and similarity may have value in detecting horizons, changes in rock properties along horizons or geological structures (Bahorich and Farmer 1995, Brouwer and Huck 2011, Chopra and Marfurt 2007, Roberts 2001, Tingdahl 2003, West et al. 2002).

The possible application of other forms of quantitative interpretation (QI) of seismic data within cooperative inversion should not be overlooked. Amplitude variations with offset (AVO), amplitude variations with azimuth (AVAz) and acoustic impedance inversion may all have beneficial roles in cooperative or joint inversion (Mahmoudian et al. 2015, Takam Takougang et al. 2015, Yilmaz 2001a).

2.2.3 Joint and Cooperative Inversion

Joint and or cooperative inversion requires a petro-physical or geometric link between parameters recovered from seismic and electromagnetic methods. For joint inversion this link tends to be explicitly included in the object function to be minimised within the inversion process, as described by Haber and Oldenburg (1997). For cooperative inversion, the link tends to be implicitly included within: (i) the design of the initial or seed model, (ii) the process of updating models within the inversion, or the distribution of inversion parameters (e.g., distribution of smoothness constraints). The exact

mathematical mechanism used to “cross pollinate” the inversion process with both seismic and MT information can be subservient to the underlying assumption that there is in fact physically a valid link.

Joint and cooperative inversion approaches are used to, in part, mitigate the inherent non-uniqueness of inversion (Gallardo and Meju 2004, Vozoff and Jupp 1975). We can divide joint and cooperative inversion into the broad and overlapping sub-categories that dominantly rely on: (i) petrophysical relationships, (ii) geometric information, (iii) mutual information, (iv) cross-gradient methods, and (v) other methods. These are briefly described these below.

2.2.3.1 Petrophysical Approaches

Joint and cooperative inversion of seismic and electromagnetic data may be based on a petrophysical connection between distribution of electrical and seismic rock properties. For example, formation porosity and fluid saturation can potentially be linked to conductivity in Archie’s equation (Archie 1942) and to velocity through Gassmann’s equation (Gao, Abubakar, and Habashy 2012). If the porosity and/or fluid saturation are first order drivers for the value of conductivity and velocity, then the petrophysical approach to joint inversion is reasonable. Unfortunately, formation resistivity may be strongly connected to spatial variations in the chemistry of the resident fluids. In this case the petrophysical approach would only be valid if fluid chemistry were accurately known. In porous media the degree of cementation is another parameter that can make such direct petrophysical connections problematic. A more robust approach may be to simply cross plot velocity against conductivity from wireline logs (if available) then base the joint or cooperative inversion process on this empirically derived petrophysical relationship within suitable subdomains, as described in the work of Takam Takougang et al. (2015).

As a sidenote, the links we described between seismic and EM information required for joint or cooperative inversion should not be confused with the seismo-electromagnetic phenomena in which a tiny portion of the seismic wavefield is converted to an electromagnetic wavefield or via versa (Garambois and Dietrich 2002, Dupuis et al. 2009).

2.2.3.2 Geometric Information

Geometric information can be used to guide joint or cooperative inversion (Gallardo and Meju 2004, Moorkamp et al. 2013, Haber and Gazit 2013). Geological circumstances may occur where structural links between acoustic impedance and electrical resistivity exist. For example, the vector direction of the seismic polar dip attribute extracted from a 3D seismic volume and the vector direction of maximum change in electrical conductivity (i.e., the conductivity gradient) will match for repeated conformable layering (Pethick and Harris 2014). We examine this possibility in detail later.

2.2.3.3 Mutual Information

Application of Mutual Information (MI) quantifies a distance metric between co-located images. In medical imaging, the metric can be used to align and position results from magnetic resonance imaging (MRI), computed tomography (CT) and other co-located medical datasets (Viola and Wells III 1997). Haber and Gazit (2013) applied MI inversion to two synthetic co-located datasets including direct current (DC) derived conductivities and seismic slowness. Mandolesi and Jones (2014) applied MI to field data from the Rhenish Shield region, Central Germany. They conducted 1D MT inversion with applied MI to obtain a conductivity distribution using a reference model derived from seismic data.

2.2.3.4 Cross-Gradient Methods

Cross-gradient inversion attempts to minimise the difference in the vector direction of the gradients between two or more earth properties such as velocity and conductivity (Gallardo and Meju 2004). Moorkamp et al. (2013) exploited the relationship between velocity and resistivity extracted from borehole data using a cross-gradient based joint inversion approach. Their cross-gradient based inversion imaged and characterised a salt dome.

In hydro-geophysics joint inversions of electrical resistivity and radar slowness have been applied (Doetsch, Linde, and Binley 2010, Linde et al. 2006). Doetsch, Linde, and Binley (2010) investigated the merits of structural cross-gradient methods by incorporating time-lapse crosshole electrical resistivity tomography (ERT) data and first-arrival ground-penetrating radar (GPR) traveltimes to recover soil moisture content changes within the vadose zone.

As noted earlier, any change of pore water conductivity could prove problematic for application of strict cross-gradient methods (Linde et al. 2006). The cross-gradient approach may also prove inappropriate where clay type (e.g., high cation-exchange clays) is key driver for distribution and direction of change of electrical conductivity.

2.2.3.5 Other Methods

The integration of seismic boundaries can be used to build a geo-electrical framework to constrain inversion and has been applied to both passive source magnetotelluric methods (Moorkamp, Jones, and Eaton 2007) and marine controlled source electromagnetic methods (Harris et al. 2009). Other cooperative inversion techniques, as used by Zhou et al. (2014), apply smoothness weights at boundaries with dependence on a priori user-defined structures. That is, smaller weightings can be allocated proximal to the edge of faults or other potential geo-electrical boundaries.

In addition, deGroot-Hedlin and Constable (1990) show that 'the penalty for roughness at known boundaries may be removed in the roughening matrix', which has the potential to permit "sharper" electrical resistivity gradients across boundaries. Conductivity models can also be engineered to support seismic inversion where a prior acoustic impedance model has aided outcomes from MT inversion (Takam Takougang et al. 2015). Here, definition of prior acoustic impedance is assisted by MT inversion combined with empirical well-log relationships between electrical conductivity and acoustic impedance to image rock property distributions across a wide range of geological environments (Takam Takougang et al. 2015).

2.2.4 Geostatistical methods in Cooperative Inversion

Selection and application geostatistical methods are often of fundament importance to cooperative inversion. Cooperative inversion generally requires the transference of information recovered from different processes such wire-line logging, petro-physical measurements on core, geochemistry and outputs from inversion. These datasets will invariably have significantly different spatial resolution. The passing of information (e.g., as a constraint) derived from different methods requires some form of averaging or geo-statistical grouping.

Examples of well-known geo-statistical methods that may have value in cooperative inversion include basic methods such as kriging or co-kriging and clustering

techniques such as k-means, Fuzzy logic, principal component analysis (PCA) and neural networking (Dubrule 2003, Di Giuseppe et al. 2014, De Benedetto et al. 2012, Kieu and Kepic 2015, Ward et al. 2014, Klose 2006, Bedrosian et al. 2007, Roden, Smith, and Sacrey 2015).

Geostatistical methods can be applied during data analysis and quality control. Basic tools of geo-statistical representations at the data analysis or QC stage, include histogram plots and scatter diagrams (Bourges, Mari, and Jeannée 2012, Takam Takougang et al. 2015). Vario-grams can be also created and these allow the spatial distribution of parameters such as seismic amplitudes, velocity and porosity to be statistically quantified (Dubrule 2003).

Geo-statistical gridding techniques such as kriging or co-kriging can also be applied to estimate values at specific locations from predicted variogram model. Bedrosian et al. (2007) use krigging to interpolate inverted MT derived electrical resistivity values onto a finer mesh corresponding to that used for seismic velocity, to perform lithological classification. Bourges, Mari, and Jeannée (2012) present an example demonstrating the benefits of co-kriging on the two dataset's porosity and acoustic impedance. They found that by performing co-located co-kriging, their estimation of the key parameter, porosity, could be improved.

Clustering techniques can also play an important role in evaluating and connecting different earth parameters. k-means clustering is one such approach. k-means "minimises the sum, over all clusters, of the within-cluster sums of point-to-cluster-centroid distances" (MathWorks 2014a). In an example by Di Giuseppe et al. (2014), distinct groups of resistivity and velocity are analysed by k-means for stress fault zone imaging.

Fuzzy logic is also known as a clustering approach. Fuzzy logic categorises parameter elements into several clusters, with each element assigned a membership level to each cluster (Bezdek, Ehrlich, and Full 1984, Kieu and Kepic 2015). Self-organised maps are a type of artificial neural network technique, which are able to transform multiple data sets into two-dimensionally maps for identifying geology characteristics of the granitic gneisses (Klose 2006).

Many of the above geo-statistical methods are broadly equivalent. In this field example we demonstrate k-means methods.

2.2.5 Incorporating seismic information within magnetotelluric inversion

The failure or success of modern 3D MT inversion may be determined by the initial or seed model conductivity distribution in combination with the distribution of smoothness constraints. The prior conductivity distribution need not be complicated; however, it must create a large scale 3D distribution of electrical conductivity, which broadly represents the true subsurface conductivity distribution.

One novel element of our research is the use of seismic attributes within automatic cooperative inversion. We will show that it is not required that the seismic attribute analysis recover high levels of detail. Rather, we seek the geometry of subvolumes that are expected to exhibit common seismic and geo-electrical characteristics. This can be done by statistically analysing the distribution of selected seismic attributes across a large volume with the objective of capturing the geometry of a limited set of subvolumes that can later be allocated values of electrical conductivity.
Two examples highlighting the link between the characteristics that can be recovered from relative apparent reflectivity (i.e., the processed seismic volume) and the geo-electrical structure of the earth include:

i. *High reflectivity boundary separating conductive cover sequences from more resistive basement:* If true relative amplitude processing has been effective, then the boundary between any conductive, weakly consolidated cover and more competent, electrically resistive higher-velocity basement should be well represented. This boundary may be extracted and identified in “energy”-based seismic attributes, provided that a suitably sized sliding window is applied over the seismic volume. The energy attribute (i.e., an amplitude based attribute) may then be used to automatically recover the geo-electrical sub-division between cover and basement.

ii. *Repeated and continuous reflections within repeated conformable layering:* Such depositional environments are common in sediments. However, they also exist within certain hard-rock settings (e.g., layered intrusions, shear zones etc.). These environments may have a common dip direction and be effectively identified by the polar dip attributes averaged over a suitably sized

3D sliding window. The polar dip seismic attribute is a geometric attribute that can be used to define large volumes with similar geological dip.

2.2.6 Some guiding principles for cooperative inversion

Before proceeding to describe our semiautomatic and automatic inversion strategies we would like to summarise several caveats and considerations that may impact outcomes arising from cooperative inversion. These are listed as general principles intended to guide the development of cooperative inversion strategies and include:

i. *True relative amplitude processing of seismic data has been applied:* for our methods we may only be seeking a limited number of geo-electrical boundaries based only on high-reflectivity boundaries such as the interface between conductive cover and crystalline basement. For example, a short window Automatic Gain Control (AGC) should never be applied. However, in general most modern processing flows would be expected to retain the key, highest relative reflectivity interfaces.

ii. *For the seismic volume, time to depth conversion has been completed:* MT inversion operates within the depth domain. So time to depth conversion of seismic data and consequently, a velocity model is required. While in many cases seismic is highly accurate, some "allowance" or "tolerance" of incorrectly located interfaces should exist in the MT inversion.

iii. *Induced polarisation and electrical anisotropy effects may exist (Zorin, Epishkin, and Yakovlev 2015) but shouldn't unnecessarily burden the inversion:* induced polarisation and electrical anisotropy in theory can certainly exist in many electrical settings. Without explicit knowledge of the existence of polarisable rocks, cooperative inversion should not be burdened with these additional degrees of freedom for full 3D inversion within a complex 3D environment. There may be value in progressively introducing these additional parameters to small subvolumes at a later stage of the inversion workflow.

iv. *Pre-processing or parameter selection for seismic attribute analysis has been completed:* our approach uses seismic attributes that are sensitive to pre-

processing that will require many input parameters. These must be thoughtfully selected with the end purpose in mind.

v. *The size of the sliding windows selected to capture seismic information should have a scale relevant to MT methods:* our approach is based on iteratively improving the prior model and updating smoothness constraints for MT inversion across key boundaries determined mostly upon seismic information. Again we should seek a limited number of well-defined subvolumes and key boundaries. We would also note that the sliding windows applied to recover or analyse seismic information can be relatively large.

vi. *Any 3D MT prior model subvolumes should be of a geo-electrically reasonable scale with reference to depth and conductivity:* the resolution of any surface-based MT method is depth dependent. There is little value to defining high levels of detail in a prior model at great depth where conductivities are not explicitly known (e.g., from wireline logging). Including geo-electrically insignificant subvolumes and/or boundaries should be avoided.

vii. *Shallow electrical conductivities can be of the highest importance:* lastly we would like to place emphasis on the role of the shallow and often electrically heterogeneous conductivity distributions. If these shallow upper often high-conductivity subvolumes fail to be suitably included in the prior model, the inversion is doomed to failure before it starts. That is, if the shallow conductivities cannot be correctly recovered from the inversion, then artefacts are inevitable at greater depth as the inversion must somehow compensate for incorrect shallow conductivity distributions. At the other extreme, if shallow conductivity distributions are recovered in detail then the MT inversion has considerably improved prospects of recovering correctly distributed deeper conductivity distributions. We will argue the any MT inversion requiring high levels of smoothness across shallow, sharp 3D interfaces will tend to distort the representation of conductivity at depth and that cooperative inversion can help remedy this problem.

Application of our semiautomatic and automatic cooperative inversion is described next (methodology), after which a comprehensive field example, including comparison of nine inversion strategies, is provided.

2.3 Methodology

For this paper, our approach is to describe our cooperative inversion strategies, then apply a set of these to an industry scale field example. The outcome will be nine 3D electrical conductive distributions stemming from the application of the nine inversion workflows. Two of these outcomes will be the results of baseline conventional unconstrained inversion and assumes that no other information is available, and seven workflows will be cooperative inversion strategies integrating MT inversion and seismic information. Results will be presented as equivalent sets of images for comparison and analysis. The strategies are designed to span a variety of unique pathways that will enable discussion around the degree to which each strategy can be automated and or generate a "true" representation of subsurface electrical conductivity in complex 3D geo-electrical settings containing both sharp geo-electrical boundaries and smooth transitional zones.

The estimation of electrical conductivity distribution from cooperative inversion requires the careful selection of suitable parameters through the data acquisition, pre-processing, inversion and validation stages. While success relies upon the correct selection of parameters at all stages, this research focuses on the pre-processing, inversion and data and model validation.

The MT inversion algorithm is a significant element of cooperative inversion and is the first concept we describe (Sect. 2.1). In particular, we will focus on the role of the prior model conductivity distribution and the prior smoothness constraint distribution as these are the main levers we use in our cooperative inversion. We then outline our semiautomatic (Sect. 2.2) and automatic (Sect. 2.3) cooperative inversion strategies. One premise for our research is that seismic attribute analysis can help bridge the gap between the rich information content found in seismic data and the inversion of magnetotelluric data. We outline the mechanics required to transfer seismic information to our cooperative inversion process via seismic attributes.

2.3.1 MT inversion and constraints

MT inversion attempts to recover the true subsurface conductivity distribution by minimising the residual percent difference between the field data and simulated data. Geo-electrical model smoothness is the rate of change in conductivity between two model cells. Model smoothness plays an important role in stabilising the inversion process. deGroot-Hedlin and Constable (1990) use the words "providing minimum possible structure" everywhere to describe the outcome of MT inversion with a single global smoothness constraint. Genuinely sharp, high-contrast geo-electrical boundaries cannot be correctly represented within such a numerical framework.

We use the ModEM code developed by Egbert and Kelbert (2012) for our experiments**.** Its objective function must satisfy both data misfit and smoothness requirements and is given as (Egbert and Kelbert, 2012):

$$\Phi(m,d) = (d - f(m))^T C_d^{-1}(d - f(m)) + \nu(m - m_0)^T C_m^{-1}(m - m_0) \qquad (2\text{-}1)$$

where, $\boldsymbol{m}$ – earth conductivity model parameter, $\boldsymbol{d}$ – field data, $\boldsymbol{C_d}$ – covariance of data errors, $\boldsymbol{f(m)}$ – forward modelling operator, $\boldsymbol{m_0}$ – the prior model, ν – Lagrange multiplier, $\boldsymbol{C_m}$ – smoothing operator.

The Lagrange multiplier ν plays a key role in balancing the misfit and smoothness requirements. $\boldsymbol{C_m}$ is the model covariance or regularisation term and is also known as a smoothing operator (Siripunvaraporn and Egbert 2000). It plays a key role in dictating sharpness or smoothness between the model elements during inversion. Theoretically, each element of $\boldsymbol{C_m}$ can be independently configured for all pairs of elements in $\boldsymbol{m}$, allowing considerable fine tuning of smoothness between adjacent cells. If the elements are set to zeroes, the smoothness criteria applying to their model parameters is not included in the inversion or sharp boundary would be defined.

Fig. 2-1 illustrates the two controls or levers that we use to drive the inversion. Seismic information can be used to assign key values for both the prior model ($\boldsymbol{m_0}$) and covariance matrix ($\boldsymbol{C_m}$). Our goals are to produce a prior conductivity model integrated with seismic structures and to populate the covariance matrix using consistent coefficients derived with the aid of seismic attributes.

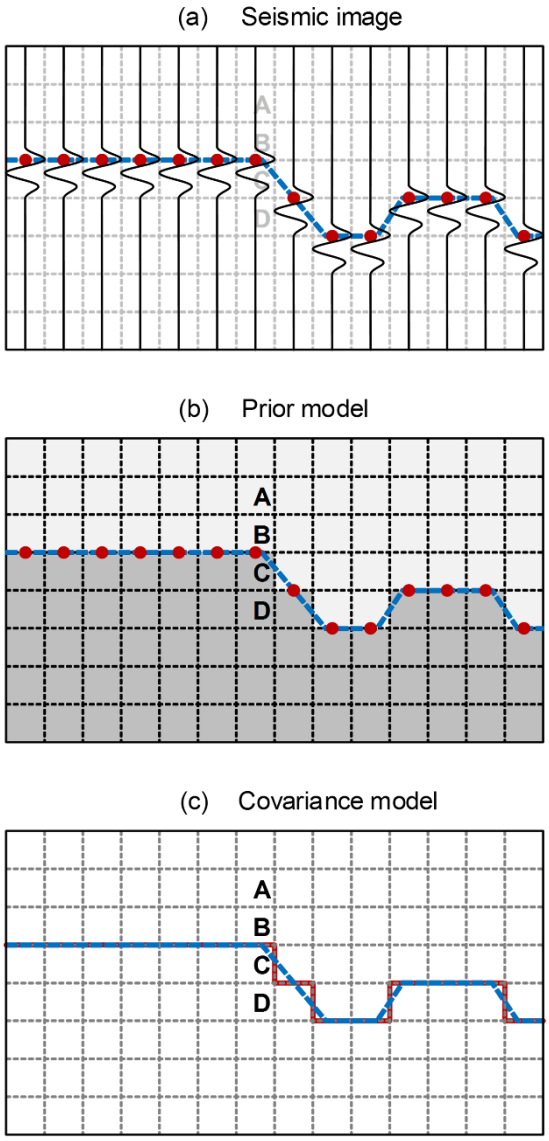

Fig. 2-1: Schematic illustrating the transference of seismic information to the MT inversion prior conductivity and covariance model. The correlation between a seismic, b the geo-electrical model and c the covariance model is shown. In theory, a sharp step change in resistivity can only be achieved if the component of the covariance matrix corresponding to that boundary contains a value of zero. For example, the covariance coefficient between cells B and C could be set to zero. Practically, a positive nonzero value up to around 0.25 is typically chosen. The rate of change in electrical resistivity possible between cells of the inverted resistivity model is inversely proportional to the corresponding covariance coefficient value. That is, the greater the covariance coefficient value, the smoother the boundary between cells

The prior model distribution for our cooperative inversion includes both conductivity and smoothness. The prior conductivity models may be derived from combinations of seismic information, MT unconstrained inversion results and drill-hole information. We will show that the prior conductivity distribution strongly influences the inversion's outcome. Seismic boundaries can be used to create distinct subvolumes, each with uniform resistivity values, as represented by the schematics in Fig. 2-1. We may infer a single representative resistivity value in each subvolume by statistical analysis of the conductivities distribution recovered from unconstrained inversion within each subvolume. This approach is used to produce sharp changes in resistivity across each subvolume boundary. While this approach does not guarantee success it is one method for automatically "loading" the prior model with reasonable conductivities within a framework recovered from seismic information.

Seismic information can also be used to assist in construction of a 3D prior distribution of smoothness constraints. That is, we assign smoothness criteria for every cell within the full model domain. The smoothness criteria can be removed or reduced at cell boundaries. Reducing the smoothness criteria at known interfaces permits the MT inversion to generate higher conductivity gradients across subvolume boundaries.

For our example of cooperative inversion strategies, we generally select a uniform covariance coefficient within each subvolume. Covariance describes the smoothness criteria between cells and the schematic in Fig. 2-1c, illustrates how smoothness criteria may be assigned based on seismic information. In the schematic four cells are labelled: A, B, C and D. Cells A and B lie within region one, while cells C and D lie within region two. The assigned covariance between cells A and B (i.e., cells in the same region) should be set to high number than the covariance between B and C (i.e., cells in adjacent regions). This procedure allows MT inversion to generate a higher-resistivity gradient between B and C compared to between A and B or C and D.

For our "semiautomatic" and "automatic" strategies our approach is to initialise the covariance coefficients globally to a constant, then modify values across boundaries where the covariance is typically assigned to a smaller number (see Fig. 2-1). This gives the MT inversion "permission" to change more rapidly across the boundary than across cells within volumes enclosed by boundaries. We will show later that seismic

attributes related to reflectivity strength along high reflectivity boundaries can potentially be a basis for automatically defining covariance.

Seismic information, in one form or another, is used to create the framework of the prior geo-electrical model. This framework may be created in a semiautomatic way by selecting high relative reflectivity seismic horizons that are expected to be coincident with key geo-electrical boundaries (e.g., the cover to basement interface).

Alternatively, the geo-electrical framework can be built automatically with the aid of seismic attribute analysis (i.e., via statistical analysis of the distribution of seismic attributes). That is, large subvolumes exhibiting common seismic characteristics are automatically extracted from attribute images. The details of semiautomatic and automatic cooperative inversion are provided below.

2.3.2 Semiautomatic cooperative inversion

Semiautomatic cooperative inversion requires some level of interpretation. In this approach, key seismic horizons with links to geo-electrical structures must be extracted from the seismic volume. Only those horizons that are interpreted as having links to the subsurface geo-electrical features are selected. Selecting all horizons would burden the inversion process with excessive and undifferentiated information. The process is called semiautomatic because the key horizons are manually selected.

A higher level of automation may be plausible if seismic attributes can be used to auto-select relevant high reflectivity interfaces and/or 3D auto-picking algorithms are used to recover the seismic horizons. Indeed, 3D auto-picking algorithms tend to be successful at recovering extensive high reflectivity boundaries as is common between cover and basement within a 3D seismic volume. More specifically seismic energy, or the squared summation of seismic amplitude in a time gate, may provide a basis for classifying or “weighting” changes occurring along a boundary of high reflectivity.

Statistical characteristics, such as application of the Grey-level co-occurrence matrix (Hall-Beyer 2007), may provide a volumetric tool for the classification of large volumes of earth. The energy texture attribute which is calculated from the application of the Grey-level co-occurrence matrix, provides a decent tool for estimating textural uniformity or defining areas of common signal character. It may also support the detection of key rock-unit boundaries or work in combination with other seismic

attributes such as energy as a multi-attribute approach to volumetric classification tailored for recovering a prior model geo-electrical framework as an input to MT inversion.

Several of our example strategies will use attribute analysis to extract subvolumes with common seismic reflectivity. The next challenge is to link or assign electrical properties to these subvolumes to build the prior conductivity and or covariance distributions necessary for MT inversion. An obvious initial approach is to search for a petrophysical relationship. Unfortunately, there is rarely sufficient data to achieve such an empirical relationship across a large variety of rock types. With respect to assigning distribution of resistivity, two important points should be considered:

i. The initial or prior resistivity model serves as a guide only, intended to gently 'nudge' the MT inversion in the correct direction. The inversion process itself will perform the numerical calculations to recover detailed conductivity distribution provided the starting point is reasonable.

ii. We never presume that any one seed model is necessarily best or correct. Equally, it would be scientifically incorrect to presume that any one final inversion outcome must be "correct" as we know there will always be equivalent models. Our approach is to create, test and compare a set of reasonable inversion strategies that may generate outcomes with equal data misfit although misfit alone may not be a good indicator of how faithfully true subsurface conductivity has been represented by the outcome of inversion.

Where there is a lack of drill-hole information, one approach that we have developed is to compute a first-pass unconstrained inversion then based on the outcome, statistically assign a single resistivity to each subvolume within the model framework generated from seismic information. That is, the limited number of subvolumes extracted from the 3D seismic reflectivity image are allocated into a new prior model conductivity based on a statistical assessment of conductivities distribution stemming from an initial unconstrained inversion. The intent of such an approach is to provide the prior model with the general large scale conductivity structures, beyond which the parallelised full MT inversion is called upon in the recovery of the detailed conductivity distribution.

2.3.3 Automatic cooperative inversion

For any high quality, co-located MT and migrated seismic datasets, our "automatic cooperative inversion" presents the potential for a fully autonomous inversion process. This cooperative inversion strategy would typically involve mapping from seismic attributes to electrical conductivity.

Unconstrained MT inversion can also be used to govern a second, constrained round of MT inversion. Put simply, the large subvolumes that form a geometric framework are based on selected characteristics of seismic reflectivity as derived from attribute analysis. The electrical conductivity is then mapped into this framework, either by an inferred relationship, or with the assistance of the conductivity distribution derived from unconstrained inversion.

For the field example of automatic cooperative inversion, we will focus on possible applications for the "polar dip" seismic attribute (Brouwer and Huck, 2011). This will demonstrate another of our approaches to cooperative inversion and will hopefully present readers with an approach that they may not have considered.

If averaged over a suitable window, the polar dip seismic attribute can provide a reasonable estimate of true geological dip. Depending on the seismic data quality and processing, the dip estimates tend to deteriorate at very high angles, however, subtle variations for shallow dipping rock are expected to be exceedingly well resolved. We will use the dip steering computation implemented within the OpendTect software (Apel 2001, Huck 2012) to help produce a polar dip vector seismic attribute.

The procedures for computing structural attributes are based on Fourier-Radon transformations and are fully described in (Tingdahl and Groot 2003, Tingdahl 2003). The procedures require the seismic data to be initially in the time-space domain, then transferred into frequency-wave number domain and then to slowness-frequency domain. Values of slowness coordinates are linked with the maximum value by integrating over the frequency axis. Finally, polar dip is derived from the slowness coordinates corresponding to the maximum value. Other methods for computing polar dip based on complex-trace analysis are described in Chopra and Marfurt (2007). Additional detail on polar dip will be provided within section 2.4.

There are as many potential cooperative-inversion pathways as there are seismic attributes and modern parallel computing is exceedingly well suited to simultaneously

testing a large numbers of inversion strategies. The set of cooperative inversions strategies we have selected aims to facilitate discussions on trade-offs between the degree to which the process can be automated, against the inversion's ability to recover true subsurface conductive distributions, with particular emphasis on a setting with thick electrically conductivity cover sequences separated by a clear 3D cover to basement interface. These setting are increasingly important as explorers extend their search for resources to mineralised terrains that descend below deep cover (Hillis et al. 2014).

2.4 A Field Example

The practical value of joint or cooperative inversion strategies can only demonstrated after application to real co-located 3D seismic and MT data. We apply our semiautomatic and automatic cooperative inversion strategies to large co-located 3D seismic and magnetotelluric datasets. These datasets were acquired by Barrick Gold Corporation in one of the Carlin Style Gold districts of north-central Nevada, USA. Collectively these districts represent, one of the world's premier gold producing provinces. It is estimated that they contain approximately six million kilograms of gold, making them the second largest accumulation in the world. It accounts for 6% of annual worldwide gold production (Muntean et al. 2011). Carlin-style gold deposits have been actively mined since 1961, although some earlier deposits were exploited at the beginning of the twentieth century (Cline et al. 2005). Palaeozoic rocks are the main host for Carlin-style gold deposits with Eocene-aged mineralisation (Cline et al. 2005, Muntean et al. 2011)).

The data used for this research was collected over an area with large variations in cover thickness. Cover depths range from less than 100 m to more than 500 m and the base of the cover sequence often has a sharp clear geo-electrical transition to more electrically resistive basement. The transition between cover and basement is an unconformity between Palaeozoic sediments that we define as "basement" and the younger "cover" sequences (Cline et al. 2005, Muntean et al. 2011, Muntean, Coward, and Tarnocai 2007, Thoreson et al. 2000).

The division between cover sequences and basement is generally well defined as a high reflectivity interface within the seismic data (see Fig. 2-5e). On mass, the cover

sequences tend to be more conductive than the Palaeozoic basement rocks below. The general characteristics of cover and basement sequences are:

(i) Drilling in the study area and the previous works (Cline et al. 2005, Muntean et al. 2011, Muntean, Coward, and Tarnocai 2007, Thoreson et al. 2000) suggest that cover rocks include unconsolidated sediments, valley-filled sediment, alluvium and interbeds of volcanics. The cover sequences are considered to be less prospective for primary gold, while basalt, mudstone, quartzite and tuff are prevalent in the Palaeozoic basement rocks. Electrical wireline logs from the study area indicate average resistivity of the order 100 Ω•m for several hundred meters in basement below the Palaeozoic unconformity.

(ii) The nature of the younger cover sequence provides a clue for the selection of seismic attribute to be used within cooperative inversion. This depositional environment is dominated by shallow dipping sequences of sand, clay, limestone and volcanics. Small changes in dip are exceedingly well defined in seismic reflectivity images and do tend to reflect significant changes in large scale depositional environment both vertically and laterally. Further the geometry of the cover to basement interface is clearly 3D and is also well defined in the 3D seismic image. In such depositional areas of varying dipping beds, reflection strength and polar dip can provide key constraints within a cooperative inversion workflow and we will integrate computation of these seismic attributes in several cooperative inversion strategies. Note that we do not promote that idea of a single best solution (i.e. the silver bullet) but do strongly advocate systematic analysis of outcomes from a diverse range of strategies in the context of the geological setting.

Howe et al. (2014) provide diagrams indicating the range of electrical resistivity that may be expected for the main rock types in the study area. In their research, a measured resistivity range for each major lithology group is defined. Their measurements indicate that areas with higher concentration of gold correlates with zones of higher electrical conductivity. They also provide an excellent example of MT inversion over a gold deposit.

For the MT data we completed a detailed QC process, in which every tensor MT sounding was reviewed and "cleaned". The QC process yielded a final data set containing 213 MT stations. All inversions were completed with this same set of 213 MT records. The locations of the MT stations are shown in Fig. 2-2. The final dataset included the impedance tensor, sampled to have 25 periods in the range of 0.0025 to 0.7880 s. Of the 213 MT soundings, 184 included the full tipper, sampled to have 21 periods in the range of 0.0042 to 0.4894 s.

Prior to inversion it is helpful to compute the MT skin depth as a rough guide to the expected depth range of investigation. Assuming a representative resistivity in the order of 25 Ω•m and MT periods in the range 0.0025 to 0.7880 s, the skin depth equation suggests an approximate depth range of investigation of between 150 m to 2500 m. Here we use skin depth $\delta = 503\sqrt{\rho \cdot T}$, where ρ is electrical resistivity in Ω·m and T is period in seconds. This simple skin depth analysis indicates that the inversion should not be expected to recover accurate conductivities for depths significantly less than 150 m or deeper than 2500 m.

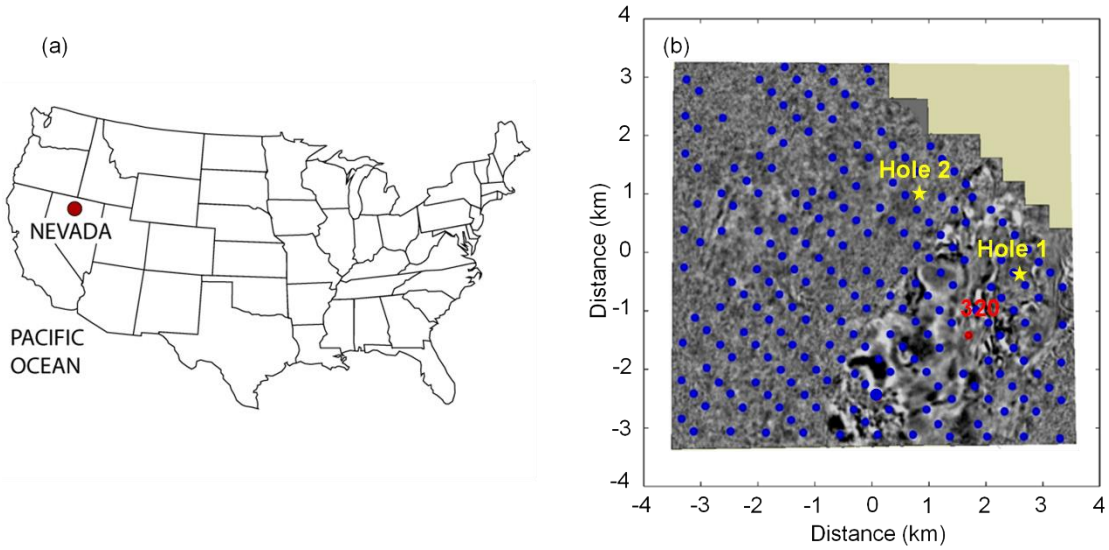

Fig. 2-2: This map shows the approximate survey location as identified by the *red dot*. The survey was carried out in Nevada, USA. **b** A plan view of the 3D migrated seismic image at depth, overlaid by the location of each MT station (i.e. the *blue points*). The position of station 320 is highlighted by a *red point*, and two significant boreholes containing electrical, geochemical and geological data are identified by the *yellow stars*. The full processed tensor MT field record for station 320 is shown in Fig. 2-3

Analysis of the tipper is helpful as it provides a coarse but important indicator of 3D geo-electrical complexity and possible large scale zonation for later inversion (Berdichevsky and Dmitriev 2008, Tietze and Ritter 2013, Becken and Ritter 2012). Fig. 2-3 provides an example of one full tensor record from the Nevada dataset, at station identifier 320 (see Fig. 2-2). 3D inversion can be carried out on this data without further pre-processing. Fig. 2-4 represents the Vozoff tippers at period 0.489 s. The Vozoff tipper vectors in Fig. 2-4a indicate directions of change from areas of high conductivity to areas of low conductivity. Fig. 2-4b presents an image of the Vozoff ellipticity. The Vozoff tippers and the ellipticity are calculated from the technique described by Berdichevsky and Nguyen included within (Berdichevsky and Dmitriev 2008). Zones of strong ellipticity (e.g., 0.3) are expected to occur at the boundary between two distinctly different geo-electrical settings (see dash blue line in Fig. 2-4b). Fig. 2-4a and Fig. 2-4b point to a complex geo-electrical environment with large 3D changes in electrical conductivity distribution.

Above we have described the site geology, data and data quality relevant to our field example. Next we will describe the application of semiautomatic and automatic cooperative inversion strategies selected for application to the field example. The methods are selected to highlight different approaches to cooperative inversion and to facilitate comparisons between the different strategies.

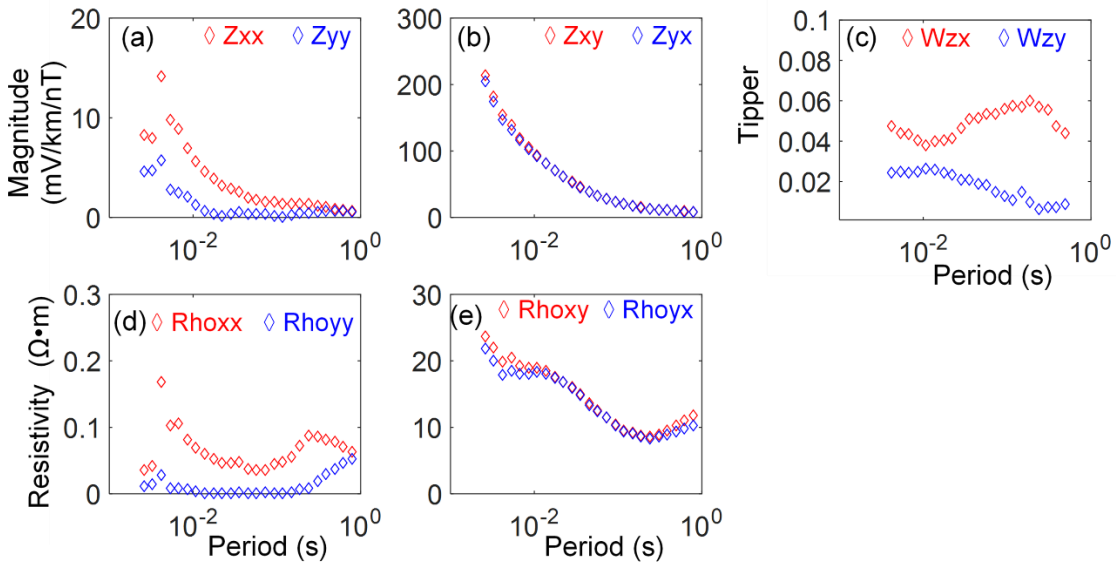

Fig. 2-3: Processed full tensor record for station 320. The figure shows the impedance tensor, Z (a, b), the tipper mode (c) and apparent resistivity versus period curves (d, e). The components of the impedance tensor (Z) refer to the ratio between the electric and magnetic

fields. The tipper mode is the ratio between horizontal and vertical magnetic fields and the apparent resistivity (Rho) and is derived from each horizontal component of tensor Z.

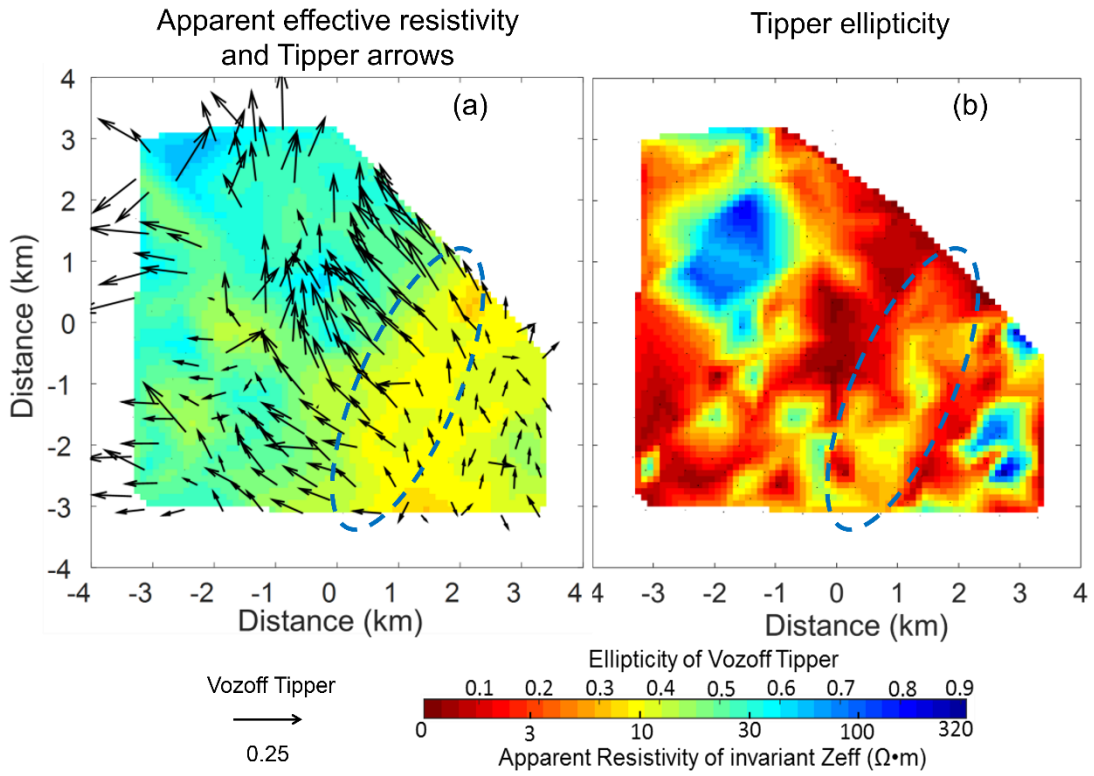

Fig. 2-4: Gridded plan views of the processed MT data at a period of T=0.48939 s. The Figure includes: (a) the apparent effective resistivity and Vozoff tipper induction vectors and (b) the ellipticity of the Vozoff tipper. A transition zone of two high and low apparent resistivity environments are highlighted by the dashed blue ellipses. The zone is also characterized by major changes in amplitude and direction of the Vozoff tippers. A zone of strong ellipticity (e.g., an approximate ellipticity ratio of 0.3) occurs within this ellipse.

2.4.1 Application of semiautomatic cooperative inversion

Next we describe semiautomatic cooperative inversion applied to the Nevada co-located seismic and MT data. This includes description methods for building or updating both prior geo-electrical and smoothness criteria models with assistance from Seismic information.

We designate strategies that require manual interpretation or inputs semiautomatic. These have limited potential for full automation. For example, where 3D seismic horizons must be manually picked the strategy is classified as semiautomatic. In the

below description we have used the OpendTect software (Apel 2001, Huck 2012) for picking horizons from the Nevada seismic volume.

2.4.1.1 Selection and application of seismic attributes for cooperative inversion

As noted in Sect. 2.2 seismic attributes such as seismic amplitudes, energy and energy texture can aid selection and classification of key seismic boundaries or subvolumes with common seismic and possibly geo-electrical character. Fig. 2-5 presents images of several seismic attributes along and key horizons picked from the seismic volume (i.e. Fig. 2-5e). Fig. 2-5b, c, d represent the large scale distribution of the seismic attributes calculated from seismic data (Fig. 2-5a) as energy, energy texture and dip angle, respectively. Each attribute provides the opportunity to subdivide the full seismic volume into a set of subvolumes.

A notable horizon is highlighted by the white line in Fig. 2-5e. It likely represents a key geological unconformity with strong acoustic impedance and geo-electrical contrast. The yellow and blue lines represent key, high reflectivity horizons within cover sequences. These sequences are later shown to enclose higher conductivity rock types. The rock types vary rapidly in both vertical and horizontal directions.

2.4.1.2 Creation and update of the prior conductivity model

Creation and update of the prior conductivity distribution is a practical and consequential part of full inversion and analysis of MT data. The set of images in Fig. 2-6 show the steps used to create prior conductivity distributions for our semiautomatic cooperative inversion strategies. For the field example only the highest reflectivity boundaries are extracted from seismic attribute volumes (e.g., based on amplitude and reflective energy) to build a prior conductivity model for MT inversion. These horizons are likely to represent key geo-electrical boundaries (Fig. 2-6a).

For the Nevada example, we have reduced the full conductivity distribution derived from unconstrained MT inversion to just five conductivities (i.e., 40 Ω•m, 30 Ω•m, 20 Ω•m, 35 Ω•m, 100 Ω•m). These five values are then mapped to the appropriate subvolumes, as shown in Fig. 2-6c. Note that unconstrained inversion, initialised with a 40 Ω•m half-space prior model, provides a basis for assigning a conductivity within each of these five large seismically derived subvolumes. As is commonly the case, there is insufficient wire-line log data to build a petrophysically based prior conductivity model.

The lower half-space subvolume is considered as a special case when assigning a value for the conductivity prior model. Neither seismic nor MT can provide a reasonable estimate over the full lower subvolume, which has no lower boundary. We use a value of 100 Ω•m in the "basement" rock as it is consistent with the average resistivity from wireline logs immediately below (i.e., within 200 m) the cover to basement interface.

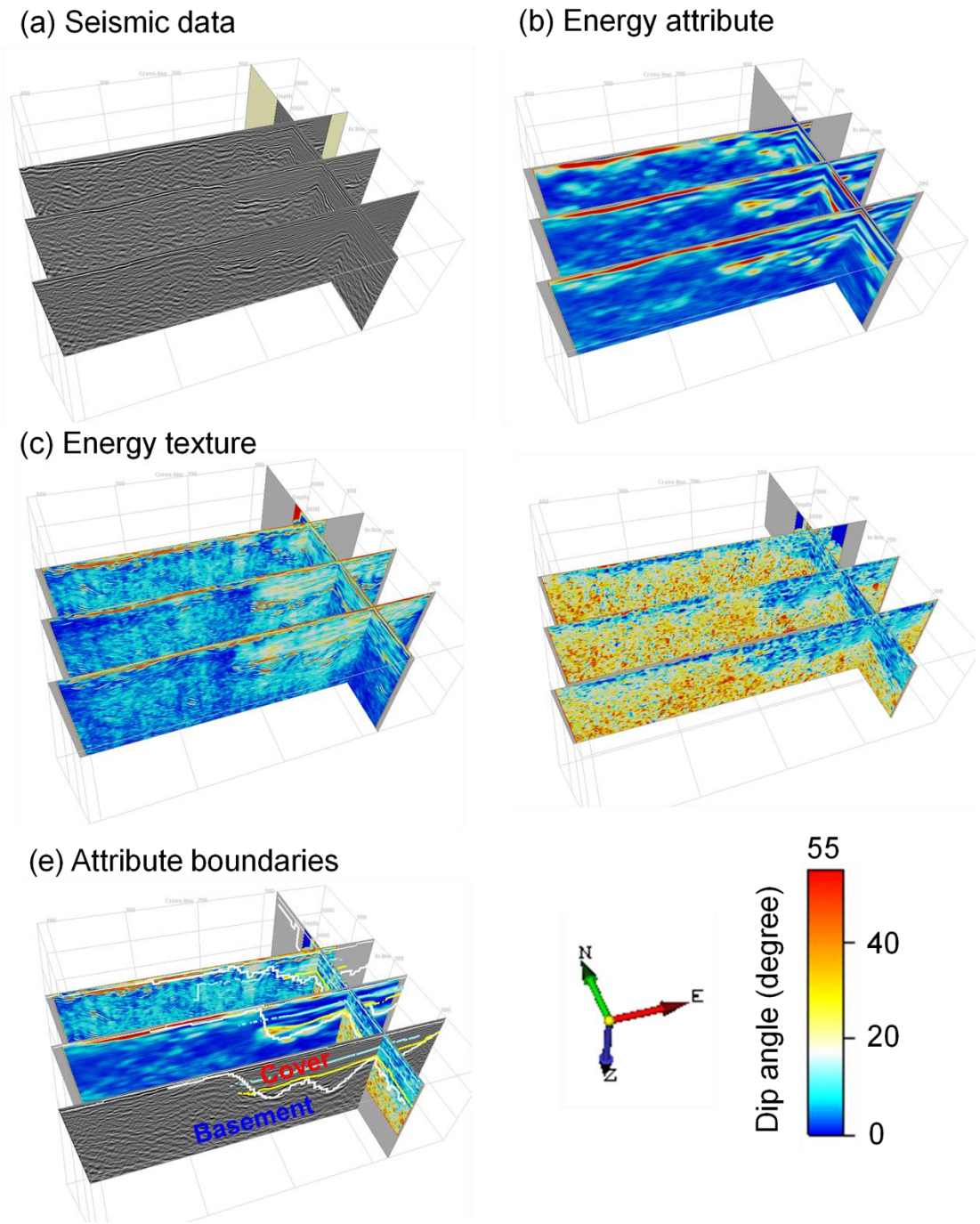

Fig. 2-5: Seismic inline and crossline slices extracted from the 3D seismic volume showing various seismic attributes within the Nevada survey area. These seismic attributes were selected to highlight various structural features. The Figure includes (a) migrated seismic lines,

(b) seismic energy attribute for highlighting strong reflectors, (c) energy texture for defining subvolumes with common seismic texture and (d) dip angle extracted from polar dip for identifying subvolumes based on structure. (e) Identifies major structural features coherent across each of the seismic attributes. The white line demarcates the basement and upper sediments.

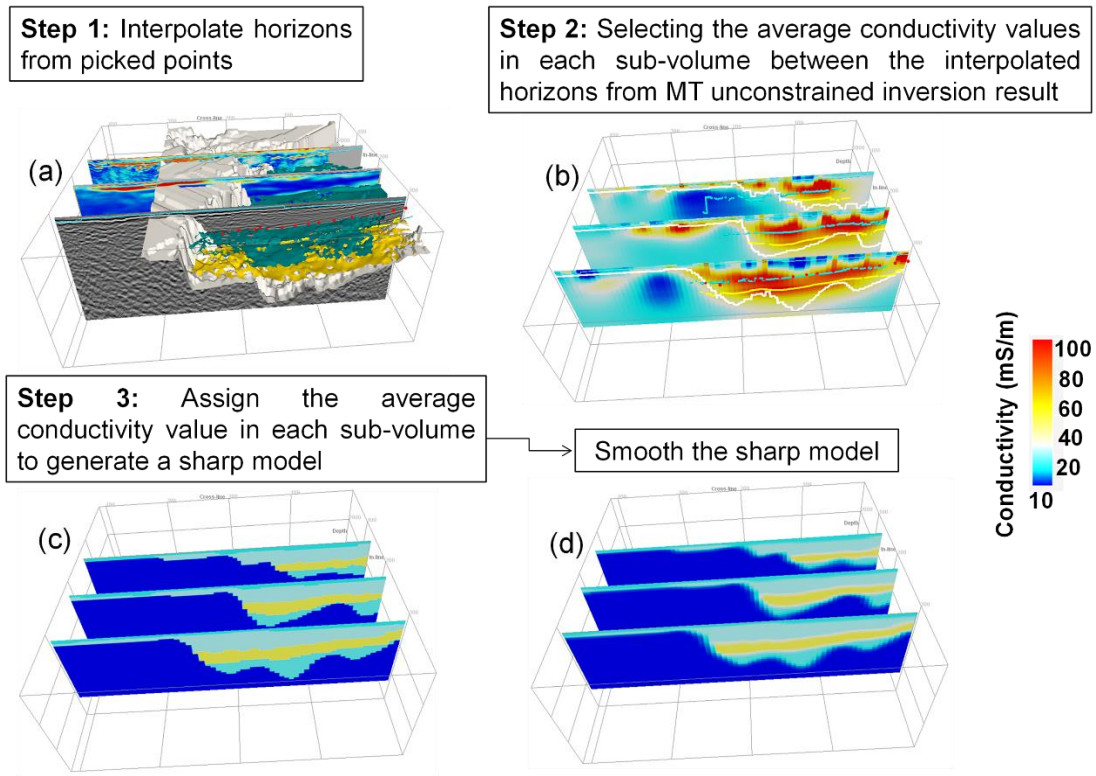

Fig. 2-6: Workflow for the semiautomatic inversion strategy. The workflow consists of three steps: (1) interpolate horizons from initial picked points (see a), (2) select the representative conductivity in the regions defined between the interpolated horizons (see b) and (3) assign this conductivity to each subvolume to generate an sharp prior model (see c). The conductivity model, b, is generated from an unconstrained MT inversion starting from a 40 Ω•m half-space prior model. A smooth boundary prior model (see d) is generated by smoothing the sharp model (c) with an averaging 3D box filter, 3-by-3-by-3 in size.

By explicitly limiting the prior model to five conductivity values we have created a starting model for inversion with sharp well defined transitions between each seismically defined subvolume (Fig. 2-6c). There will always be a degree of uncertainty as to the exact boundary placements. Therefore, a 3D smoothing filter is

applied to “soften” each boundary, generating a second smoothed conductivity prior model (see Fig. 2-6d). The filter is a 3-by-3-by-3 box filter with usage defined by the Matlab (version R2014b) built-in code, smooth3.m.

2.4.1.3 Creation and Update of the prior covariance model

The prior covariance coefficients must be assigned across all cells (see Eq. 2-1). Kiyan, Jones, and Vozar (2014) illustrate inversion with different covariances in synthetic data to evaluate the extent and conductivity of a 2D conductor. They found that the default covariance model with 0.3 gave an acceptable result. Similarly, we find that a covariance coefficient of 0.3 in all directions is generally suitable for unconstrained inversion strategies.

For semiautomatic cooperative inversion, the distribution of the covariance coefficients is uniform (i.e., 0.3) within subvolumes and reduced across subvolume boundaries. The obvious question is what value of covariance coefficient should be set across subvolume boundaries. To answer this question, we complete a small semi-empirical study where we run 3D MT inversion with different covariance coefficients set across the key geo-electrical interfaces. We then assess how representative the resultant conductivity changes across the interface in the vicinity of a deep drill hole. The test is completed with the resistivity prior model shown in Fig. 2-6c which includes clearly defined horizons. MT Inversion is completed with covariance coefficients set across the key boundaries at 0.00, 0.10, 0.20, 0.25, 0.27, and 0.30.

The results of these covariance coefficient tests are captured in Fig. 2-7. A coefficient of value 0.3 at boundaries means that no seismic horizon is recognised in the covariance model (i.e., 0.3 everywhere). Fig. 2-7 includes a seismic reflectivity image showing three key horizons in the cover (i.e., marked in cyan) and the main horizon representing the cover to basement interface. The panel to the right of the seismic image shows the six different inverted conductivity curves and a wireline conductivity log at the position of well 1.

We observe that the inversion results, where covariance coefficients across boundaries are set at 0.2 or less tend to overshoot at the interfaces of the high conductivity layer. Results where values were set at 0.27 and 0.3 could be considered over smoothed as boundaries are expected to be sharp. The curve with a covariance of 0.25 (red) was

selected as providing the optimal smoothness across geo-electrical boundaries. It provided the best match to the picked horizons whilst also maintaining the high conductivity value within most conductive layer. After considerable trial and error, we concluded that covariance coefficients between 0.25 and 0.30 tended to generate stable results. Later we will consider semiautomatic strategies with:

i. Uniform covariance values throughout the full model domain (e.g., a global constant covariance coefficient of 0.3).

ii. A reduced covariance value across all subvolume boundaries (e.g., a global constant covariance coefficient of 0.3 is set everywhere except at subvolume boundaries where a value of 0.25 is used).

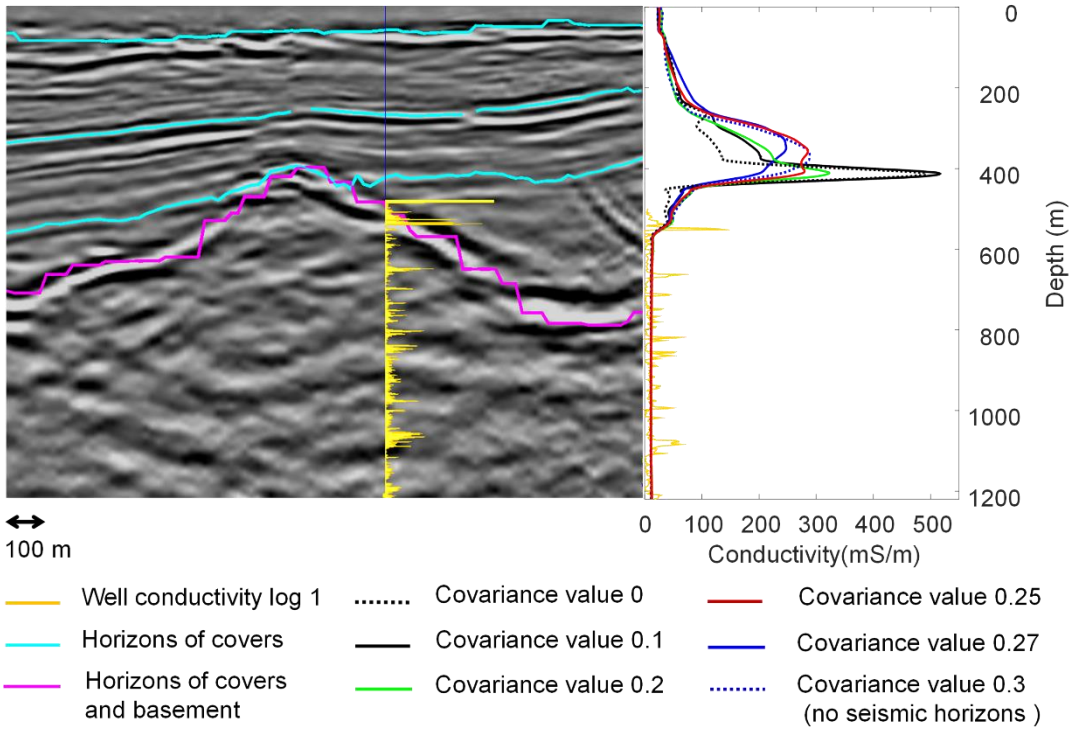

Fig. 2-7: Image illustrating the consequence of using six different covariance coefficient values across four selected seismic horizons within 3D MT inversions of the Nevada MT data. The left panel provides a greyscale seismic reflectivity image (i.e. section view) along with the four picked seismic horizons and the well location. The strong lower horizon marked in magenta is the interface between cover and basement. The right panel provides a comparison of conductivity distribution at the well location after inversions with covariance coefficients set to 0, 0.1, 0.2, 0.25, 0.27, and 0.3. Setting the covariance coefficient to 0 across the boundaries of the high conductivity central layer tends to result in ‘‘overshoot’’. In contrast

we suspect that leaving the covariance at 0.3 everywhere may ‘‘over-smooth’’ what are likely to be sharp high geo-electrical contrast boundaries. After analysis of the results we have taken a value for the covariance coefficient of 0.25 across the key seismic horizons to be a reasonable compromise

2.4.2 Application of automatic cooperative inversion strategies

Given a valid seismic reflectivity volume and co-located MT data after QC, those strategies with potential to be fully automated are classified as “Automatic Cooperative Inversion”. For example, structural or amplitude based attributes may be selected to automatically partition the full model domain into subvolumes. These partitions may then be automatically allocated resistivities according to a predefined set of rules. We will also show that considerable success can be achieved by allocating a limited number of plausible electrical resistivities based on a statistical analysis of first-pass unconstrained MT inversion (another process with potential to be fully automated).

2.4.2.1 Application of the seismic polar dip attribute in cooperative inversion

Geological dip is a fundamental characteristic of any geological setting. Under certain circumstances, the dip of formations, layering, bedding, faults or shears, can be extracted from seismic data via the ‘polar dip’ seismic attribute. If used with care, the polar dip attribute can play a central role in building prior models for cooperative inversion.

Fig. 2-8 provides a schematic representation for true polar dip. Polar dip can be particularly useful in differentiating extensive shallow dipping subvolumes. At the other extreme the polar dip attribute can be either inaccurate or provide little to no value in differentiating volumes of massive crystalline rock and or steep-dipping intrusive bodies.

For our research, we always apply dip steering with the Fast Fourier Transform algorithm available within the OpendTect software for recovery of structural attributes like polar dip. Methods for recovering structural attributes are also described in (Tingdahl 2003, Tingdahl and Groot 2003) and (Chopra and Marfurt 2007).

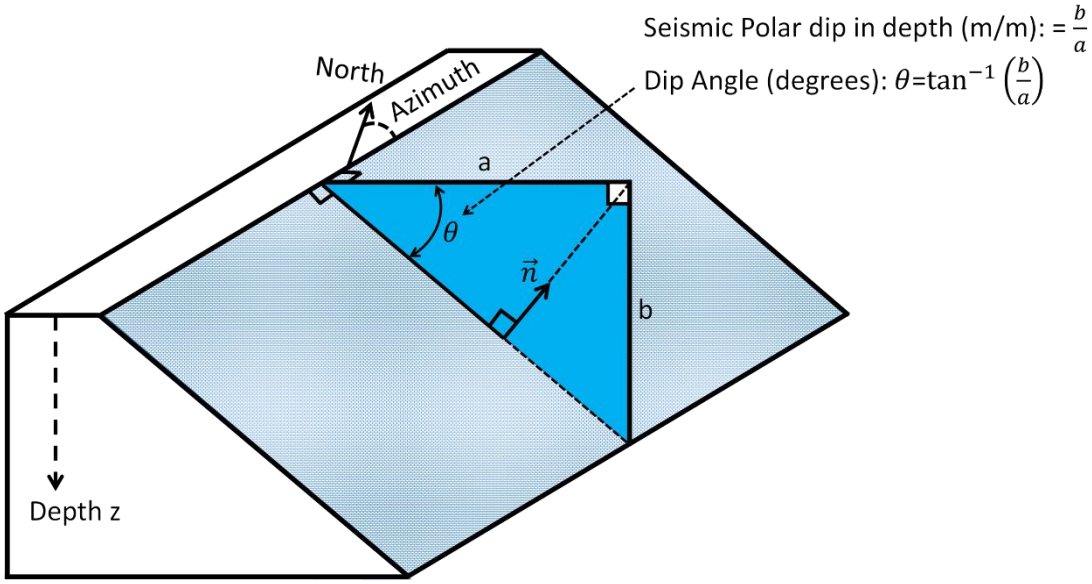

Fig. 2-8: Illustration of the seismic polar dip vector modified from (Nelson 2009). The vector direction of polar dip attribute is the vector $(\overrightarrow{n})$ oriented normal to the seismic structure (i.e., bedding) (Pethick and Harris 2014). The dip angle, Θ, is the inverse tangent function of the polar dip attribute.

Typically, the polar dip attribute is given in units of milliseconds/meters if derived from seismic images in time or metres/meters for depth converted seismic images. Put simply these structural seismic attributes are based on a ratio between a vertical and horizontal distance for sufficiently similar seismic events (dGB Earth Sciences 2015). For our research we converted the seismic polar dip attribute in meter/meter to a dip angle attribute in degrees.

We will provide several examples of automatic cooperative inversion that uses the polar dip seismic attribute to assist populating prior model subvolumes with electrical conductivity. For our Nevada example the dip angle attribute is used to group large volumes within the cover sequences. Here we expect large packages of rock with common depositional and structural history to have common geo-electrical properties.

2.4.2.2 Application of automatic strategies for mapping seismic attributes to conductivity

Processes that can be automated present a possible efficiency dividend. We explore methods for automatic mapping of geo-electrical properties into large subvolumes with common seismic character. We will demonstrate two possible directions for

automatic cooperative inversion. The first method is a direct mapping from a seismic attribute value to a limited number of electrical conductivities. The second method uses statistical analysis of the spatial distribution of both seismic attribute values and electrical conductivity-derived unconstrained MT inversion.

Direct mapping

For our Nevada field example, we use a fast, gross automatic direct mapping of the seismic dip angle attribute to a limited number of electrical conductivities within the cover sequences. The logic followed here is that extensive subvolumes containing common dip angle are likely to have common depositional and structural histories, which is a simple reasonable criterion for large scale geo-electrical grouping within the cover sequences. No attempt is made to extend this direct mapping to the much older basement subvolume (i.e., the lower half-space) where dip angle based on seismic is poorly resolved.

A schematic illustrating direct mapping of dip angle to resistivity is shown in Fig. 2-9 When viewed at a large scale, a relationship between dip angle and electrical resistivity distribution derived from unconstrained inversion in the cover certainly seems to exist (Pethick and Harris 2014). The direct mapping relies on grouping of dip angle into a limited number of clusters then mapping resistivity into these subvolumes based on a simple rule. For example, within cover thick layers with uniform shallow dip tend to be more conductive than areas with higher dip angle.

A strategy that directly maps conductivities based on dip angle is not going to be universally applicable. However, under suitable conditions (e.g., within conductive cover), it can be a component of an effective and fully automatic strategy for setting up a prior conductivity distribution for MT inversion, especially where no other constraints are available. We reiterate that for our Nevada example an objective is to create a set of reasonable prior model conductivity distributions where little or no information other that the seismic and MT are available.

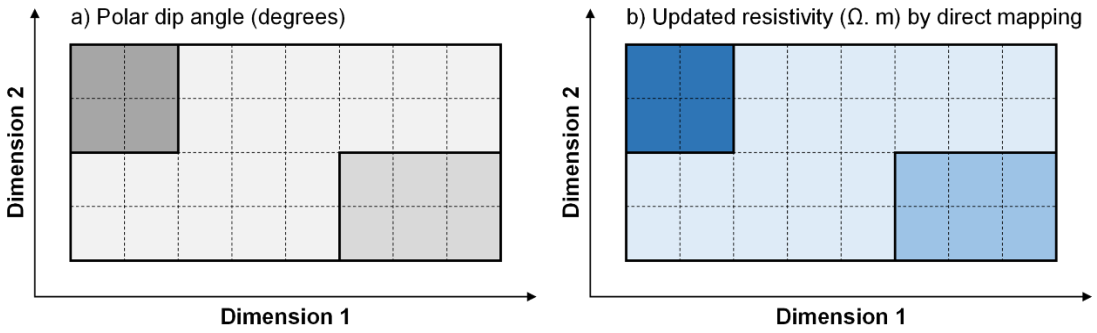

Fig. 2-9: Schematic illustrating model generation during automatic cooperative inversion. This is based on directly mapping conductivities into a geometric framework as defined by common seismic attribute analysis. For the Nevada example, the dip angle attribute was chosen. This process relies on a broad link between the seismic attribute and the large scale geo-electric structure of the earth

While we observe these large scale relationships between areas of common dip angle in cover and electrical conductivity for the Nevada example, such relationships are by no means universal and should be assessed on a case by case basis. One clear advantage of this method is its simplicity. Once the broad geo-electrical structure is set it is the inversion (run on a supercomputer) that will hopefully arrange conductivities in detail via minimisation of misfit between field data and model data (see equation 1, section 2.1). Posterior analysis of inversion statistics and more directly conductivity distribution should be compared for the full set unconstrained and cooperative inversion strategies completed.

Statistical mapping based seismic attribute subvolumes and unconstrained MT inversion conductivity distribution

For the second and perhaps more universal automatic cooperative inversion technique we use k-means clustering of the average dip angle seismic attribute to form a small number of subvolumes based on dip angle "groups". These large subvolumes form an initial "empty" framework.

Each subvolume needs to be filled with a sensible discrete electrical conductivity. The discrete conductivity can be extracted via analysis of the conductivity distribution recovered from unconstrained MT inversion. The intended outcome is a prior

conductivity model that has both seismic and MT characteristics. This prior model is then passed to a new round of MT inversion, which we run on a Cray Cascade system at the Pawsey Supercomputing system in Perth Western Australia (Pethick and Harris 2016).

We have produced a schematic as Fig. 2-10 to explain our how conductivity from unconstrained inversion can be mapped into seismic attribute subvolumes. The methods indicated in Fig. 2-10 can be compared with that for direct mapping in Fig. 2-9.

Below we will systematically work through the main steps as illustrated in the schematic in Fig. 2-10 as applied to the Nevada field example.

Step 1 - Establish a subvolume framework based on analysis of the seismic dip angle attributes (see Fig. 2-10a):

Firstly, the seismic dip angle attribute is computed. Its three-dimensional distribution is then statistically simplified into a finite number of spatial groupings. Here the number of dip angle groups is decided by analysing a histogram of dip angles extracted from the seismic attribute volume. The histogram for the Nevada seismic volume is provided as Fig. 2-11a. Spatial sampling within the seismic volume is orders of magnitude greater than that required for the MT finite element mesh, so resampling onto nodes of the MT conductivity model finite difference mesh is required, as shown in Fig. 2-11b. For the Nevada dataset, four distinct average dip angle groups can be recovered from the observed dip angle histogram resampled into the MT model domain. These include the dip angle in the ranges: (i) 0^o to 12^o, (ii) from 12^o to 25^o, (iii) from 25^o to 40^o, and (iv) from 40^o to 80^o. A k-means clustering algorithm (i.e., MATLAB built-in code, kmeans.m) is then applied to categorise all observations of dip angle into the five predetermined clusters in which each observation belongs to the cluster with the nearest mean. This nearest mean represents the characteristic value of the cluster or group. The five average values within each group were found to be 10, 20, 27, 58 as shown in Fig. 2-11c, and value representing maximum dip angles is located at 83^o. These group means correspond to the index numbers 1, 2, 3, 4, and 5. In summary, this first step takes a complex

distribution of seismic dip angle attribute values and simplifies this into five classes, each with its index number. Note that for this strategy it is possible to have many separated 3D zones having the same index category.

Step 2: Compute the electrical conductivity distribution (see Fig. 2-10c)

The second step is to compute unconstrained MT inversions to establish a first-pass background electrical conductivity distribution. This first-pass conductivity distribution is necessary to assist in the mapping of discrete conductivity values into the subvolumes recovered from seismic information. It may be necessary to commence unconstrained inversion with several different half-space resistivities.

Step 3: The last step is to assign conductivity distributions into closed subvolumes defined by analysis of seismic attribute distributions (see Fig. 2-10c).

In this step each subvolume, with characteristic dip angle attributes, is allocated with a value of conductivity. The method we use is to average all values of electrical conductivity resulting from unconstrained inversion in each subvolume. This average value in each subvolume becomes the single conductivity for that subvolume within the prior model. Finally, a smoothing convolution filter (i.e., a box filter) is applied to the resulting 3D conductivity distribution. This approach accommodates subvolume boundary locations that may be approximate. It is the position of each mean dip angle subvolume that helps to form the model skeleton in which one average conductivity value represents one 3D separate closed zone. Histograms of conductivity distribution are shown in Fig. 2-12 for unconstrained inversion (Fig. 2-12a), sharp automatic (Fig. 2-12b), and smooth automatic (Fig. 2-12c)

For the Nevada field example, the prior conductivity distribution is shown in Fig. 2-13 and the steps taken to build the prior conductivity distribution for this second automatic cooperative inversion option are summarised. It should be noted that the resulting prior conductivity models (i.e., see Fig. 2-13e) after grouping shares the similar structure seen in the dip angle attribute volume (i.e., see Fig. 2-13c).

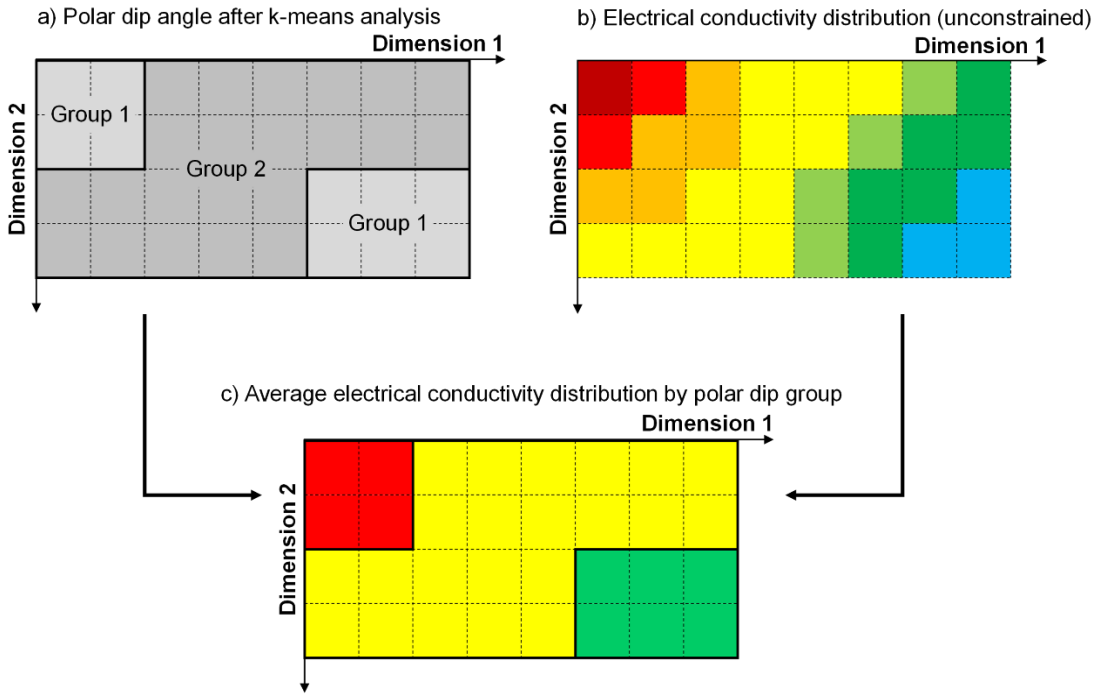

Fig. 2-10: Schematic illustrating automatic cooperative inversion based on mapping conductivity from unconstrained inversion into geometric framework defined by statistical analysis of the distribution of seismic attributes or multi-attributes. In short the prior model framework is derived from seismic information and the discrete conductivity value for each subvolume through unconstrained inversion. In principle, any attribute or combinations of attributes, can be used. However, for the Nevada example the subvolumes framework is recovered from statistical analysis of the distribution of the seismic dip attribute in the cover. From the schematic it is clear that a group with a common seismic characteristic (i.e., group 1) can be populated with completely different electrical conductivities. This is a highly significant difference with the automatic cooperative inversion based on a direct mapping illustrated in Fig. 2-9. We should reiterate that only large subvolumes are used to create the prior conductivity model after which full 3D MT inversion is applied to recover detailed conductivity distribution and associated fitting error statistics for comparison with other strategies

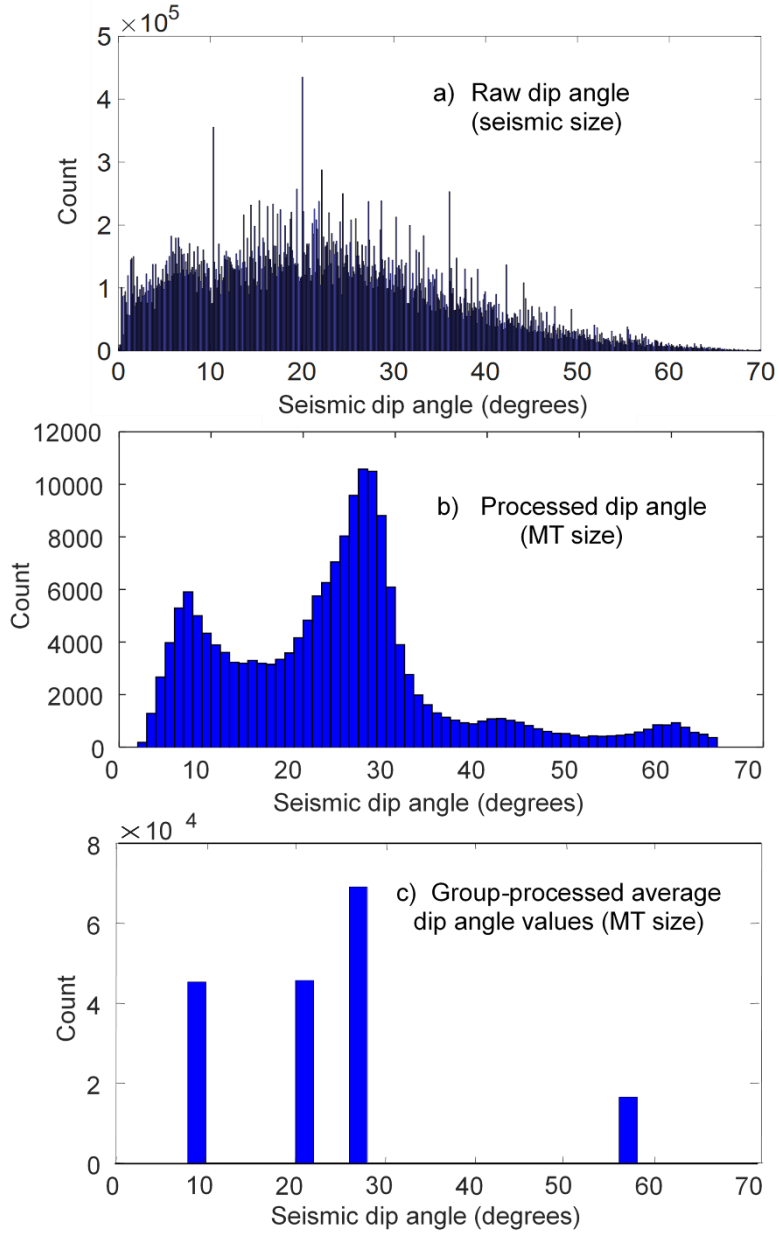

Fig. 2-11: Histograms of the seismic dip angle (a) at the seismic scale and (b) in MT model domain and (c) dip angle derived from k-means grouping. (a) Histogram expressing distribution of the seismic dip angle attribute from the full seismic volume (total number of samples in the seismic volume = 4.5343E+09). It should be noted that the histogram is computed at a finer resolution to that of the MT. (b) The histogram after processing the seismic dip angle volume at MT model resolution. This is performed by averaging the values in each MT subvolume (total number of cells = 173,387). The depth size of each 3D subvolume increases according to depth. This explains why the shape of MT-sized distribution of dip angle are grossly similar with the seismic-sized distribution of dip angle. (c) The resulting histogram after applying a k-means clustering method. Five groups are generated after it is applied to the dip angles seen in b. The seismic area is smaller in extents than the MT volume and must be padded by any specific number (i.e., the maximum dip angle value). In this case,

the four groups with blue bars extracted from seismic dip angle information (b) and one red-bar group is set by the manually padded group (total number of cells = 223,776).

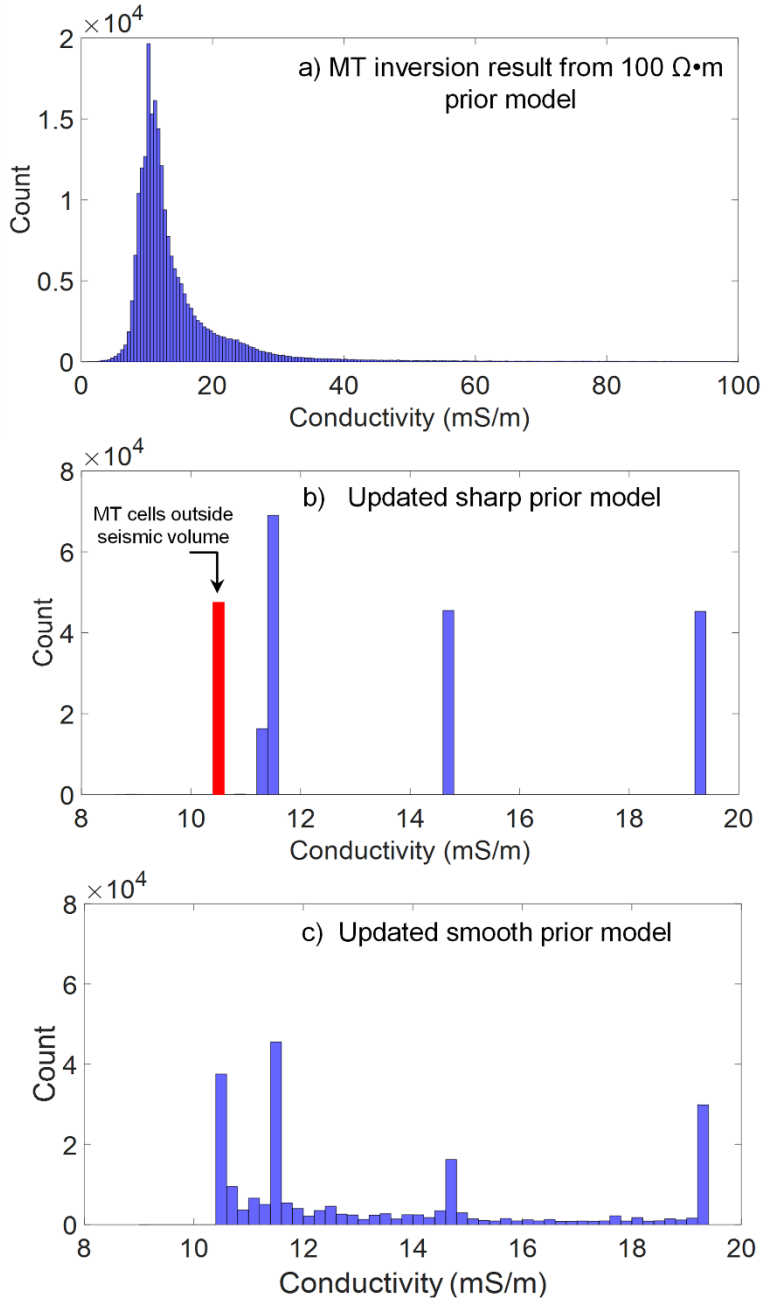

Fig. 2-12: Histograms of conductivity derived from unconstrained inversion and seismic dip angle information (a) The histogram showing the distribution of conductivities computed by an MT unconstrained inversion from 100 Ω•m homogenous half-space prior model (total number of cells = 223776). (b) The updated sharp prior conductivity model histogram after grouping the conductivities by those established through the k-means clustering of dip angle seen in Fig 11c (total number of cells = 223776). The blue bars show conductivity extracted from seismic dip angle and unconstrained inversion conductivity. Again, the red bar shows conductivity locating outside seismic area in which dip angle could not be computed. (c) The

updated smooth prior model histogram of conductivity (total number of cells = 223776). It is created by smoothing the sharp conductivity model (e) with an averaging 3D box filter, 3-by-3-by-3 in size

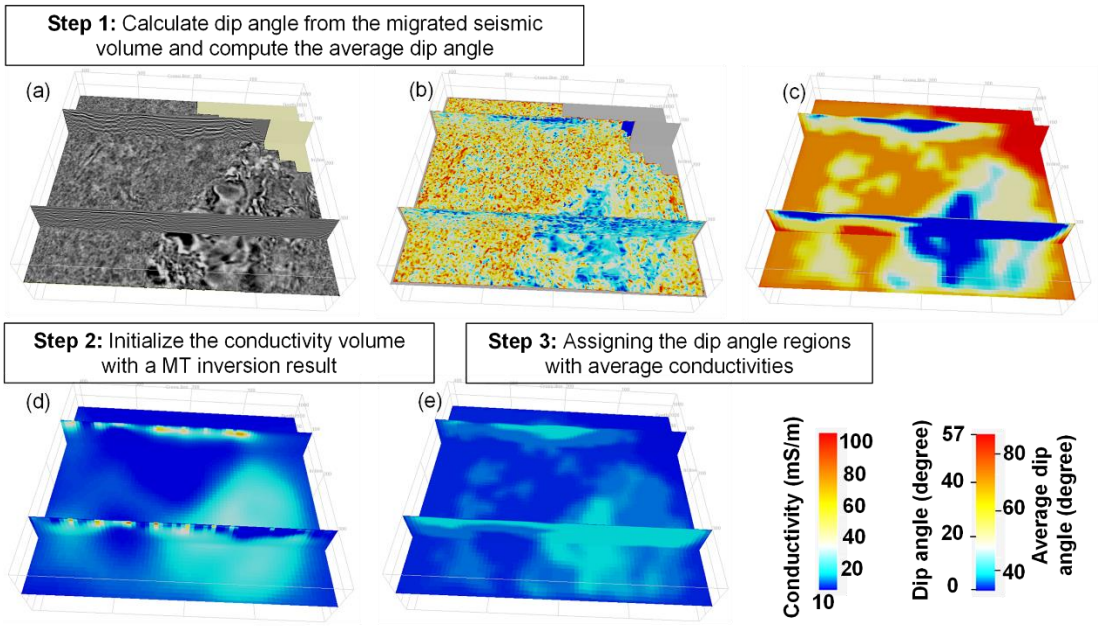

Fig. 2-13: Images representing the steps taken to create the conductivity prior model for an automatic cooperative inversion strategy. The Figure shows (a) a migrated seismic image, (b) a raw dip angle seismic attribute image, (c) the dip angle volume after rescaling to MT resolution and application of k-means clustering, (d) the conductivity distribution resulting from unconstrained MT inversion based on a 100 Ohm.m halfspace and (e) the resulting prior model conductivity distribution ready final MT inversion. The resulting conductivity volume should reflect the structures found in the seismic whilst maintaining a reasonable conductivity distribution. Our geometric mapping method has one significant advantage. That is, subvolumes with similar seismic character can be used to automatically allocate separate individual regions of conductivity in the prior model as would occur if the same formation was physically separated (e.g., by faulting) or had regions of different solute concentrations

2.4.3 Preparation and analysis of Nevada drill-hole logs and geochemical data

Drill-hole data are precious. It presents one fundamental method for assessing the outcome of inversion. Comparison of inversion outcomes along drill-holes can be based on geological logging, wireline logs and or geochemical analysis. For the two reference drill holes located at the Nevada site we have used geostatistical methods to

divide the rock into classes based on a suite of geochemistry elements. For the geochemical data PCA and k-means clustering techniques have been used to reduce the data dimension to highlight a limited number of geo-chemically similar rock types (Alférez et al. 2015, Roden, Smith, and Sacrey 2015, Nanni et al. 2008, Grunsky and Smee 2003, Jolliffe 2002). The purpose of the analysis was to check the consistency of geochemical groupings with seismic boundaries, prior model conductivity distributions and the final conductivity distribution from semiautomatic and automatic cooperative inversion strategies.

First we removed high noise data (e.g., elemental concentration that are negligible) and then used simple range scaling from 0 to 1, as suggested by Samarasinghe (2006). We then applied principal component analysis based on 15 elements to extract nine components after which the k-means algorithm was applied to group these new components.

Note that we broadly follow the methodologies expressed in (Roden, Smith, and Sacrey 2015), with the main difference being that Roden, Smith, and Sacrey (2015) used self-organising maps (SOM) for clustering, while we use the k-means method (Nanni et al. 2008, Alférez et al. 2015). The end result of the analysis of bore hole geochemical analysis is a limited number of geochemical classes.

In the "Results" section below we will compare lithology, well-log data and geochemical clusters to seismic boundaries, and conductivity distribution obtained from cooperative inversion strategies at the two reference drill-hole locations.

2.5 Results

In Sect. 2, automatic and semiautomatic cooperative inversion strategies were described. This was followed by description of the application of semiautomatic / automatic cooperative inversion with the aid of a field example from Nevada USA. In the results section we will describe, analyse and compare the outcomes from application of nine MT inversion strategies.

Note that multiple strategies were run simultaneously on the Magnus Super computer located at the Pawsey Supercomputing Centre in Perth; Western Australia. Run times for each strategy were of the order 24 hours on the Cray Cascade system. Pethick and Harris (2016), provide a detailed account of applied parallel computing for EM

methods. They include analysis of speed up and wall time for standard Intel processors versus the optimised Cray Cascade system that was also used for the current research.

There are limitless combinations of seismic attributes and MT inversion methods that could be attempted. We elected to systematically work through nine strategies we label S1 to S9. These strategies were selected to facilitate comparison of misfit and final inverted conductivity distribution for: conventional unconstrained inversion (S1-S2), automatic cooperative inversion (S4-S6) and semiautomatic cooperative inversion (S3, S7-S9).

The "base case" unconstrained inversions are named S1 and S2. The seven cooperative inversion strategies, S3 to S9, use seismic information to aid development of the prior model conductivity distribution, ($\boldsymbol{m_0}$) and/or covariance matrix values, ($\boldsymbol{C_m}$) needed for input to subsequent rounds of 3D MT inversion (see equation 1). We have organised the main points that differentiate these nine inversion strategies into summary Table 1 and provide more complete descriptions below.

2.5.1 Unconstrained inversion (S1-S2):

For the first two strategies, S1 and S2, the half-space prior model resistivity is set to 100 Ω•m and 40 Ω•m, respectively (see Table 2-1). The value 100 Ω•m (S1) is selected to be consistent with the average wireline log resistivity measurements immediately below cover (i.e., in basement). The value 40 Ω•m (S2) is selected to be consistent with the gross resistivity of the younger cover rocks above basement. Strategies S1 and S2 use a uniform covariance coefficient of 0.3.

2.5.2 Semi-Automatic inversion (S3):

Strategy S3 is identical to the unconstrained inversion strategy S2, except that for strategy S3 the covariance coefficient is reduced from 0.3 to 0.25 for cells that cross key high-impedance contrast interfaces picked from the seismic volume. An example of a high acoustic impedance interface is the boundary between cover and basement.

2.5.3 Automatic cooperative inversion (S4-S6):

Automatic cooperative inversion strategies can, in principle, be automated. For the Nevada field example, the structural seismic attribute, dip angle, is used to create the geometric framework (see subsection 3.2). However, the ideas presented can certainly be adapted to take advantage of other seismic attributes or combinations of attributes.

Strategy S4 uses “direct mapping” of the seismic dip angle attribute to electrical conductivity distribution for the prior model (see schematic in Fig. 2-9). Direct mapping is in essence a mapping of some characteristic extracted from the seismic data to an electrical conductivity. This mapping is usually based either on a presumed or empirically determined petrophysical relationship possibly established by crossplot of velocity and conductivity from wireline logs.

Given enough wells and good quality wireline log data a neural network approach could, in principle, be adopted to build nomogram connecting parameters derived from seismic and electromagnetic data (Bauer, Muñoz, and Moeck 2012). However, as with the Nevada example, there is rarely sufficient log data to build the relationships.

Strategies S5 and S6 use the distribution of dip angle to divide the complete seismic volume into smaller subvolumes with a common seismic character. Each subvolume is subsequently assigned an electrical resistivity based on analysis of the distribution of conductivity derived from unconstrained inversions S1 and S2 respectively (seeFig. 2-14). We call this type of mapping from unconstrained inversion into a framework defined by seismic information “geometric mapping”.

For the Nevada example, five classes of subvolumes are created based on k-means cluster analysis of the distribution of the dip angle seismic attribute (See Fig. 2-11c). A resistivity value is then assigned to each subvolume by statistical analysis of the conductivity distribution derived from unconstrained inversion using half-space models of 100 Ω•m (S1) and 40 Ω•m (S2). In this way the seismic information provides a geo-electrical framework and the unconstrained inversion is used to generate a discrete conductivity that is assigned to each subvolume. It should be remembered that the prior model needs only to have a simple relatively gross and broadly correct 3D conductivity distribution for the subsequent rounds of inversion to yield a vastly improved final outcome.

2.5.4 Semiautomatic inversion (S7 to S9):

Cooperative inversion strategies S7 to S9 are designated semiautomatic because the key seismic boundaries that form the geo-electrical framework were picked by a partly manual and subjective process. For these strategies seismic attributes like amplitude, energy and energy texture were highly useful in identifying key horizons. After identifying key horizons, an auto-picking algorithm (Huck 2012) was used to recover

them through the seismic volume. The auto picking tended to be successful for recovery of the main high acoustic impedance contrast horizons. The result is that the seismic volume was readily partitioned into large subvolumes that ultimately formed a prior geo-electrical model framework for S7, S8 and S9.

Table 2-1 contains three broad classes of inversion. These are unconstrained inversion (S1 to S2), automatic cooperative inversion (S4 to S6) and semiautomatic cooperative (S3, S7 to S9)

Inversion strategy	**Prior model conductivity distribution (see Fig. 2-14)**	**Covariance coefficient (i.e., sharpness)**	
		Coefficient within subvolumes	*Coefficient at boundaries*
S1 Unconstrained Inversion	100 Ω•m Half-space	0.3	N/A
S2 Unconstrained Inversion	40 Ω•m Half-space	0.3	N/A
S3 Semiautomatic Cooperative inversion Boundary coefficient (0.25)	40 Ω•m Half-space	0.3	0.25
S4 Automatic Cooperative Inversion by Direct Mapping	• The geometric framework is based on the dip angle seismic attribute. Assignment of conductivity is based on "direct mapping" • Smooth model	0.3	N/A
S5 Automatic cooperative inversion Geometric mapping - S1	• The geometric framework is based on distribution of the dip angle seismic attribute. • Conductivity is mapped in the framework with the aid of conductivity distribution from strategy S1 (unconstrained inversion) • Smooth model	0.3	N/A
S6 Automatic cooperative inversion Geometric mapping – S2	• The geometric framework is based on distribution of the dip angle seismic attribute. • Conductivity is mapped in the framework with the aid of conductivity distribution from strategy S2 (unconstrained inversion) • Smooth model	0.3	N/A
S7 Semiautomatic Cooperative inversion Geometric Mapping Smooth	• The geometric framework is based on seismic horizons selected with the aid of seismic attributes. • Conductivity is mapped into the framework with the aid of results from unconstrained inversion strategy S2. • Smooth model	0.3	N/A
S8 Semiautomatic Cooperative inversion Geometric Mapping Sharp	• The geometric framework is based on seismic horizons selected with the aid of seismic attributes. • Conductivity is mapped into the framework with the aid of results from unconstrained inversion strategy S2. • Sharp model	0.3	N/A
S9 Semiautomatic Cooperative inversion Geometric mapping Sharp Boundary Coefficient (0.25)	• The geometric framework is based on seismic horizons selected with the aid of seismic attributes. • Conductivity is mapped into the framework with the aid of results from unconstrained inversion strategy S2. • Sharp model	0.3	0.25

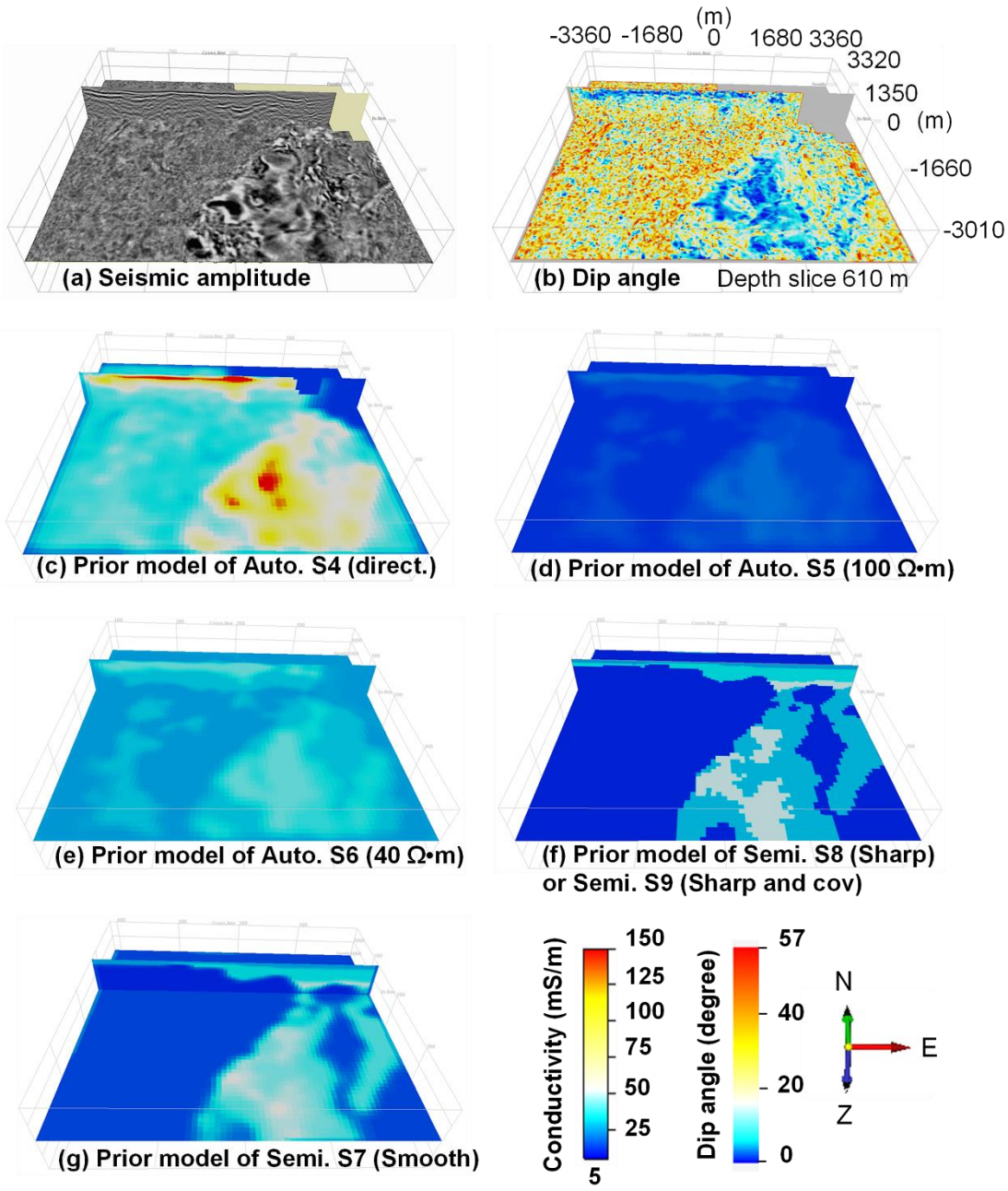

Fig. 2-14: Image representations of the prior model conductivity distributions for cooperative inversions applied for the Nevada field example. Each image includes an elevation slice at 610 m below average ground level for the study area. These prior model conductivity distributions are created according to the methods outline in Table 2-1; where inversion strategies S1 to S9 are outlined. Fig. 2-14a and Fig. 2-14b are included as reference images of seismic amplitude the polar dip attribute respectively. Fig 14c shows prior conductivity model for strategy S4 (i.e., direct mapping), Fig. 2-14d, and Fig. 2-14e show prior conductivity distributions for automatic cooperative inversion strategies S5 and S6 respectively (i.e., geometric mapping). Fig. 2-14g and Fig. 2-14f show prior model conductivity distribution for semiautomatic cooperative inversion strategies S7 and S8 respectively. The prior models for strategies S8 and S9 are identical; however, for strategy S9 the covariance coefficients are reduced for cells that

cross geo-electrical boundaries. The key point from Fig. 2-14 is that there are many valid pathways for creating the prior model conductivity and covariance coefficient distribution. While all models do have a common gross distribution, details clearly vary from model to model. Fig. 2-15 shows how these differences impact on the final conductivity distribution for each cooperative inversion strategy

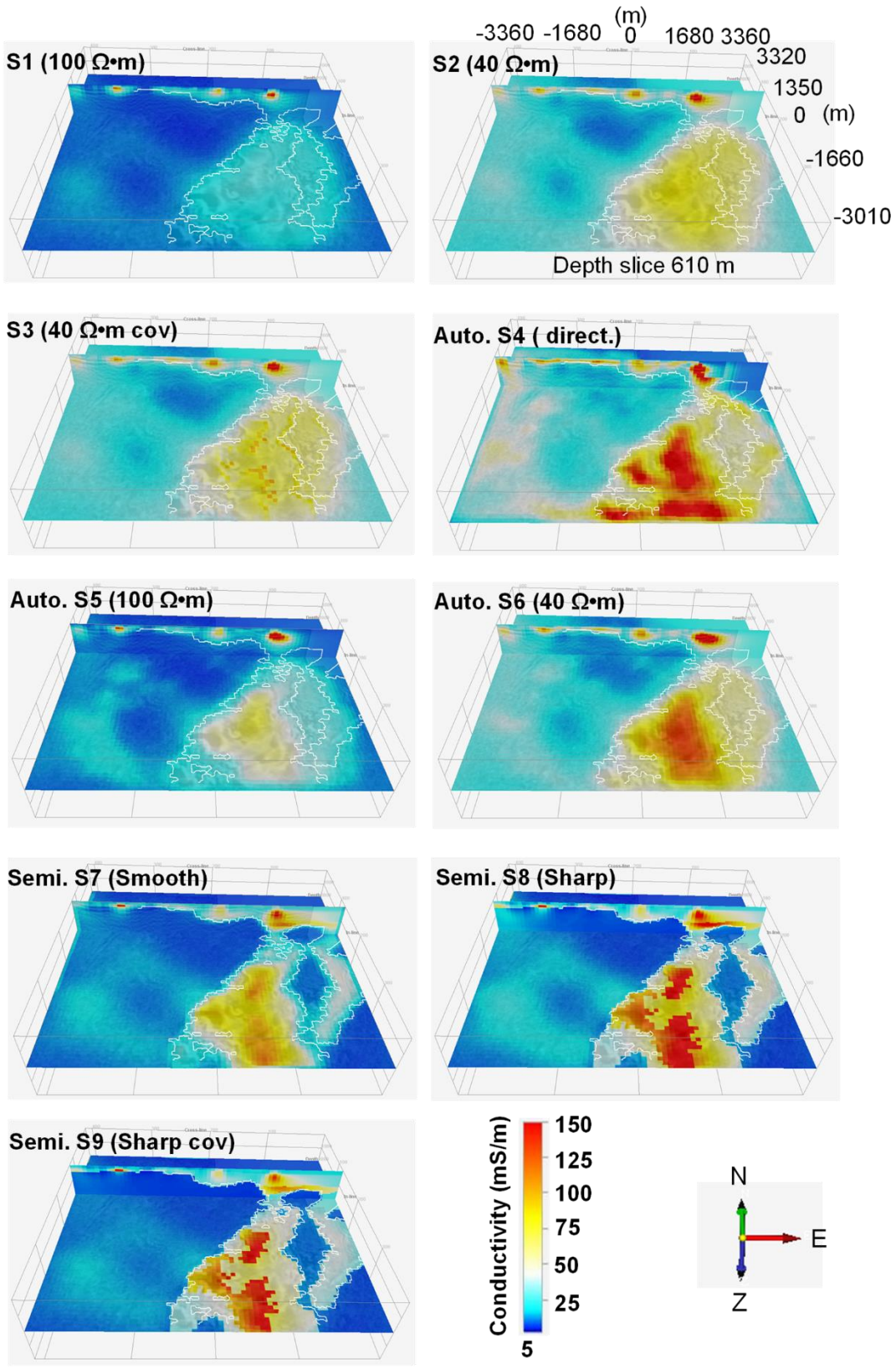

Fig. 2-15: Image representations of the final 3D electrical conductivity distributions after application of MT inversion strategies S1 - S9 (See Table 2-1). Each image shows an elevation slice at 610 m below average ground level for the study area. The white lines represent the key

boundary between basement and covers rocks. Note that inversion strategies S1 - S3 all fail to recover a higher resistivity basement ridge protruding into cover on the right of these images. This ridge is clearly mapped within the seismic reflectivity volume. This ridge is clearly resolved in strategies S7 - S9. While strategies S7 - S9 have exceptional resolution in cover, strategy S4 appears to resolve linear features in basement on the left hand side of the images. Our example is intended to highlight the possibly uncomfortable reality that no single strategy will adequately recover conductivity distribution across a large volume containing diverse geo-electrical settings

The prior model framework for semiautomatic cooperative inversion strategies S7, S8 and S9 included just four interpreted horizons (see Fig. 2-6a and Fig. 2-6b) and five large subvolumes. The largest subvolume was the lower basement half space. A resistivity was assigned to each of the other subvolumes by "geometric mapping" (see Fig. 2-9) based on statistical analysis of resistivity distribution derived from unconstrained inversion using a 40 Ω•m half-space model (see strategy S2). The four subvolume resistivity values assigned to the cover rocks were 40 Ω•m, 30 Ω•m, 20 Ω•m, and 35 Ω•m. A resistivity of 100 Ω•m was mapped into the full basement subvolume because it is broadly consistent with outcome from unconstrained inversion (S1) and wireline log resistivity (see section 3.1.2) immediately below cover.

Fig. 2-14 provides an image representation of the original seismic reflectivity, the dip angle seismic attribute distribution and prior models conductivity distributions for cooperative inversion strategies S4 to S9. The nine strategies are included to compare advantages and disadvantages of inversion strategies.

We immediately see that automatic cooperative inversion strategies S4 to S6 permit prior model conductivity detail within basement that is not permitted for semiautomatic strategies S7 to S9. For strategies S4 to S6, the geo-electrical framework comes directly from the volumetric distribution of a seismic attribute whereas for S7 to S9 the framework is based explicitly on selected seismic horizons. One approach is likely to provide accurate 3D geo-electrical boundaries while the other provides an objective, mapping conductivities onto subvolumes with common seismic character.

2.5.5 The final conductivity distribution for Inversion strategies S1 to S9

Next we provide final conductivity distributions for inversion strategies S1 to S9 and analyse these outcomes with respect to fitting errors, the original seismic reflectivity and drill-hole data. A representation of final conductivity distributions from inversion strategies S1 to S9 are provided in Fig. 2-15. All nine final inverted conductivity models broadly represent the geometry of the more conductive cover. However, as anticipated there are considerable differences in the distribution of conductivity in cover and below cover between the nine different strategies.

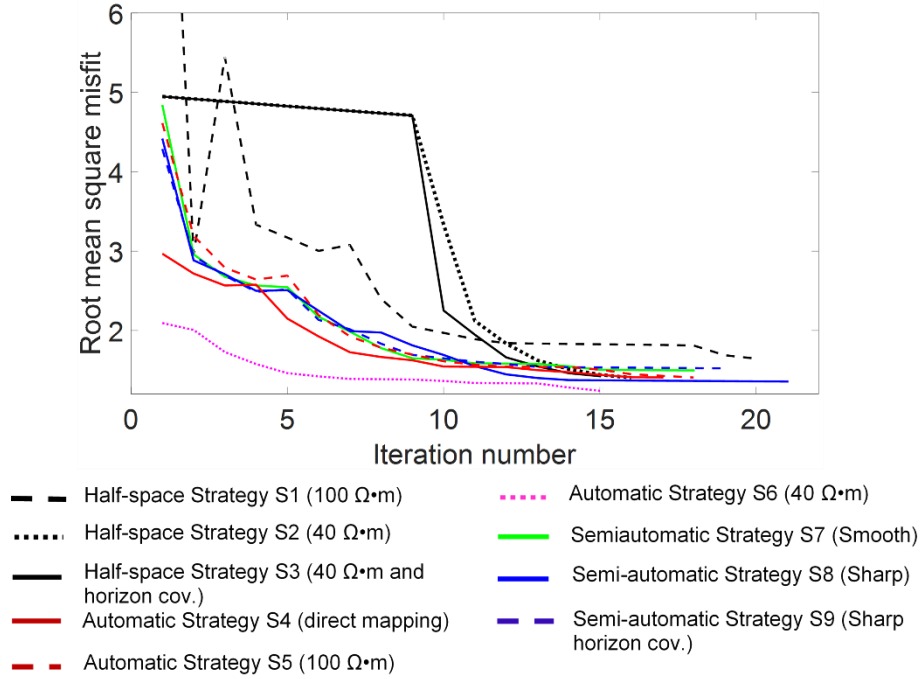

Fig. 2-16: The total root mean square misfit error at each inversion iteration step for each of the nine inversion strategies (S1 to S9). The fastest rate of convergence and lowest global RMS misfit is achieved with automatic inversion strategy S6. However, all RMS misfits are between 1.65 and 1.33, which is exceedingly low. A closer investigation of misfit is required

We will return to the analysis and comparison of these conductivity distributions after considering model convergence and data misfit for the nine inversion strategies.

2.5.6 Assessing Inversion strategies S1 to S9: convergence and misfit

For each 3D MT inversion strategy, a suitable error floor needs to be specified. The error floors for off-diagonal elements (Zxy and Zyx) are set to 5% of the root mean square (RMS) absolute of their complex multiplication. Diagonal elements (Zxx and

Zyy) share the same error floor with the off-diagonal elements because both are small and tend to be noisy. The error floor of tipper values is set to 0.02.

Table 2-2: Number of iteration and global RMS misfit of the nine inversion strategies. Misfit is similar for all inversion strategies. Global RMS misfit is not a suitable measure of fit and more detailed analysis is always required

Inversion strategy	Number of iteration (Fig. 2-16)	Global RMS misfit (Fig. 2-16)
S1	20	1.65
S2	16	1.41
S3	15	1.42
S4	17	1.41
S5	18	1.41
S6	15	1.33
S7	18	1.50
S8	21	1.35
S9	19	1.52

Assessing the fit between field and synthetic data is not straight forward. The rate of convergence for inversion strategies S1 to S9 is shown in Fig. 2-16 and details are included in Table 2-2. At a basic level we could consider rate of convergence and global RMS error as indicators of the relative success for each inversion. However, this would be misleading and further analysis is required.

The global RMS error (Table 2-2) alone is a blunt instrument for analysing fit, which can be assessed for each sounding. Fig. 2-17 shows a complete representation of field data and final inversion outcomes from all strategies for tensor MT station 320. The location of station 320 is provided in Fig. 2-2. The inversion strategies S1, S2 and S3 using halfspace prior models generally do not achieve the rate of change observed in the field MT apparent resistivity curves. This is likely because unconstrained inversion strategies S1 and S2 do not contain the information necessary to accommodate high geo-electrical contrasts in their prior models. These high geo-electrical contrast interfaces are accurately located in the seismic volume and this information is transferred to the MT inversion by different methods in strategies S4 - S9.

A different way to assess the nine inversion strategies is to compare apparent resistivity and tipper values of the real field and synthetic data at each period for all MT stations that were included in inversion strategies S1 to S9. In Fig. 2-18 we show a map of apparent resistivity and tipper at period of 0.092367 s for the nine inversion strategies. Fig. 2-18 shows that the model apparent effective resistivity for all strategies is similar to the field values. However, Vozoff tipper directions at the measurement area edge tend to diverge from the tipper derived from the field data.

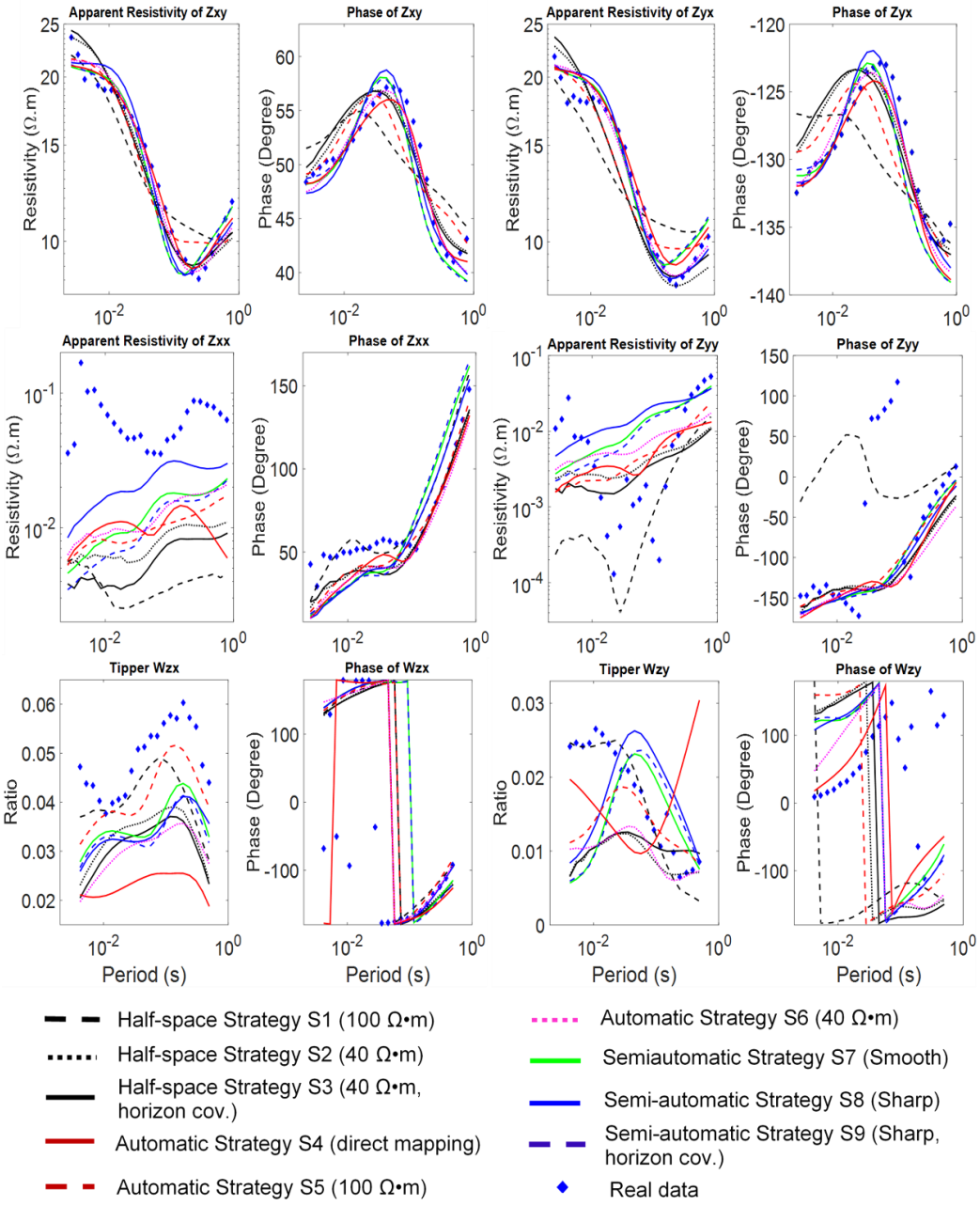

Fig. 2-17: Comparison of field MT data and final computed model MT data resulting from nine inversion strategies for MT station 320 (see Fig. 2-2). The apparent resistivity and phase for Zxy and Zyx fit exceedingly well to the MT data generated at the end of most inversion

strategies (see fit for strategy S9). As expected the signal to noise levels in the Zxx and Zyy component data are exceedingly low and as such a close fit is not anticipated (i.e., some elements of the data are not reliable)

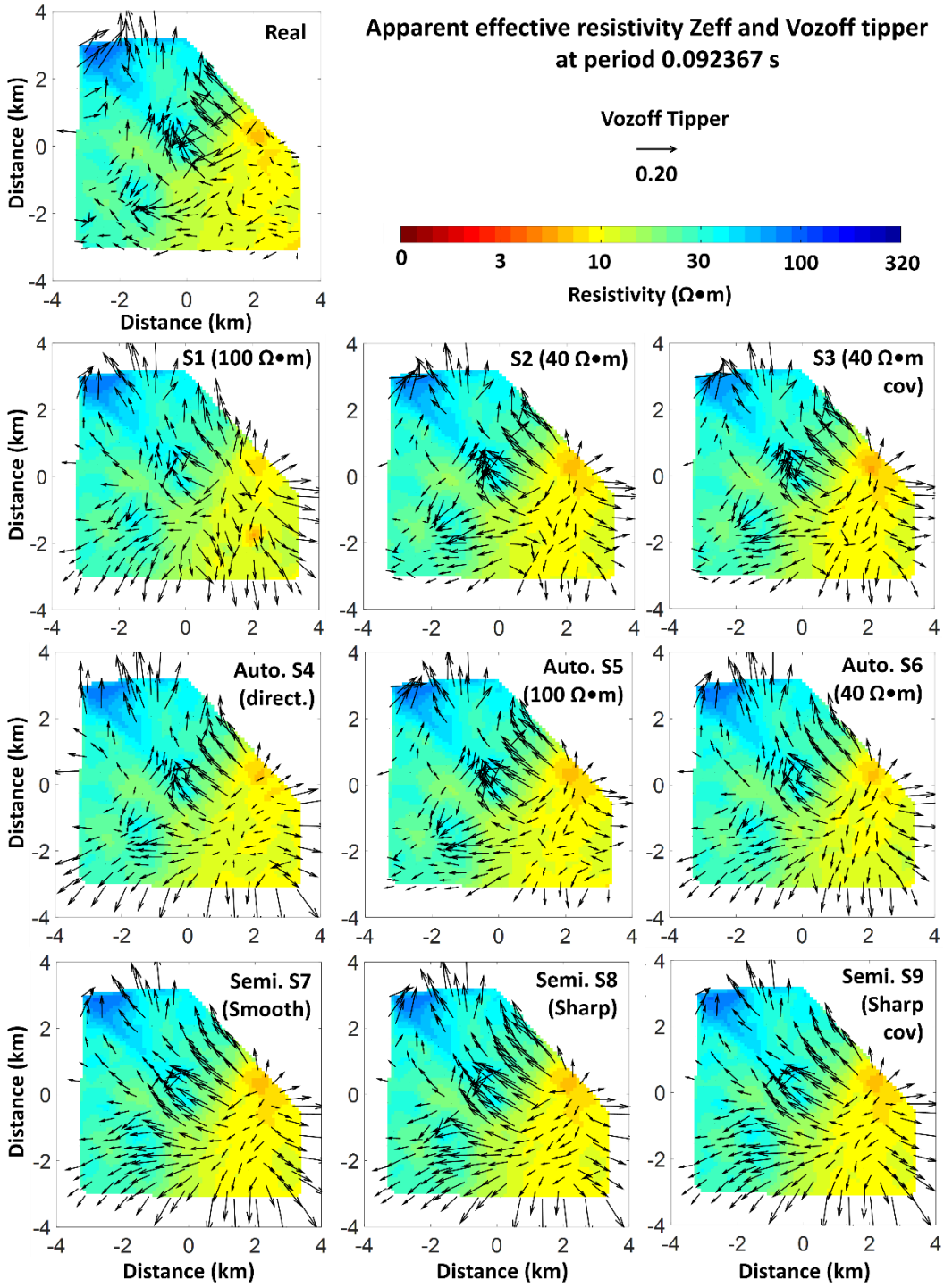

Fig. 2-18: Ten plan view slices of MT apparent effective resistivity and Vozoff tipper vector at a constant period (0.092367 second), providing a direct comparison of the real field data

and synthetic MT data after application of inversion strategies S1 to S9. The difference between field and model derived tipper vectors tends to increase towards the model boundaries where both seismic and MT coverage ends

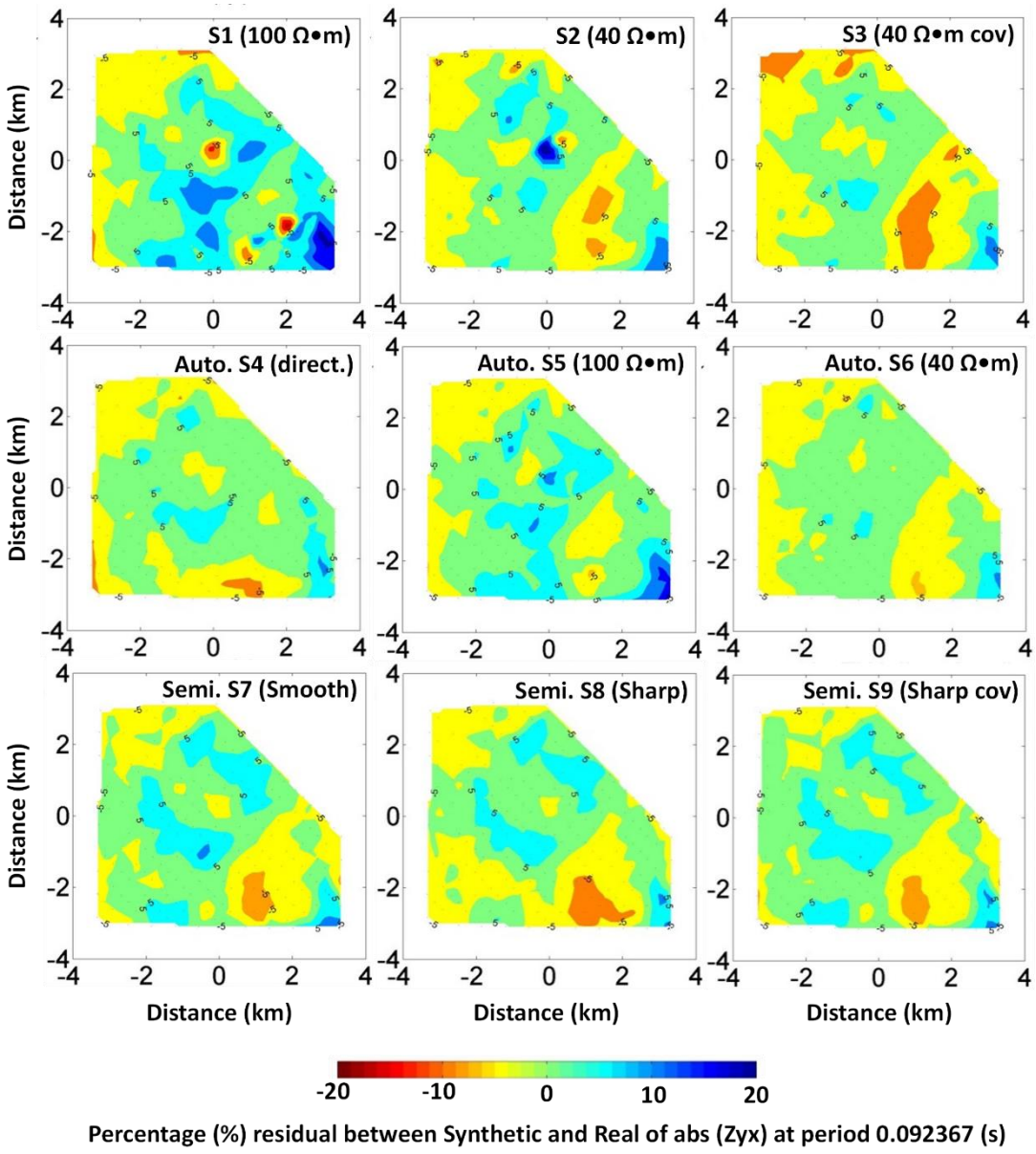

Fig. 2-19: Plan view slices of percentage residuals (i.e., synthetic data subtracted by the field data as a percentage normalised by the field data) of the abs(Zyx) at a constant period (0.092367 s) for all inversion strategies. Percent residuals from the automatic and semiautomatic cooperative inversion strategies demonstrate a reduction in zones of high local misfit that is apparent in strategies S1 and S2

Fig. 2-19 shows residuals between synthetic and field data at the same period for the nine cooperative inversion strategies. This provides a better diagnostic of the quality

of the fit between modelled and real data than the global RMS value. Localised, high misfit areas can be readily identified.

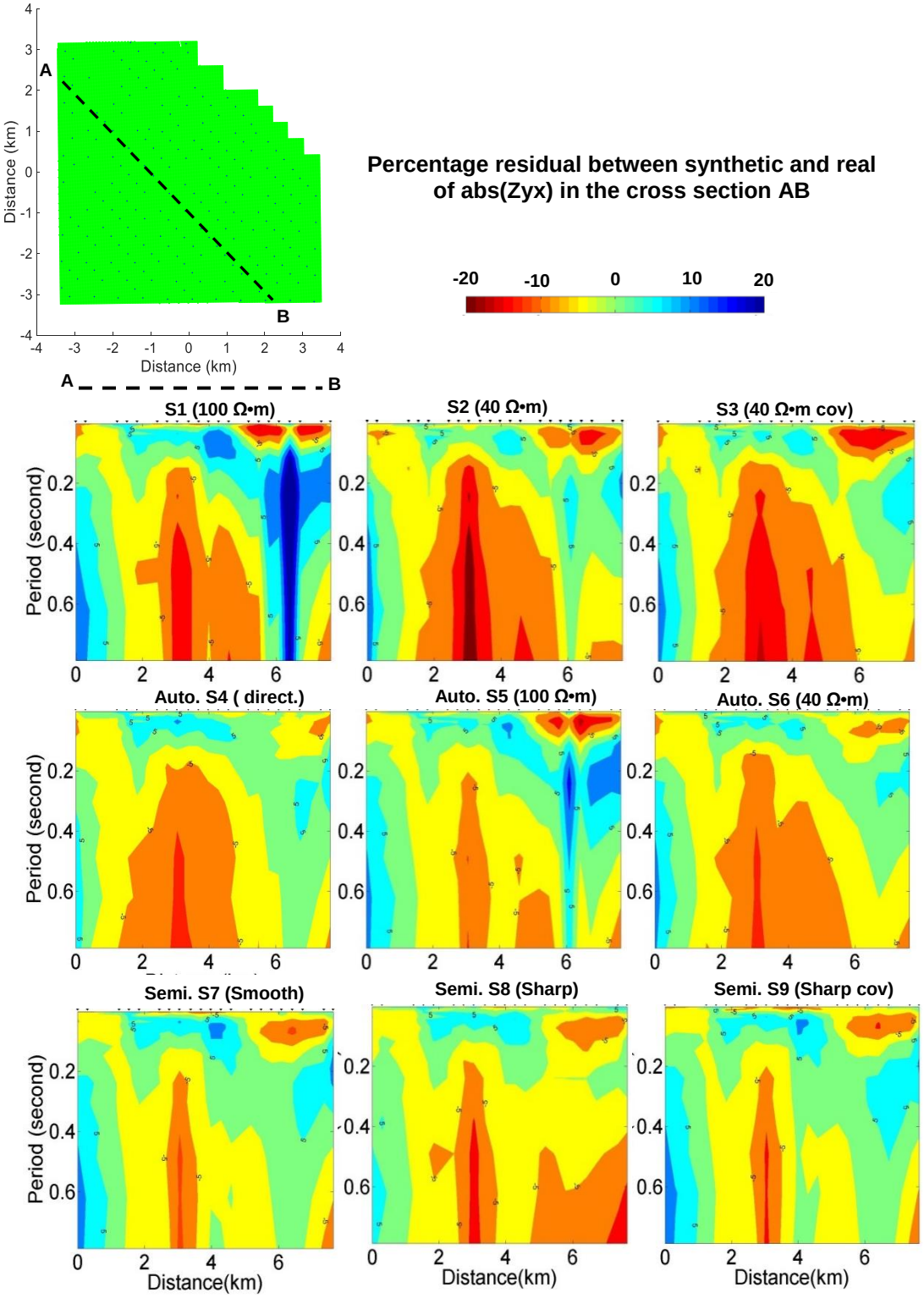

Fig. 2-20: Images showing cross-section views of percentage residuals of the abs(Zyx) for strategies S1 to S9. The location of the cross-section is identified by the black dashed line AB

in the plan view. The addition of seismic information to inversion strategies S4 to S9 appears to have considerably reduced zones of localised high misfit that exist in strategies S1 and S2

The percent residual maps for strategies S1 and S2 show distinct localised high residual areas (i.e., localised high misfit) when compared to residuals from strategies S3 to S9. Fig. 2-20 shows residuals along a section mark as AB on the survey map. Again, percent residuals for strategies S1 and S2 exhibit localised zone of exceedingly poor fit. The red and dark blue zones in Fig. 2-19 and Fig. 2-20 represent over 20% residual error between synthetic and real data for the absolute (abs) value of Zyz. The light blue to light green on these images represents areas of good fit between synthetic and field data after inversion. In the section views provided in Fig. 2-20 localised misfit is substantially reduced for strategies S7 and S9. The simple message is that misfit can and should be assessed throughout the full data volume.

2.5.7 Assessing inversion strategies S1 to S9: Conductivity distribution

Fig. 2-15 shows images of the final electrical conductivity distributions after inversion for strategies S1 to S9. Each strategy uses a different prior model conductivity and or covariance coefficient to seed the inversion (seeTable 2-1 and Fig. 2-14). In all cases (S1 to S9) final inversion resulted in significant reduction in RMS error and a substantial change to the conductivity distribution compared to the prior model. Gross distribution of electrical conductivity is broadly similar for all strategies and clearly represents more conductive cover over basement. However, a closer review of the nine images leads to a salient conclusion: in detail, all strategies yield different 3D conductivity distributions and as usual a “good fit” is a necessary but not sufficient condition for the actual subsurface conductivity distribution to be recovered by inversion.

The unconstrained MT inversions using halfspace prior models S1 and S2 result in a highly smoothed representation showing a usual “blurred” image of conductive cover against the higher resistivity basement. There is little detail in either cover or basement rock volumes and certainly no sharp boundaries for these unconstrained inversions. These results are typical and often accepted outcomes from the application of the MT method. We know these conductivity distributions must be incorrect, as sharp geo-

electrical boundaries certainly exist (i.e., from wireline logs, logged geology, core geo-chemistry and seismic reflectivity).

Semiautomatic inversion strategy S3 uses a prior root mean squared covariance of 0.25 across key seismic boundaries along with a 40 Ω•m half-space prior model. Lowering the covariance coefficient across the boundaries appears to play a minor role in directing the outcome of the inversion. While the lower covariance permits rapid change in electrical conductivity at the high reflectivity boundary it does yield a significantly different result to strategy S2, which has its covariance coefficient set to 0.3 everywhere.

Automatic cooperative inversion strategy S4 is interesting in that the prior model is initialised via direct mapping of a seismic attribute to electrical resistivity for all cells in the MT model domain (see Table 2-1). This type of "direct mapping" has the advantage of being straight forward to implement. However, a distinct risk in applying such a strategy is that it requires an inferred link between conductivity and the selected seismic attribute. Even if this is based on wireline log data such a relationship may only apply locally.

For Nevada example, the result for S4 is surprisingly effective. In particular, S4 was the only strategy to recover possible linear features that may be associated with faulting in basement. What we suspect is that faulted zones in basement have a recoverable dip angle attribute and so are mapped to slightly higher electrical conductivity in the prior model compared to basement rock. A close look at the far left of the image representation of strategy S4 on Fig. 2-14 reveals slightly higher conductivity along linear seismic features. The global RMS misfit and percentage residual images (Fig. 2-16, Fig. 2-19 and Fig. 2-20) indicate good model fit to data. In the absence of information to the contrary, we must consider the conductivity distribution generated from automatic cooperative inversion strategy S4 as a possible and valid representation. We highlight this example because for exploration, fault systems are often of high significance. Representing their existence within the prior geo-electrical model may permit full inversion to reveal important information concerning subsurface rock properties proximal to faults.

Strategies S5 and S6 use the dip angle seismic attribute to assist in construction of the geometric framework for the prior conductivity model. For automatic cooperative

inversion strategies S5 and S6, we have used geostatistical methods to restrict the number of "index groups" to five, which ultimately means that the large scale seismic structures are retained and represented in the prior geo-electrical model by a small set of discrete conductivities (see schematic Fig. 2-10). In contrast to discrete conductivity values filling each subvolume for strategies S5 and S6, the prior conductivity model derived from direct mapping used for strategy S4 permits continuous variations in conductivity that follow the seismic character of the model domain.

Semiautomatic cooperative inversion strategies S7, S8 and S9 result in considerable vertical and lateral detail in conductivity distribution in cover. What is particularly exciting about these results is that the final inversions (S8 and S9) created detailed conductivity distributions that follow geometries clearly in the seismic reflectivity that were not included in the prior model. That is the inversions have "found" clear geo-electrical units within the framework of the prior model that appear to match the detail of the reflectivity image. S7 results in the smoothest image due to the higher, default covariance boundary value of 0.3 and the smooth prior conductivity model. Strategy S9 provides the sharpest image and the greatest contrast in conductivity between key subvolumes. It includes a prior model with sharp conductivity changes at boundaries and boundary-defined covariance that will enable the inversion process to maintain these sharp boundaries (see Table 2-1).

Fig. 2-21 provides a conductivity slice at 466 m below average ground level with an intensity overlay from the 3D seismic volume at the same depth. The prior conductivity model for strategies S8 and S9 are identical and are presented at depth 466 m in Fig. 2-21a. At this depth slice the prior model conductivity distribution consists of just 3 conductivities. Small arrows in each image point to selected prominent seismic reflections that are not incorporated in the prior model for S8 or S9. We observe that the application of semiautomatic cooperative inversion strategies S8 and S9 reveal detailed conductivity distributions that correlate with seismic information not provided to the prior model.

Semiautomatic cooperative inversion strategy S9 differs from S8 in that the boundary or covariance coefficient is reduced at the prior model boundaries. What this does is to allow more rapid changes of conductivity across the boundaries. The outcome is that several features close to high contrast boundaries may be better resolving in S9 compared to S8. Such features are represented by yellow and tan arrows in Fig. 2-21c.

Certainly the relatively small feature highlighted by Fig. 2-21c matches the seismic and appears to be accurately resolved by strategy S9. It's difficult to fully appreciate the detail resulting from strategy S9 in 2D images so 3D representation of conductivity distribution of S9 is provided in Fig. 2-25.

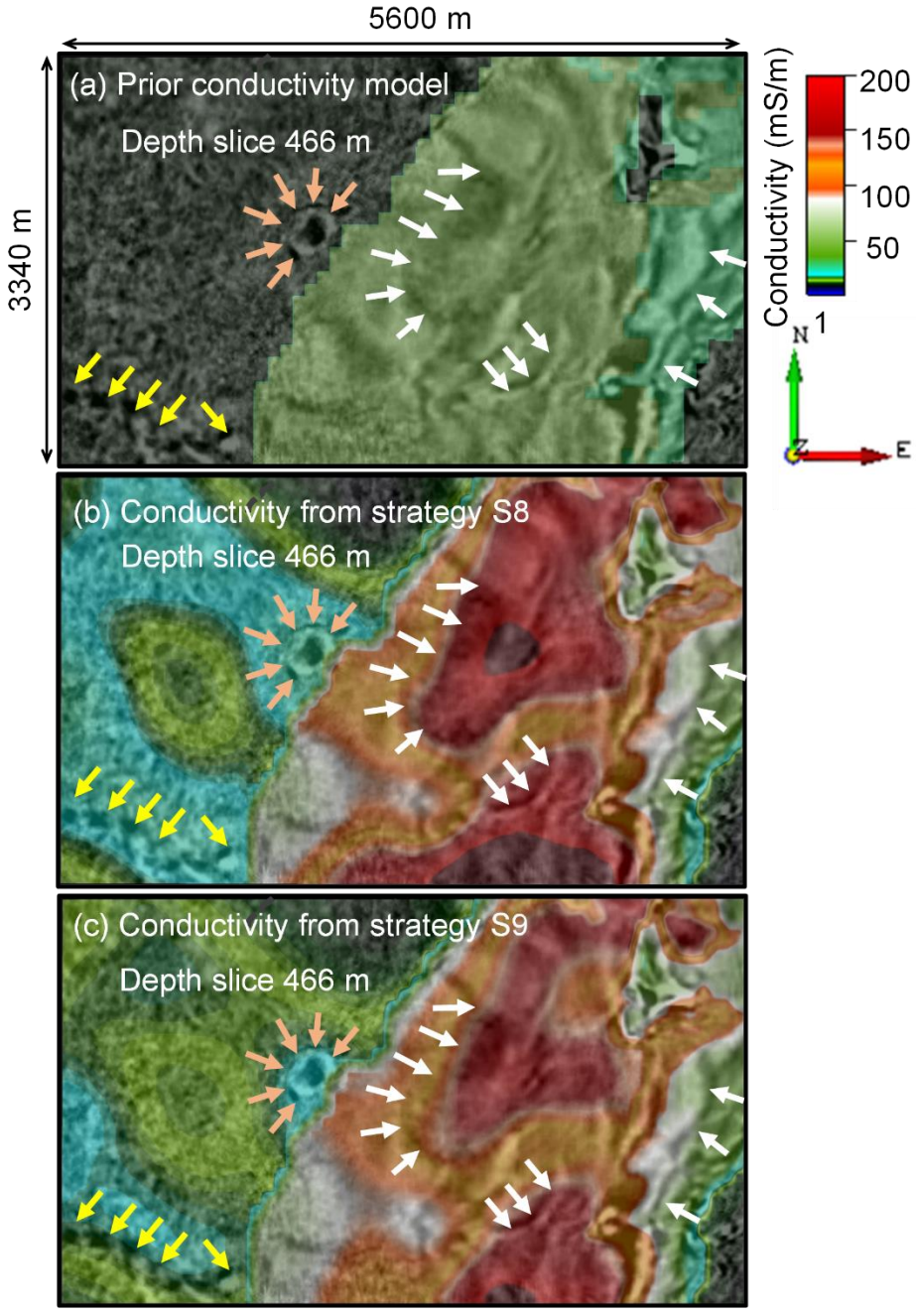

Fig. 2-21: Depth slice images 466 m below average surface level comparing seismic reflectivity with the prior model conductivity and final inverted conductivity distribution for semiautomatic cooperative inversion strategies S8 and S9. Strategies S8 and S9 generate a prior conductivity model (Fig. 2-21a) with sharp boundaries. Strategies S8 and S9 use the same prior conductivity model. Strategy S9 permits more rapid changes in conductivity across

subvolumes by reducing the covariance coefficients across the boundaries. Note that inversion strategy S9 (Fig. 2-21c) accurately recovers subtle conductivity distributions that are clear in the seismic reflectivity but not included in the prior model. This indicates that even the small changes in the covariance coefficient from 0.3 to 0.25 at seismically defined boundary can significantly improve resolution of subtle conductivity distributions proximal to that boundary. The white arrows highlight reflectors to the right of the major fault that appear to have been represented in the outcome for both strategies S8 and S9

We suspect that strategy S9 is the most likely to represent the true subsurface conductivity distribution in cover because results are consistent with (i) the wireline log data, (ii) seismic data, (iii) geo-chemical information and lithological information. We would also suggest that recovery and resolution of subtle conductivity features proximal to the large faults is substantially enhanced by changing smoothness constraints across the fault, which is accurately located in the seismic reflection data.

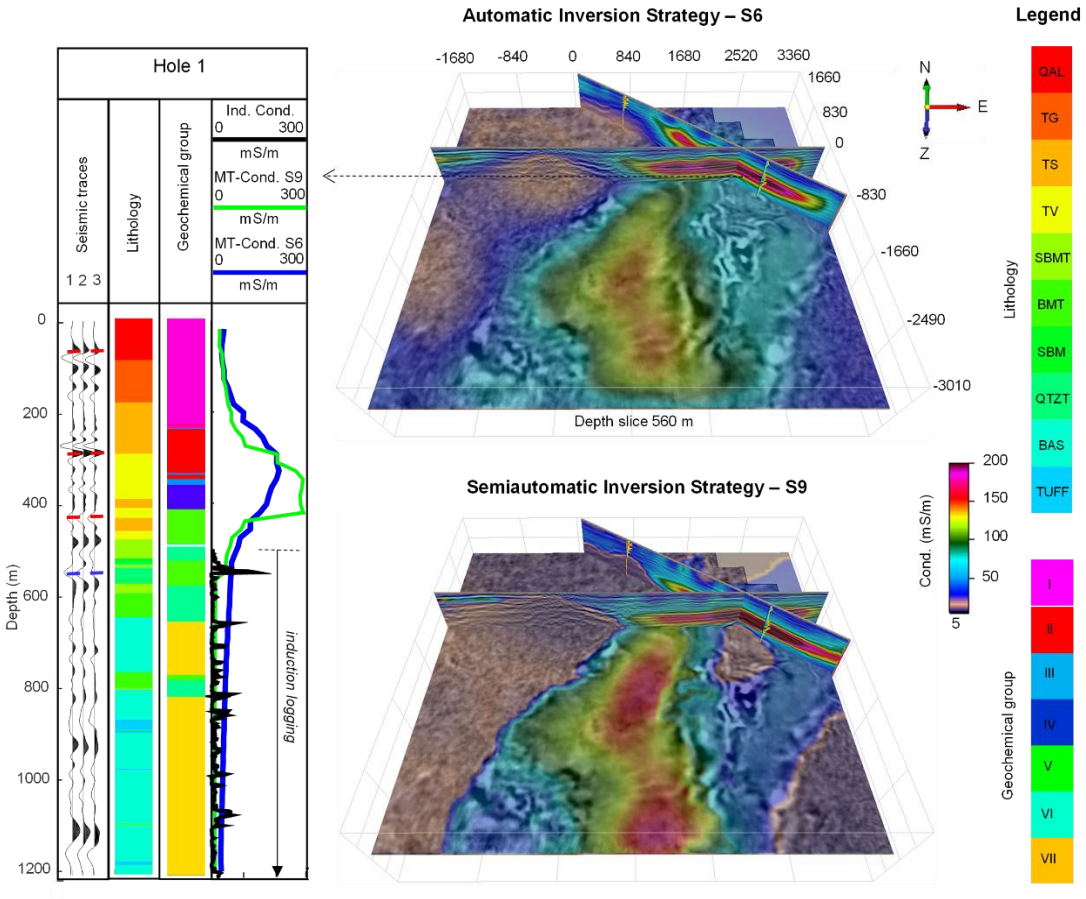

Fig. 2-22: 3D image comparison of electrical conductivity distribution obtained from automatic and semiautomatic cooperative inversion strategies S6 and S9 respectively, with drill-hole information. The available drill-hole information included: (i) the wireline electrical log, (ii) geochemistry (geostatistical groups) and (iii) lithology. As is common practice, the

wireline log from which the conductivity profile was obtained (i.e., black line) is only recorded below the surface casing (steel casing) that is set against cover sediments. In the "seismic traces" panel on the left of Fig. 2-22, the dashed red lines are high reflectivity boundaries within cover, while the dashed blue line identifies the interface between cover and basement rock. Conductivity profiles have been extracted at hole 1 from the final 3D conductivity distribution at S6 and S9 and are displaced as blue and green profiles in the left hand panel. K-means clustered groups based on 15 geochemical elements along with lithological groups and seismic traces are also provided in the left hand panel. Abbreviation for the lithology log is detailed below: QAL Tertiary volcaniclastics, tuffs, and siltstones. TG Rhyodacite volcanics - Tuffaceous silt and clay. TS Tuffaceous silt and clay. TV Green glassy volcanics. SBMT Siliceous mudstone with tuff. BMT Mudstone with tuff. QTZT Quartzite. BAS Basalt. TUFF Tuff

Next we will compare automatic cooperative inversion strategy S6 and semiautomatic cooperative inversion strategy S9 with available drill-hole information. Fig. 2-22 shows a comparison between "smooth" strategy S6 and "sharp" inversion strategy S9. The 3D image representation includes a depth slice of 560 m below average surface level. The final conductivity distribution after application of strategies S6 and S9 is overlaid on the 3D seismic image. Detailed information at drill hole 1 is provided in the left hand panel.

Within cover, conductivity distributions derived from strategies S6 and S9 broadly match with lithology and geochemistry information (see section 3.3). However, in detail semiautomatic inversion strategy S9 results in discrete clear conductivity zones that appear to give a superior match to the lithological and geochemical rock groupings. Also, strategy S9 recovers the correct resistivity in basement according to the wireline log. Strategy S9, which includes definition of a specific covariance value across key boundaries (dashed lines), also provides the closest agreement with average basement resistivity as recovered from induction logging (approx. 100 Ω•m).

A key observation from the lithological and geochemical groupings for hole 1 (Fig. 2-22) is that at several locations they simply do not match. Further, we should not expect that distribution of pore water chemistry is necessarily matched to lithological or geochemical groupings. As noted earlier the distribution of solute concentration will be determined by both local effects and large scale basin hydrodynamics. These are some of the reasons why strict forms of joint inversion (e.g., cross-gradient methods)

or cooperative inversion-based direct mapping of seismic to electromagnetic properties may fail to generate a sensible outcome.

Fig. 2-23 and Fig. 2-24 show a comparison of drill holes' 1 and 2 information with conductivities extracted from final inverted results from all strategies. These are included to highlight the range of possible solutions generated by inversion strategies S1 to S9 at the two well locations. Table 2-3 provides the key observations from the strategies.

Table 2-3: Key observations from application of inversion strategies S1–S9 to the Nevada co-located 3D seismic and MT data sets

Types of prior models	Key observations
Half-space (S1, S2, S3)	• Unconstrained inversion S1 and S2 used a half space prior model conductivity representing basement (100 Ohm.m) and cover (40 Ohm.m) rocks respectively. While S2 (40 Ohm.m halfspace prior model) arguably recovers the best representation of subsurface conductivity, in general unconstrained inversions fails to recover both the geometry of conductive layers within the correct basement resistivity as shown in Fig. 2-22, Fig. 2-23 and Fig. 2-24. • Although final RMS misfit is less than 2% across all strategies, Fig. 2-19 and Fig. 2-20 indicate that inversion strategies S1, S2, and S3 generate high localised misfit between field data and synthetic model data. • For strategy S3, addition information from the 3D seismic is included by making a small reduction in covariance coefficient across key boundaries. For the Nevada field example this made little difference to the inverted result when compared to the outcome from S2 (i.e., see S3 result).
Automatic (S4, S5, S6)	• Automatic cooperative inversion strategy S4 applies direct mapping of a seismic attribute to a conductivity throughout the MT model domain. This is a higher "risk" strategy as certainly there will be areas where the assumed relationship between the selected volumetric seismic attribute and conductivity will not hold. Interestingly, inversion strategy S4 was the only strategy able to generate detailed conductivity distributions that identified north south linear features near to or in basement at the far West of the survey are. These linear features are also clear in the seismic (See Fig. 2-15).

	• In contrast to strategy S4, strategies S5 and S6 incorporate a geometric mapping of a discrete conductivity value derived from an unconstrained inversion into each large subvolume within a framework recovered from volumetric analysis of a seismic attribute. Both strategies appear to produce a conductivity distribution similar in shape but with a final conductivity biased towards the halfspace resistivity that was used for the unconstrained inversion. • In general strategies S4, S5 and S6 did not generate a clear match to that which appeared to be achieved by S7, S8 and S9 at drills 1 and 2 (see Fig. 2-23 and Fig. 2-24).
Semiautomatic (S7, S8, S9)	• Semiautomatic cooperative inversion Strategies S7, S8 and S9 create a prior model geo-electrical framework around four exceedingly well defined high-reflectivity boundaries, which separate five large subvolumes. The key geo-electrical and seismic horizon is the basement to cover interface. The result of S7, S8 and S9 are consistent with drill hole (see Fig. 2-23 and Fig. 2-24) and seismic data (see Fig. 2-21 and Fig. 2-24), especially in cover rocks. • A key observation from a comparison of the outcomes from strategies S8 and S9 was that by introducing a small reduction in the covariance co-efficient at the subdomain boundaries, subtle features proximal to these key boundaries could be resolved in detail (see Fig. 2-21a, Fig. 2-21b and Fig. 2-21c). These observations may have significant implications in exploration for conductive mineralisation expected to be associated with faulting.

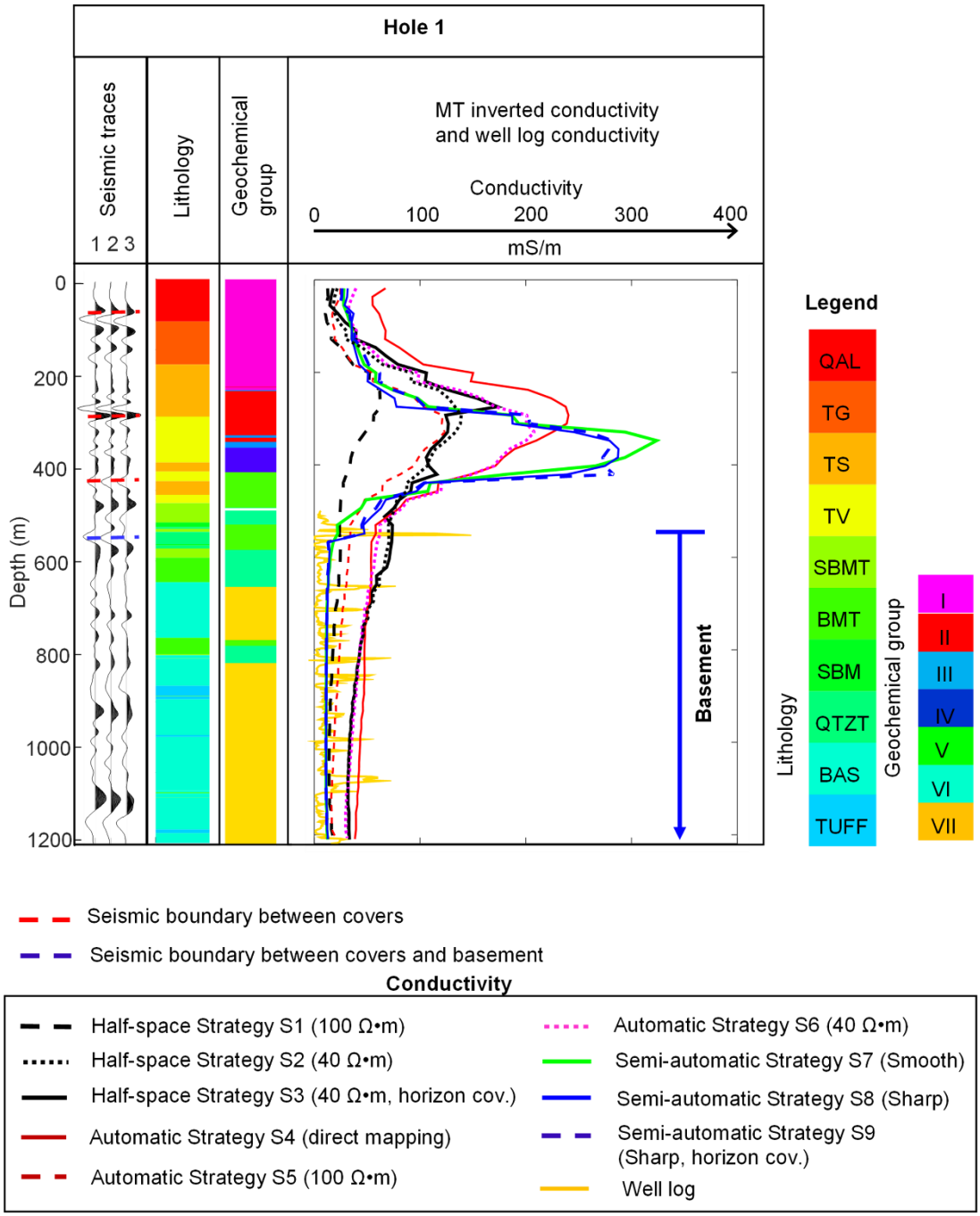

Fig. 2-23: Measured well-log conductivity (yellow) and the corresponding equivalent profiles derived from the nine inversion strategies at hole 1. While all of the inversion strategies capture the transition between the sediment and the basement, the resistivity of the sedimentary structures varies significantly between each inversion strategy. It is evident that inversion strategies S1, S5, S7, S8 and S9 capture the average resistivity of the basement. Abbreviation of lithology is mentioned below: QAL Tertiary volcaniclastics, tuffs and siltstones. TG Rhyodacite volcanics—Tuffaceous silt and clay. TS Tuffaceous silt and clay. TV Green glassy volcanics. SBMT Siliceous mudstone with tuff. BMT Mudstone with tuff. QTZT Quartzite. BAS Basalt. TUFF Tuff

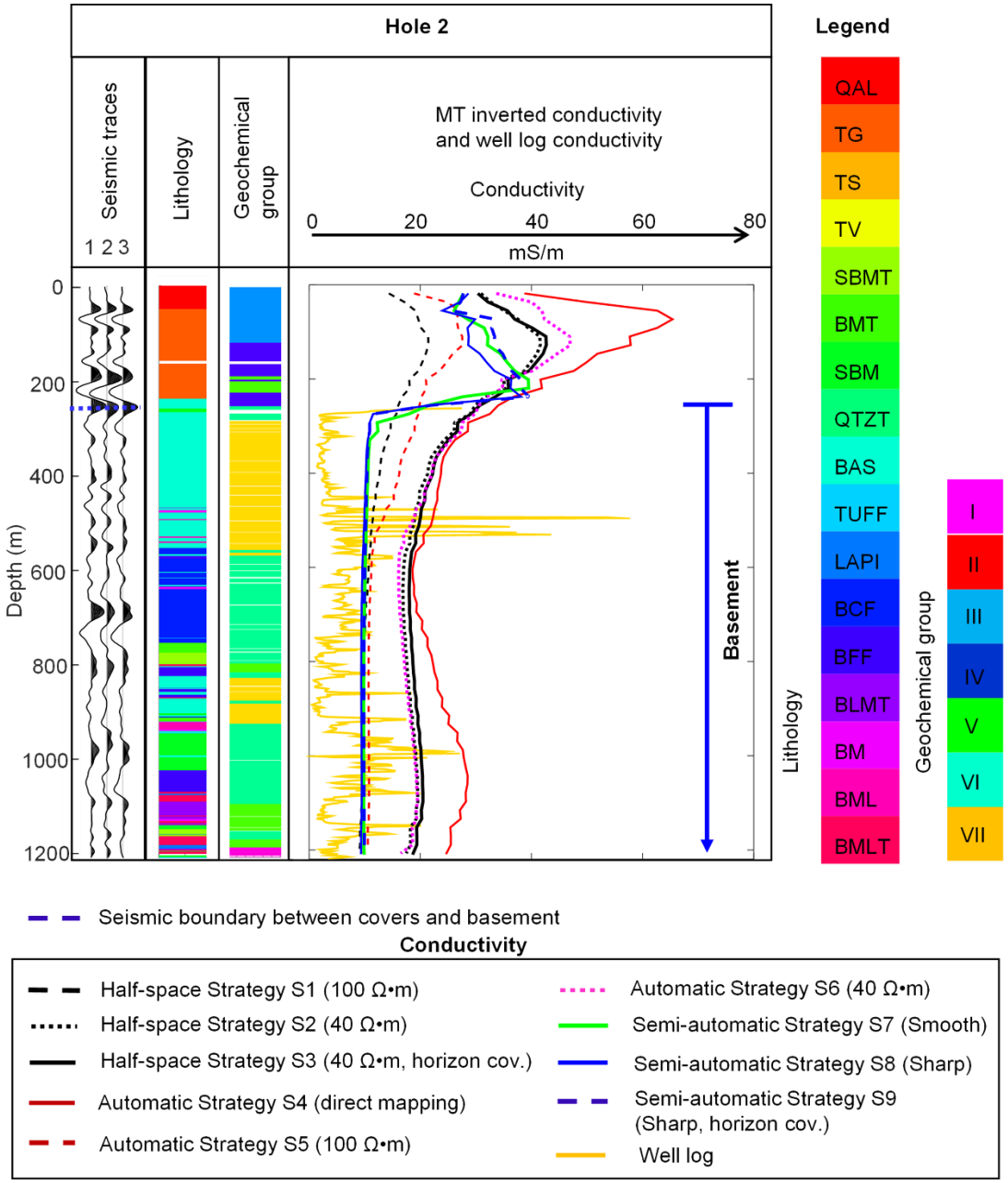

Fig. 2-24: Measured well-log conductivity (yellow) and the corresponding equivalent profiles derived from the nine inversion strategies at hole 2. All of the inversion strategies capture the transition between the sediment and the basement. There is also a significant variation in sediment formation resistivity between each of the inversion strategies. It is evident that inversion strategies S1, S5, S7, S8 and S9 capture the average resistivity of the basement. Abbreviation of lithology is mentioned below: QAL Tertiary volcaniclastics, tuffs and siltstones. TG Rhyodacite volcanics—Tuffaceous silt and clay. TS Tuffaceous silt and clay. TV Green glassy volcanics. SBMT Siliceous mudstone with tuff. BMT Mudstone with tuff. QTZT Quartzite. BAS Basalt. TUFF Tuff LAPI: Lapilli Tuff. BCF Mudstone with tuff. BFF

Fine Fragmental Mudstone with tuff—breccia. BLMT Mudstone, limestone with tuff. BM Mudstone. BML Mudstone, limestone. BMLT Mudstone, limestone with tuff

All strategies other than S7, S8 and S9, fail to recover conductivities that match wireline log conductivity in the basement with S2, S3, S4 and S6 being the main offenders. However, S4 did provides a level of detail proximal and below the basement not present in other strategies and in this sense represented valuable information about conductivity distribution now not present in other outcomes. A message from our analysis is that many possible inversion outcomes (i.e., strategies) must be considered when interpreting MT data. The information that is desired may not exist because of the inversion strategy selected.

For cooperative strategies S4 to S9, outcomes show details consistent with the seismic image. The inversion process refined the conductivity distribution to match remarkably well within the detailed seismic reflectivity image not included in the prior model.

2.6 General Discussion

We would like to reiterate three key points that arose from our detailed analysis of automatic and semiautomatic cooperative inversion:

i. In the semiautomatic approach, seismic attributes such as seismic amplitude, seismic energy and energy texture are used to build a skeleton of the prior model. Subsequent unconstrained inversion results in resistivity values that are then included in the skeleton to build the prior model. We can see that this cooperative approach is appropriate due to the fact that the inverted conductivity model inherits the general trend of the prior resistivity model volume and still keeps reliable sharp/smooth seismic boundary and resistivity information from the MT method.

ii. A highlight of our results is cooperative inversion strategies S4, S5 and S6, all of which have the potential to be automated. Volumetric analysis of seismic attributes such as dip angle (see Fig. 2-8) can be automated, generating subvolume regions of a prior model geo-electrical framework that can then be automatically filled by direct mapping or geometric mapping based on unconstrained inversion (see Fig. 2-9 and Fig. 2-10).

iii. Our most focused strategies were S7, S8 and S9. In particular, S9 contained the prior model conductivity and covariance coefficient distributions based on the auto-picking of high-reflectivity boundaries. The prior model directs the inverted result to the imbedded seismic structures and the reduction in the model covariance permits rapid changes in conductivity across high contrast boundaries. This allowed both more gradual changes within subvolumes and relatively sharp changes across high-contrast conductivity interfaces where seismic and geology imply that high contrast should exist.

2.7 Conclusions

We have created, described and tested a set of practical cooperative inversion strategies. These include semiautomatic and automatic methods for converting co-located 3D seismic reflection and magnetotelluric data to subsurface rock properties throughout large volumes of earth. These strategies have been applied to a large, modern dataset from the well-known gold mining districts of Nevada USA. While unconstrained inversion of MT data has a limited capacity to provide a detailed 3D subsurface image of conductivity distribution, both semiautomatic and automatic methods provided dramatically improved detail and resolution when outcomes are compared to seismic and all available core and log data.

The key to the semiautomatic strategies is to pick boundaries from the seismic volume and automatically assign a prior model based on an unconstrained inversion. A second round inversion is conducted with the new prior model.

Our automatic cooperative inversion strategies require MT data and a migrated seismic volume, beyond which, little human intervention is necessary. One method uses a combination of seismic attributes averaged over large volumes of earth and unconstrained inversion to create a set of prior models. The set of prior models forms a new starting point for a second round MT inversion. In essence, subvolumes with common seismic characteristics (attributes) provide the geometry within which electrical conductivity is to be distributed. Subsequently, each subvolume can be populated by conductivities extracted from the unconstrained inversion of the MT data. In a second class of cooperative inversion strategies, seismic attributes are more

directly converted to a conductivity distribution by a “transfer function” to create the prior model. Such methods can only be applied in subvolumes where a clear link between the value of an attribute (or combinations of attributes) and electrical conductivity is reasonably justified.

Our cooperative inversion strategies generate conductivity distributions generally consistent with both seismic and drill-hole data from the trial site. This set of plausible 3D geo-electrical models may then direct the interpreter’s attention to possibilities that otherwise may not have been considered. Similar strategies would have value across a wide range of subsurface research (e.g., crustal geophysics) and industrial applications (e.g., mineral, hydrocarbon, groundwater and geothermal industries).

2.8 Acknowledgements

The work has been supported by the Deep Exploration Technologies Cooperative Research Centre whose activities are funded by the Australian Government's Cooperative Research Centre Programme. This is DET CRC Document 2015/730. We also acknowledge and thank Barrick Gold for use of their comprehensive geophysical datasets. This work was supported by resources provided by the Pawsey Supercomputing Centre with funding from the Australian Government and the Government of Western Australia. We would like to thank Gary Egbert, Anna Kelbert and Naser Megbel for permitting us access to the 3D MT inversion code ModEM3D. We are thankful for the helpful discussions and assistance with software given by our colleagues including Thong Duy Kieu, Michael Carson, Mahyar Madadi and Robert Verstandig from Curtin University. We appreciate dGB Earth Science for providing software. We are also grateful to Lee Sampson from Barrick Gold Corporation, and one referee for valuable suggestions on improving our paper.

2.9 Author contributions

C.V.A.L ran 3D unconstrained/cooperative inversion. C.V.A.L has processed seismic and MT data. C.V.A.L and B.D.H interpreted the geophysics results. All the authors constructed and wrote the paper.

2.10 Supplementary

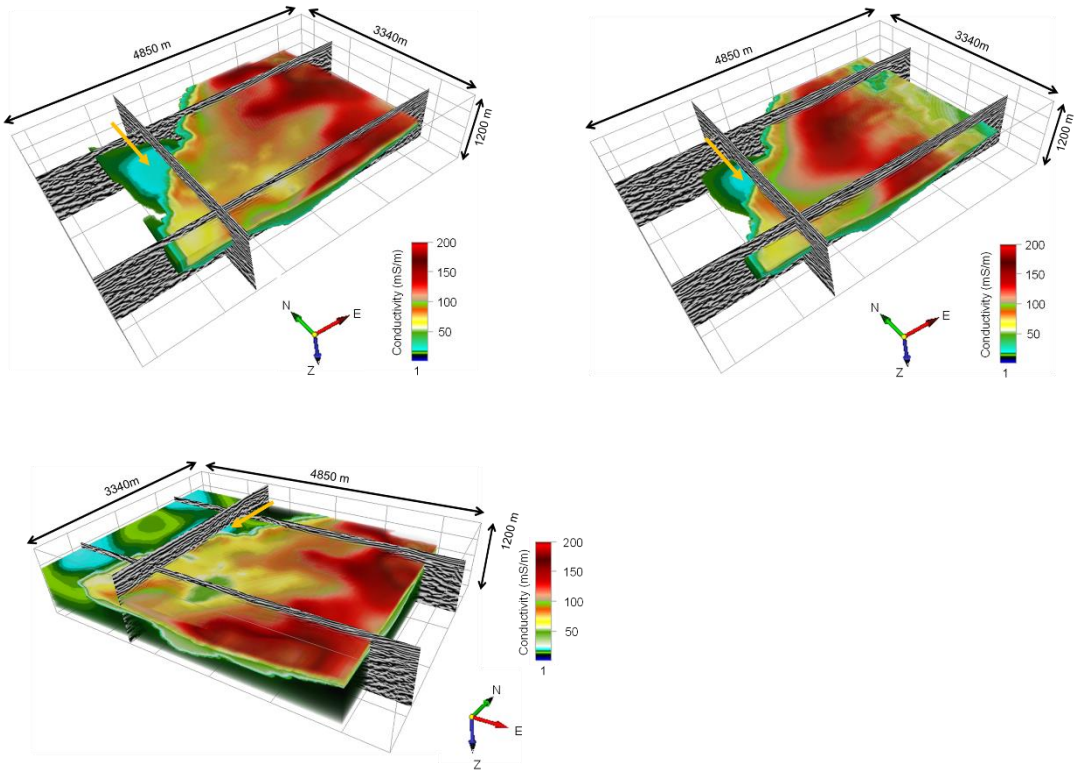

Fig. 2-25 Different views of 3D conductivity distribution extracted from S9 strategy. The tan arrow points to the similar feature shown in Fig. 2-21

2.11 References

Alférez, Germán H, Jocksan Rodríguez, Benjamin Clausen, and Lance Pompe. 2015. "Interpreting the Geochemistry of Southern California Granitic Rocks using Machine Learning." Proceedings on the International Conference on Artificial Intelligence (ICAI).

Apel, Marcus. 2001. "Development of a 3D GIS - based on the 3D modeller Gocad." Proceedings of the International Association for Mathematical Geology Annual Meeting.

Archie, Gustave E. 1942. "The electrical resistivity log as an aid in determining some reservoir characteristics " *Transactions of the AIME* 146 (01):54-62.

Bahorich, Mike, and Steve Farmer. 1995. "3-D seismic discontinuity for faults and stratigraphic features: The coherence cube." *The Leading Edge* 14 (10):1053-1058. doi: 10.1190/1.1437077.

Bauer, K, G Muñoz, and I Moeck. 2012. "Pattern recognition and lithological interpretation of collocated seismic and magnetotelluric models using self-organizing maps." *Geophysical Journal International* 189 (2):984-998. doi: 10.1111/j.1365-246X.2012.05402.x.

Becken, Michael, and Oliver Ritter. 2012. "Magnetotelluric Studies at the San Andreas Fault Zone: Implications for the Role of Fluids." *Surveys in Geophysics* 33 (1):65-105.

Bedrosian, PA, N Maercklin, U Weckmann, Y Bartov, T Ryberg, and O Ritter. 2007. "Lithology-derived structure classification from the joint interpretation of magnetotelluric and seismic models." *Geophysical Journal International* 170 (2):737-748.

Berdichevsky, Mark N, and Vladimir I Dmitriev. 2008. *Models and methods of Magnetotellurics*: Springer.

Bezdek, James C, Robert Ehrlich, and William Full. 1984. "FCM: The Fuzzy C-means clustering algorithm." *Computers & Geosciences* 10 (2):191-203.

Bourges, Matthieu, Jean-Luc Mari, and Nicolas Jeannée. 2012. "A practical review of geostatistical processing applied to geophysical data: methods and applications." *Geophysical Prospecting* 60 (3):400-412.

Brouwer, F., and A. Huck. 2011. " An Integrated Workflow to Optimize Discontinuity Attributes for the Imaging of Faults." *2011 Proceedings: Attributes: New Views on Seismic Imaging—Their Use in Exploration and Production, edited by KJ Marfurt, D. Gao, A. Barnes, S. Chopra, A. Corrao, B. Hart, H. James, J. Pacht, and NC Rosen*:496-533.

Chopra, Satinder, and Kurt J. Marfurt. 2007. *Seismic attributes for prospect identification and reservoir characteriztion*. Edited by Stephen J. Hill, *SEG Geophysical Development Series No. 11*. United States of America: Tulsa, Okla. (8801 South Yale St., Tulsa OK 74137-3175) : Society of Exploration Geophysicists

Cline, Jean S., Albert H. Hofstra, John L. Muntean, Richard M. Tosdal, and Kenneth A. Hickey. 2005. "Carlin-Type Gold Deposits in Nevada: Critical Geologic Characteristics and Viable Models." *Economic Geology 100th anniversary volume*:451-484.

Colombo, D., G. McNeice, E. Curiel, and A. Fox. 2013. "Full tensor CSEM and MT for subsalt structural imaging in the Red Sea: Implications for seismic and electromagnetic integration." *The Leading Edge* 32 (4):436-449. doi: 10.1190/tle32040436.1.

De Benedetto, Daniela, Annamaria Castrignano, Donato Sollitto, Francesca Modugno, Gabriele Buttafuoco, and Giuseppe lo Papa. 2012. "Integrating geophysical and geostatistical techniques to map the spatial variation of clay." *Geoderma* 171:53-63. doi: 10.1016/j.geoderma.2011.05.005.

deGroot-Hedlin, C., and S. Constable. 1990. "Occam's inversion to generate smooth, two-dimensional models from magnetotelluric data." *Geophysics* 55 (12):1613-1624. doi: 10.1190/1.1442813.

dGB Earth Sciences. 2015. "OpendTect dGB Plugins User Documentation version 4.6." Accessed 02/05/2016. http://opendtect.org/relman/4.6.0/unpacked/4.6.0/doc/User/dgb/chapter2.3_attributes_with_steering.htm.

Di Giuseppe, Maria Giulia, Antonio Troiano, Claudia Troise, and Giuseppe De Natale. 2014. "k-Means clustering as tool for multivariate geophysical data analysis.

An application to shallow fault zone imaging." *Journal of Applied Geophysics* 101:108-115.

Doetsch, Joseph, Niklas Linde, and Andrew Binley. 2010. "Structural joint inversion of time-lapse crosshole ERT and GPR traveltime data." *Geophysical Research Letters* 37:L24404. doi: 10.1029/2010GL045482.

Dubrule, Olivier. 2003. *Geostatistics for seismic data integration in Earth models: 2003 Distinguished Instructor Short Course*. United States of America: Tulsa, OK : Society of Exploration Geophysicists.

Dupuis, Christian, K Butler, Anton Kepic, and Brett Harris. 2009. "Anatomy of a seismoelectric conversion: Measurements and conceptual modeling in boreholes penetrating a sandy aquifer." *Journal of Geophysical Research: Solid Earth* 114 (B10):B10306.

Egbert, Gary D., and Anna Kelbert. 2012. "Computational recipes for electromagnetic inverse problems." *Geophysical Journal International* 189 (1):251-267. doi: 10.1111/j.1365-246X.2011.05347.x.

Gallardo, Luis A., and Max A. Meju. 2004. "Joint two-dimensional DC resistivity and seismic travel time inversion with cross-gradients constraints." *Journal of Geophysical Research: Solid Earth* 109 (B3). doi: 10.1029/2003JB002716.

Gao, Guozhong, Aria Abubakar, and Tarek M. Habashy. 2012. "Joint petrophysical inversion of electromagnetic and full-waveform seismic data." *Geophysics* 77 (3):WA3-WA18.

Garambois, Stéphane, and Michel Dietrich. 2002. "Full waveform numerical simulations of seismoelectromagnetic wave conversions in fluid-saturated stratified porous media." *Journal of Geophysical Research: Solid Earth* 107 (B7):ESE.

Grunsky, Eric C, and Barry W Smee. 2003. "Enhancements in the interpretation of geochemical data using multivariate methods and digital topography." *CIM Bulletin* 96 (1068):39-43.

Haber, Eldad, and Michal Holtzman Gazit. 2013. "Model fusion and joint inversion." *Surveys in Geophysics* 34 (5):675-695.

Haber, Eldad, and D Oldenburg. 1997. "Joint inversion: a structural approach." *Inverse problems* 13 (1):63.

Hall-Beyer, M. 2007. "GLCM Texture Tutorial." Accessed 03 May 2016. http://www.fp.ucalgary.ca/mhallbey/tutorial.htm.

Harris, Peter, Zhijun Du, Lucy MacGregor, Wiebke Olsen, Rone Shu, and Richard Cooper. 2009. "Joint interpretation of seismic and CSEM data using well log constraints: an example from the Luva Field." *first break* 27 (5):73-81.

Hillis, R., D. Giles, S. Van Der Wielen, A. Baensch, J. Cleverley, A. Fabris, S. Halley, B. Harris, S. Hill, P. Kanck, A. Kepic, S. Soe, G. Stewart, and Y. Uvarova. 2014. "Coiled Tubing Drilling and Real-Time Sensing: Enabling Prospecting Drilling in the 21st Century?" In *Building exploration capability for the 21st century*, edited by Karen D. Kelley and Howard C. Golden, 243-259. Colorado, United States of America: Society of Economic Geologists, Inc.

Howe, Brendan D., Bill Doerner, Jared Townsend, and Pamela Patraskovic. 2014. "Three-dimensional magnetotelluric inversion and petrophysical interpretation of the Turquoise Ridge gold deposit, Nevada, USA." SEG Technical Program Expanded Abstracts 2014.

Huck, Helene. 2012. "The road to open source: Sharing a ten years' experience in building OpendTect, the open source seismic interpretation software." 74th EAGE Conference and Exhibition, Copenhagen, Denmark.

Jolliffe, Ian T. 2002. "Principal Component Analysis " In, 1-28. Wiley Online Library.

Kieu, Duy Thong, and Anton Kepic. 2015. "Incorporating prior information into seismic impedance inversion using fuzzy clustering technique." SEG New Orleans Annual Meeting, USA.

Kiyan, Duygu, Alan G. Jones, and Jan Vozar. 2014. "The inability of magnetotelluric off-diagonal impedance tensor elements to sense oblique conductors in three-dimensional inversion." *Geophysical Journal International* 196:1351-1364.

Klose, Christian D. 2006. "Self-organizing maps for geoscientific data analysis: geological interpretation of multidimensional geophysical data." *Computational Geosciences* 10 (3):265-277.

Linde, Niklas, Andrew Binley, Ari Tryggvason, Laust B. Pedersen, and Andre´ Revil. 2006. "Improved hydrogeophysical characterization using joint inversion of cross-hole electrical resistance and ground-penetrating radar traveltime data." *Water Resources Research* 42:W12404.

Mahmoudian, Faranak, Gary F. Margrave, Joe Wong, and David C. Henley. 2015. "Azimuthal amplitude variation with offset analysis of physical modeling data acquired over an azimuthally anisotropic medium." *Geophysics* 80 (1):C21-C35.

Mandolesi, Eric, and Alan G. Jones. 2014. "Magnetotelluric inversion based on mutual information." *Geophysical Journal International* 199 (1):242-252. doi: 10.1093/gji/ggu258.

MathWorks. 2014. "MATLAB." Accessed 03 May 2016. http://au.mathworks.com/help/stats/k-means-clustering.html.

Moorkamp, M., A. G. Jones, and D. W. Eaton. 2007. "Joint inversion of teleseismic receiver functions and magnetotelluric data using a genetic algorithm: Are seismic velocities and electrical conductivities compatible?" *Geophysical Research Letters* 34 (16):L16311.

Moorkamp, M., A. W. Roberts, M. Jegen, B. Heincke, and R. W. Hobbs. 2013. "Verification of velocity-resistivity relationships derived from structural joint inversion with borehole data." *Geophysical Research Letters* 40:3596-3601.

Muntean, John L., Jean S. Cline, Adam C. Simon, and Anthony A. Longo. 2011. "Magmatic–hydrothermal origin of Nevada's Carlin-type gold deposits." *Nature geoscience* 4 (2):122-127. doi: 10.1038/ngeo1064.

Muntean, John L., Michael P. Coward, and Charles A. Tarnocai. 2007. "Reactivated Palaeozoic normal faults: controls on the formation of Carlin-type gold deposits in north-central Nevada." *Geological Society, London* Special Publications:571-587.

Nanni, Arthur, Ari Roisenberg, Jandyra MG Fachel, Gilberto Mesquita, and Cristiano Danieli. 2008. "Fluoride characterization by principal component analysis in the hydrochemical facies of Serra Geral Aquifer System in Southern Brazil." *Anais da Academia Brasileira de Ciências* 80 (4):693-701.

Nelson, Eric. 2009. Spreadsheet to Convert Rake to Plunge & Trend. edited by Rake Diagram. Computer Applications in Structural Geology: Colorado School of Mines.

Onajite, Enwenode. 2013. *Seismic data analysis techniques in hydrocarbon exploration*: Amsterdam : Elsevier

Pethick, Andrew, and Brett Harris. 2016. "Macro-parallelisation for controlled source electromagnetic applications." *Journal of Applied Geophysics* 124:91-105. doi: 10.1016/j.jappgeo.2015.11.013.

Pethick, Andrew M., and Brett D. Harris. 2014. "Structural constraints in joint inversion of seismic and EM data: Analysis and visualization." SEG Technical Program Expanded Abstracts, USA.

Roberts, A. 2001. "Curvature attributes and their application to 3D interpreted horizons." *first break* 19 (2):85-100.

Roden, Rocky, Thomas Smith, and Deborah Sacrey. 2015. "Geologic pattern recognition from seismic attributes: Principal component analysis and self-organizing maps." *Interpretation* 3 (4):SAE59-SAE83. doi: 10.1190/INT-2015-0037.1.

Samarasinghe, Sandhya. 2006. *Neural Networks for Applied Sciences and Engineering From Fundamentals to Complex Pattern Recognition*: Auerbach Publications.

Simpson, Fiona, and Karsten Bahr. 2005. *Practical Magnetotellurics*. Cambridge University Press.

Siripunvaraporn, Weerachai, and Gary Egbert. 2000. "An efficient data-subspace inversion method for 2-D magnetotelluric data." *Geophysics* 65 (3):791-803. doi: 10.1190/1.1444778.

Takam Takougang, Eric, Brett Harris, Anton Kepic, and Cuong V. A. Le. 2015. "Cooperative joint inversion of 3D seismic and magnetotelluric data: With application in a mineral province." *Geophysics* 80:1-13. doi: 10.1190/GEO2014-0252.1.

Taner, M. T., F Koehler, and R. E Sheriff. 1979. "Complex seismic trace analysis." *Geophysics* 44 (6):1041-1063.

Taner, M. Turhan. 2001. "Seismic attributes." *CSEG Recorder* 26 (7):48-56.

Thoreson, RF, ME Jones, FJ Breit Jr, MA Doyle-Kunkel, and LJ Clarke. 2000. "The geology and gold mineralization of the Twin Creeks gold deposits, Humboldt County, Nevada." In *GUIDEBOOK SERIES of the SOCIETY OF ECONOMIC GEOLOGISTS: Part II. Geology & Gold deposits of the Getchell region*, edited by Elizabeth Jones Crafford, 175-187. Colorado, United States of America: Society of Economic Geologists.

Tietze, K., and O. Ritter. 2013. "3D magnetotelluric inversion in practice - the electrical conductivity structure of the San Andreas Fault in Central California." *Geophysical Journal International* 195 (1):130-147.

Tingdahl, Kristofer M. 2003. "Improving seismic chimney detection using directional attributes." In *Soft computing and intelligent data analysis in oil exploration*, edited by M. Nikravesh, F. Aminzadeh and L.A. Zadeh, 157-173. Elsevier Science Publishers, Amsterdam.

Tingdahl, Kristofer M., and Paul F. M. De Groot. 2003. "Post-stack dip and Azimuth Processing." *Journal of Seismic Exploration* 12:113-126.

Viola, Paul, and William M. Wells III. 1997. "Alignment by Maximization of Mutual Information." *International Journal of Computer Vision* 24 (2):137-154.

Virieux, J., and S. Operto. 2009. "An overview of full-waveform inversion in exploration geophysics." *Geophysics* 74 (6):WCC127–WCC152.

Vozoff, K, and DLB Jupp. 1975. "Joint inversion of geophysical data." *Geophysical Journal International* 42 (3):977-991.

Vozoff, Keeva. 1972. "The magnetotelluric method in the exploration of sedimentary basins." *Geophysics* 37:98-142.

Ward, W.O.C., P.B. Wilkinson, J.E. Chambers, L.S. Oxby, and L. Bai. 2014. "Distribution-based fuzzy clustering of electrical resistivity tomography images for interface detection." *Geophysical Journal International* 197:310-321.

West, B., S. May, J. E. Eastwood, and C. Rossen. 2002. "Interactive seismic facies classification using textural and neural networks." *The Leading Edge* 21:1042-1049.

Yilmaz, Ö. 2001a. "Reservoir Geophysics." In *Seismic Data Analysis: Processing, Inversion, and Interpretation of Seismic Data*, edited by Stephen M. Doherty, 1794-1896. United States of America: Tulsa, OK : Society of Exploration Geophysicists.

Yilmaz, Ö 2001b. "3-D Seismic Exploration." In *Seismic Data Analysis: Processing, Inversion, and Interpretation of Seismic Data*, edited by Stephen M. Doherty, 1001-1008. United States of America: Tulsa, OK : Society of Exploration Geophysicists.

Zhou, J., A. Revil, M. Karaoulis, D. Hale, J. Doetsch, and S. Cuttler. 2014. "Image-guided inversion of electrical resistivity data." *Geophysical Journal International*. doi: 10.1093/gji/ggu001.

Zorin, Nikita, Dmitrii Epishkin, and Andrey Yakovlev. 2015. "A telluric method for natural field induced polarization studies." *Journal of Applied Geophysics*. doi: 10.1016/j.jappgeo.2015.10.017.

CHAPTER 3. SEISMIC TEXTURE FOR ROCK VOLUME CLASSIFICATION AND COOPERATIVE INVERSION

Key points:

- We convert 3D seismic reflectivity images into a volume containing seismic textures.
- The distribution of seismic texture recovered from 3D seismic imaging may map to the volumetric distribution of rock texture with potential applications for minerals, hydrothermal, hydrocarbon and groundwater industries as well as crustal research.
- K-means clustering is used to recovers discrete seismic textures with inputs being four dip steered, textural seismic attributes.
- Volumetric distribution based on seismic texture clusters can be used as a guiding framework to significantly improve cooperative inversion of lower resolution electromagnetic, or potential fields methods.
- We provide methods and examples of how to calculate seismic texture for industry scale land based seismic data sets from Nevada USA and Kevitsa Finland.

This chapter content is submitted to Nature: Scientific Reports. Its authors are Le, Cuong V.A., B.D. Harris, and A.M. Pethick.

3.1 Abstract

Seismic methods are fundamental to solid earth research and exploration. High resolution three-dimensional (3D) seismic reflection data is tremendously rich, yet the challenge of recovering information connected to geological process or macroscopic rock texture remains unresolved. We introduce a suite of methods for volumetric classification or "domaining" of seismic reflectivity data based on texture. They have potential to reveal geological and geotechnical domains that would otherwise remain hidden, particularly for hard-rock settings where changes in average velocity may be negligible across rock volumes that exhibit significant change in rock texture. Dip steered seismic texture attributes like; contrast, entropy, and homogeneity, are used as input to cluster based geo-statistical techniques to recover new volume rendered images and a seismic texture reference diagram. Seismic texture domaining is tested on seismic surveys in Nevada, USA and Kevitsa, Finland. For the Nevada data, the technique delivers distinct textural domains that map to cover sequences and textures within fault zones. Here texturally similar domains are sufficiently resolved to be integrated within cooperative inversion of magnetotelluric and seismic data to recover vastly improved subsurface conductivity distributions. In Finland, seismic textural domains are linked to the distribution of Ni at the polymetallic Kevitsa mine site.

3.2 Seismic texture and geology

The seismic reflection method aims to map the distribution of true relative reflectivity amplitudes, which can be interpreted to recover the distribution of geological boundaries and structures (Yilmaz 2001b). The method is deployed extensively and successfully by the hydrocarbon industry. Detailed subsurface structures, ranging from salt bodies (Yilmaz 2001a, Jones and Davison 2014) to conventional hydrocarbon seal and reservoir systems are routinely imaged in remarkable detail. More recently, seismic reflection methods were applied in the hard-rock environment, with 3D seismic starting to play a crucial role in delineating a wide range of mineral ore deposits (Harrison and Urosevic 2012, Malehmir et al. 2012). However, there remain many challenges for seismic reflection imaging and one is to develop methods able to provide volumetric information concerning distribution of rock type and texture.

Texture is a very 'human property'. It may relate to any combination of shape, size, roughness, smoothness, orderliness, randomness, contrast, and homogeneity of an object or elements of an object. Rock texture is often associated with the specific nature, composition or arrangement of mineral crystals. However, at a larger scale, rock mass may also be linked to a multitude of macroscopic textures associated with jointing, faulting, metamorphic processes, metasomatic processes or depositional/post-depositional processes in sediments (Malehmir et al. 2012, Koivisto et al. 2012, Muntean et al. 2011, Cline et al. 2005).

In hard rock settings it is possible or even common for two rock volumes to have similar average acoustic velocity (Salisbury, Harvey, and Matthews 2003, Malehmir et al. 2014) but dramatically different seismic and rock texture. Discriminating between such volumes can be critical, especially when exploring for economic ores. We will show how "seismic texture domaining" can be achieved with a combination of seismic attributes and multivariate statistics.

Seismic attributes are extensively used in the hydrocarbon industry. For example they routinely provide indications of 4D reservoir fluid movements in time and space (Liner 2004, Grochau et al. 2014). A comprehensive table of applications for seismic attributes is provided by Roden, R., Smith, T. and Sacrey, D (2015) (Roden, Smith, and Sacrey 2015).

The techniques we develop can automatically classify domains with common seismic texture, based on dip-steered textural attributes and statistical clustering. In essence, four textural attributes, energy texture, entropy, homogeneity and contrast (Chopra and Marfurt 2007, Haralick, Shanmugam, and Dinstein 1973, Gao 2003, Chopra and Alexeev 2006, Di and Gao 2017, Amtmann et al. 2017) become the input to k-means clustering to produce new volume rendered images containing domains with common seismic texture. Computational details for our seismic texture domaining is included in the section 3.8, Methods.

Three examples are provided to show the application and value of "textural domaining". These focus on (i) characterisation of deep cover and basement at a site in Nevada USA (ii) rock mass characterisation at the Kevitsa mine in Finland, and (iii) textural domains as input to cooperative inversion. Background on each site is provided as supplementary information. Fig. 3- 1 shows the test site locations and a diagram that graphically illustrates the inputs and outputs needed for our volumetric domaining based on seismic texture. The volume rendered images in Fig. 3- 1 are for a 5 km by 5km by 2 km cube at the Nevada site. This diagram provides a high level view of the conversion of a 3D seismic reflectivity data to domains with common seismic texture. It also represents an outcome from the rapidly evolving discipline of cooperative inversion (Moorkamp 2017, Lines, Schultz, and Treitel 1988) (see section Example 3: Seismic texture and cooperative inversion).

3.3 Examples

3.3.1 Example 1: Seismic texture domains in cover and basement rock, Nevada USA

Partitioning of the seismic reflectivity volume to a finite number of domains (or clusters) with common seismic texture is achieved with k-means analysis (see the Methods section 3.8). For k-means analysis it's possible to generate outcomes with any number of clusters; however, the outcome may fail to have value if the number of clusters are too high or low.

Internal Cluster validation measures (Davies and Bouldin 1979) provide a possible rational for determining the optimal number of clusters. They are statistical guides based on coherences within clusters and distances between cluster subvolumes. Specifically, we've employed the Davies-Bouldin and Calinski-Harabsz validation

measures (Davies and Bouldin 1979) to help choose the number of clusters as described in the section 3.8, Methods. These suggest that between 3 and 10 clusters would be reasonable for the Nevada data set (also see Fig. 3- 1 for outcomes with 5, 6, 7, and 8 clusters) and we'll explore a seven-cluster image and accompanying seven cluster seismic texture reference diagram. In selecting seven clusters we are partly guided by the validation measures and partly by the recognition of at least three significant seismic textural domains within basement and cover rocks for the Nevada reflectivity volume.

Once the number of clusters is selected, the mean values of the centroids from the clustering, based on the four input seismic texture attributes can be plotted. This is graphically expressed as the "seven-cluster seismic texture reference diagram" which provides the seismic texture combinations that characterise each cluster (i.e. domain). Some clusters will be distinct and map out a distinct rock mass while sets of clusters can be more gradational in nature.

Fig. 3- 2 provides depth slice images at 400 m below ground level for the; seismic reflectivity image (Fig. 3- 2A), energy texture (Fig. 3- 2B), homogeneity texture (Fig. 3- 2C), entropy texture (Fig. 3- 2D), contrast texture (Fig. 3- 2E), seven cluster seismic texture cluster image (Fig. 3- 2F), and the seven cluster seismic texture reference diagram (Fig. 3- 2G). Note that the clusters shown in the reference diagram (Fig. 3- 2G), and seismic texture domain image (Fig. 3- 2F) are colour-matched so that the spatial distribution textural character is clear.

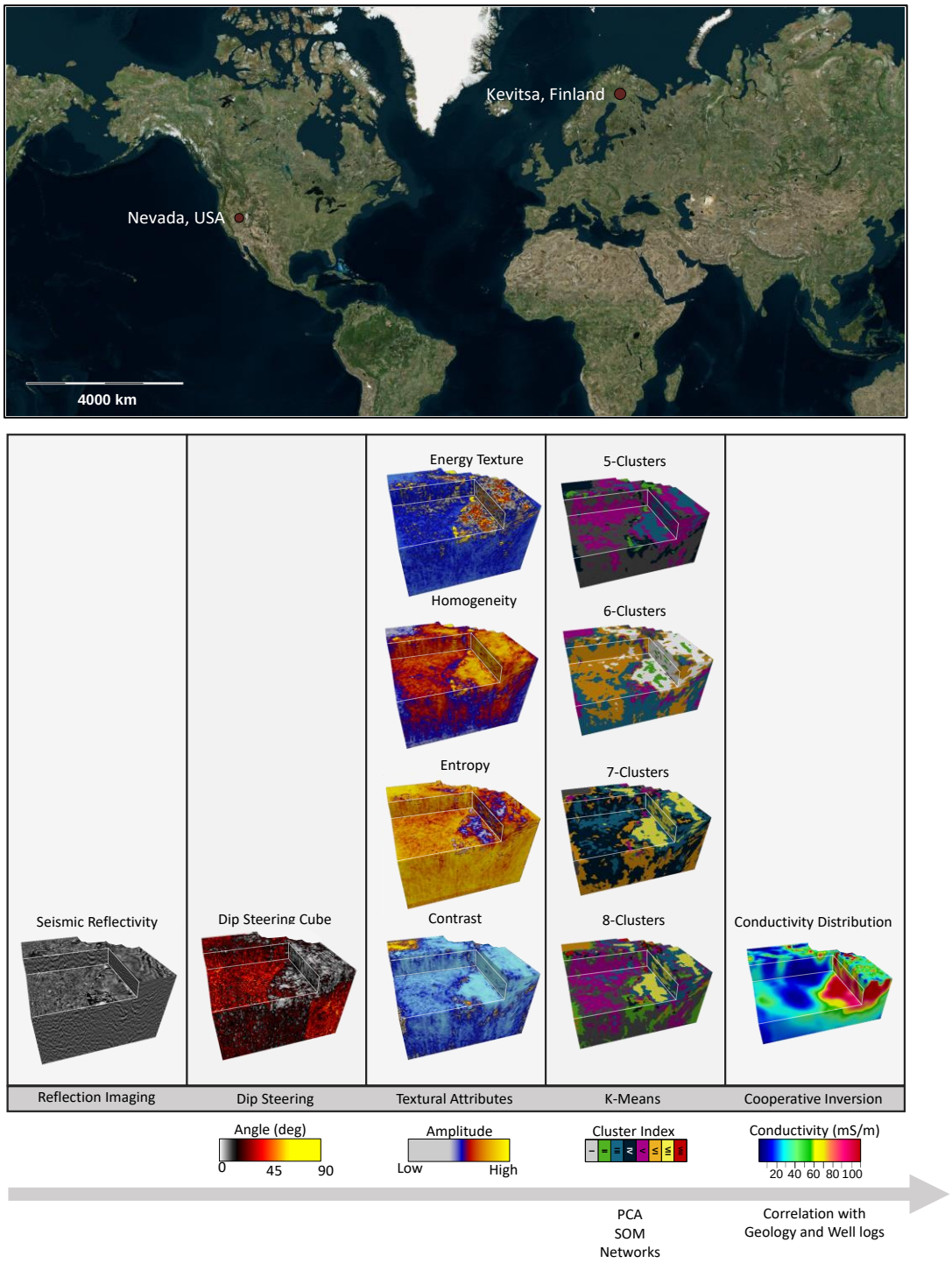

Fig. 3- 1: World map (Microsoft 2017) showing the location of the 3D seismic surveys from the Carlin gold district in Nevada, USA, and the polymetallic Kevitsa mine site in Finland (Upper). A graphic overview representing the major steps and outcomes for seismic texture domaining (Bottom). Each image is an approximate 5 km by 5 km by 2 km cube. The reflectivity image is post-stack seismic data. The schematic provides the steps required to take the Nevada seismic reflectivity volume, from dip-steered textural attributes, to the outcome of k-means analysis for 5, 6, 7 and 8 clusters, and finally to an electrical conductivity distribution derived from cooperative inversion.

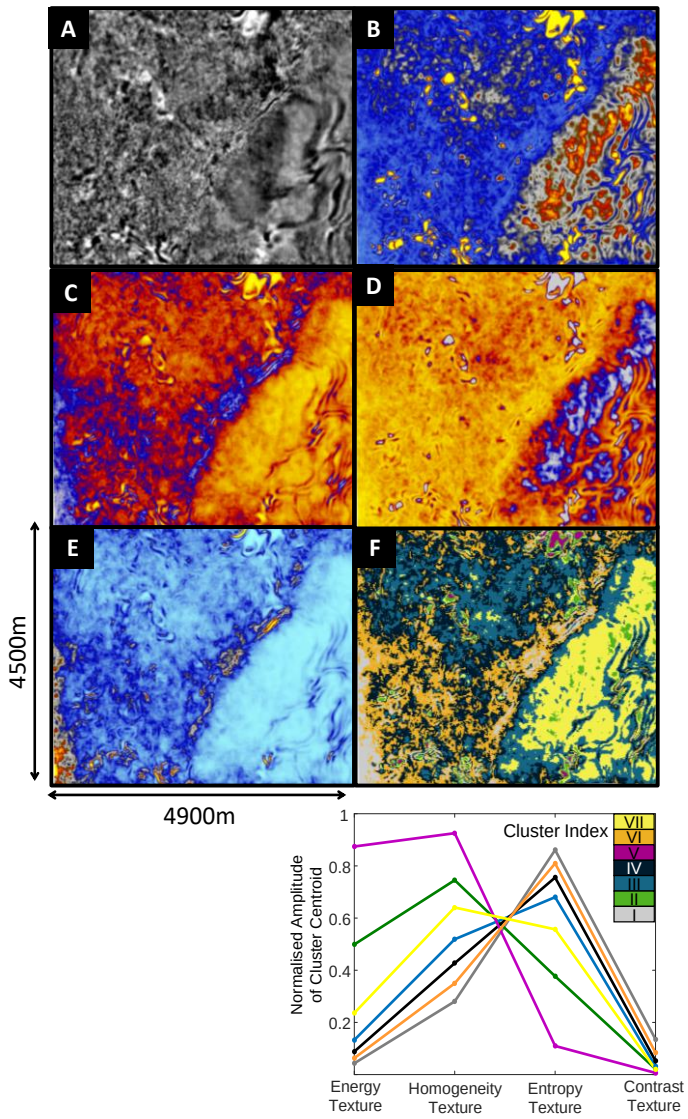

Fig. 3- 2: Horizontal slices extracted from the Nevada seismic volumes at 400 m below ground level for A) Seismic reflectivity, B) energy texture, C) homogeneity texture, D) entropy texture, E) contrast texture and F) seven cluster seismic texture image. The relationship between seismic texture of each of the seven clusters is shown. In the above, the seismic reflectivity volume is converted to volumetric domains with common seismic texture.

The depth slice in Fig. 3- 2F immediately reveals the sharp transition from Palaeozoic basement rock to younger cover, which is dominated by the cluster VII (yellow). However, the value of textural domaining lies with volumetric analysis. Fig. 3- 3 provides several representations of the 3D distribution of textual domains along with a comparison with geochemical analysis (Ca and Fe) obtained from cores in two drill holes.

For Fig. 3- 3A, B, C and D we have completed an additional processing step. A volume statistics filter that replaces the centre value of a sliding 3D calculation window with the most frequent occurrence value is applied (dGB Earth Sciences 2015). We use a calculation window of five inline and five crossline traces, with a depth gate of 15 m. Fig. 3- 3D provides a vertical section showing seismic texture domains with logs of Fe and Ca concentrations recovered from cores at two drill holes. The largest changes in chemistry are broadly mapped textural domains hinting at connections between cluster distribution geological environments and geological processes. In particular, the large difference between basement and cover sequences at approximately 257 m in Hole 2 and at 594 m in Hole 1 are clear. Both geochemistry and distribution textural domains indicate a complex, transitional zone from cover to basement.

In Fig. 3- 3, Cluster VII (yellow) is distinct and exhibits simultaneously medium homogeneity and entropy texture but low energy and contrast texture. Cluster VII is an expansive seismic texture domain that has a strong link to shallow dipping electrically conductive packages of rock in cover. It is almost exclusively found within the cover sequences.

In contrast to Cluster VII (yellow), Cluster I (grey) exhibiting the highest entropy and contrast texture but lowest homogeneity and energy texture cluster centroids. Cluster I maps to specific relatively narrow 3D subvolumes in or behind the major faulted transition zone in Palaeozoic basement rock. Cluster I (grey) could be thought of the extreme of the volumetrically more extensive Cluster VI (orange).

Cluster V (magenta), maps out a textural domain with high energy and homogeneity texture but low entropy and contrast texture centroids. Cluster I (grey) and Cluster V (magenta) are distinct textural extremes that are almost never spatially associated.

Some seismic texture domains are almost exclusive to cover or basement for the Nevada example (e.g. Cluster VII); however, others (see Clusters III or IV in Fig. 3-3) are represented in both cover and basement. This is not unreasonable as expansive packages of volcanic rock are indeed found in cover and the Palaeozoic basement rock. More generally it’s incorrect to impose an expectation that textural domaining should provide a direct map of solid geology. What it does is offer a tool to significantly improve volumetric interpretation of seismic data where some volumes with common macroscopic rock texture may be mapped.

Seismic texture domaining can also identify important but subtle textural changes across and along faults. There are several examples in the Nevada images. Point A in Fig. 3- 3E highlights a vertical feature in the seismic textural domains that would be exceedingly difficult recognized with the original reflectivity data.

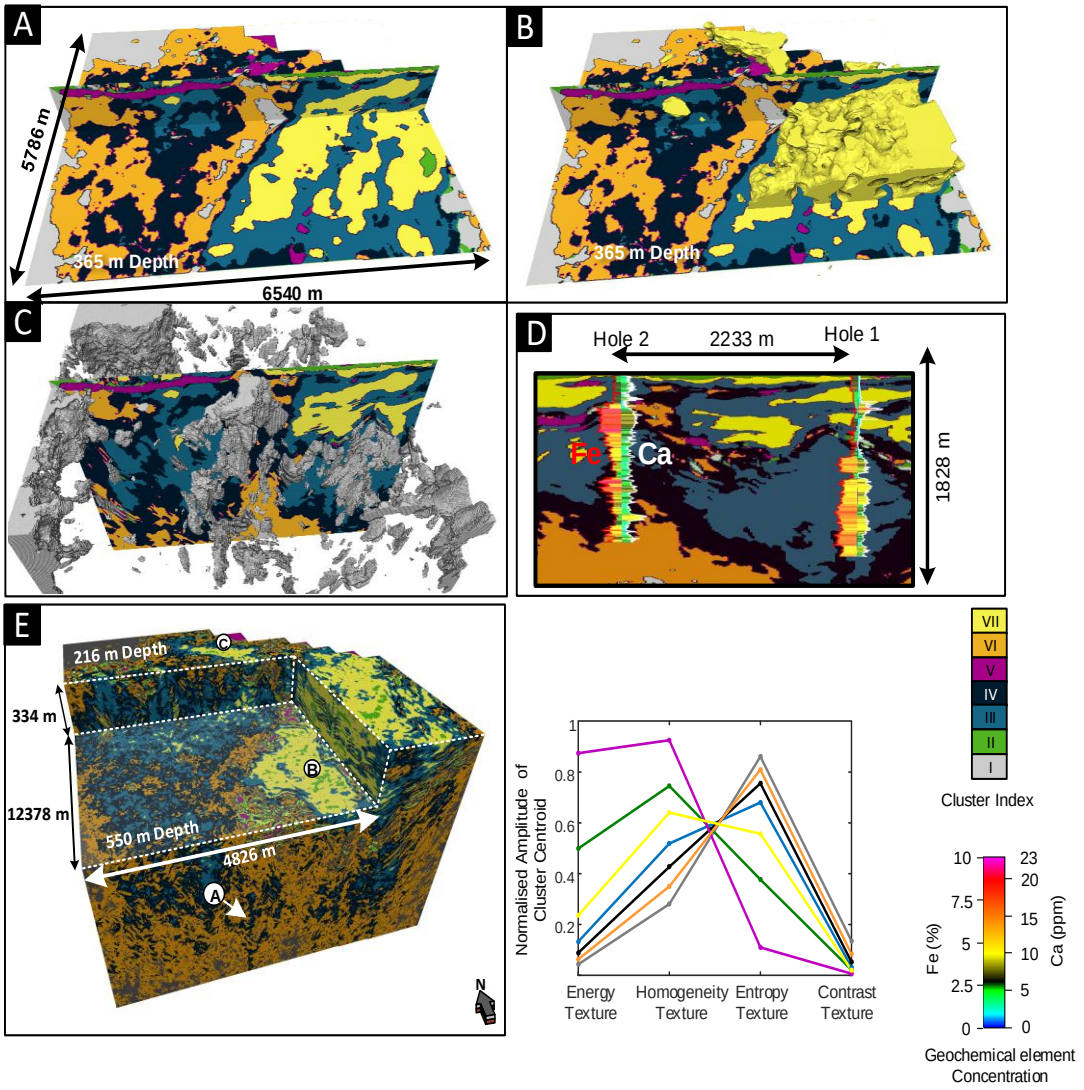

Fig. 3- 3: Volume rendered 3D images from seismic textural domaining of the Nevada USA reflectivity data. A) A crossline and plan-view section extracted from the filtered 3D cluster volume at 365 m depth. B) A 3D rendering of the Cluster VII (yellow), which relates to a distinct group of sediments in cover. C) A 3D rendering of Cluster I (grey) that maps out narrow sub-volumes nested along the major fault. D) A cross section view through drill holes 1 and 2 showing distribution of Fe and Ca relative to the seismic textural clusters. E) Seven cluster seismic texture image. The relationship between seismic texture of each of the seven clusters is shown. The major fault is down-thrown to the right of the images and Clusters III, IV and VI dominate the basement rock.

3.3.2 Example 2: Seismic Texture and Rock Mass Characterisation, Kevitsa Finland

The same steps taken to create seismic texture domains for the Nevada seismic reflectivity image have been followed for the Kevitsa data. Here k-means cluster analysis is tested for the range from 2 to 11 clusters. As with the Nevada data set, the Davies-Bouldin and Calinski-Harabasz cluster validation measures are computed. When viewed together they suggest anywhere between 5 and 10 clusters would be reasonable. For Kevitsa we examine images with 10 clusters, which is three additional clusters compared to the example from Nevada. We select a higher number of clusters to examine the potential influence of low signal-to-noise zones on the margins of the seismic data coverage. That is, we deliberately include very low fold seismic data at the north of the seismic image and examine how anomalously lower quality (e.g. low or inconsistent seismic fold) data may be represented by textural domaining.

Fig. 3- 4 shows depth slice images at 500 m below ground level, for the Kevitsa seismic data. It includes the four GLCM seismic texture attribute images (Fig. 3- 4B, C, D and E), a horizontal slice through the seismic textural domains (Fig. 3- 4F) and the associated 10-cluster seismic texture reference diagram (Fig. 3- 4). Superimposed on each panel is a 0.15% Ni cut-off contour to broadly represent the shape of the Kevitsa Ni mineralisation. The images of seismic textures are provided with an intensity overlay of the cosine of phase seismic attribute which gives a detailed impression of the seismic reflectivity distribution.

The northern limit of the images is characterised by Clusters IV (purple), V (magenta) and X (rose). These clusters map out the anomalous textural extremes associated with the poor seismic fold connected to low or inconsistent coverage of seismic source and receiver combinations (i.e. deliberately included at the Northern margin).

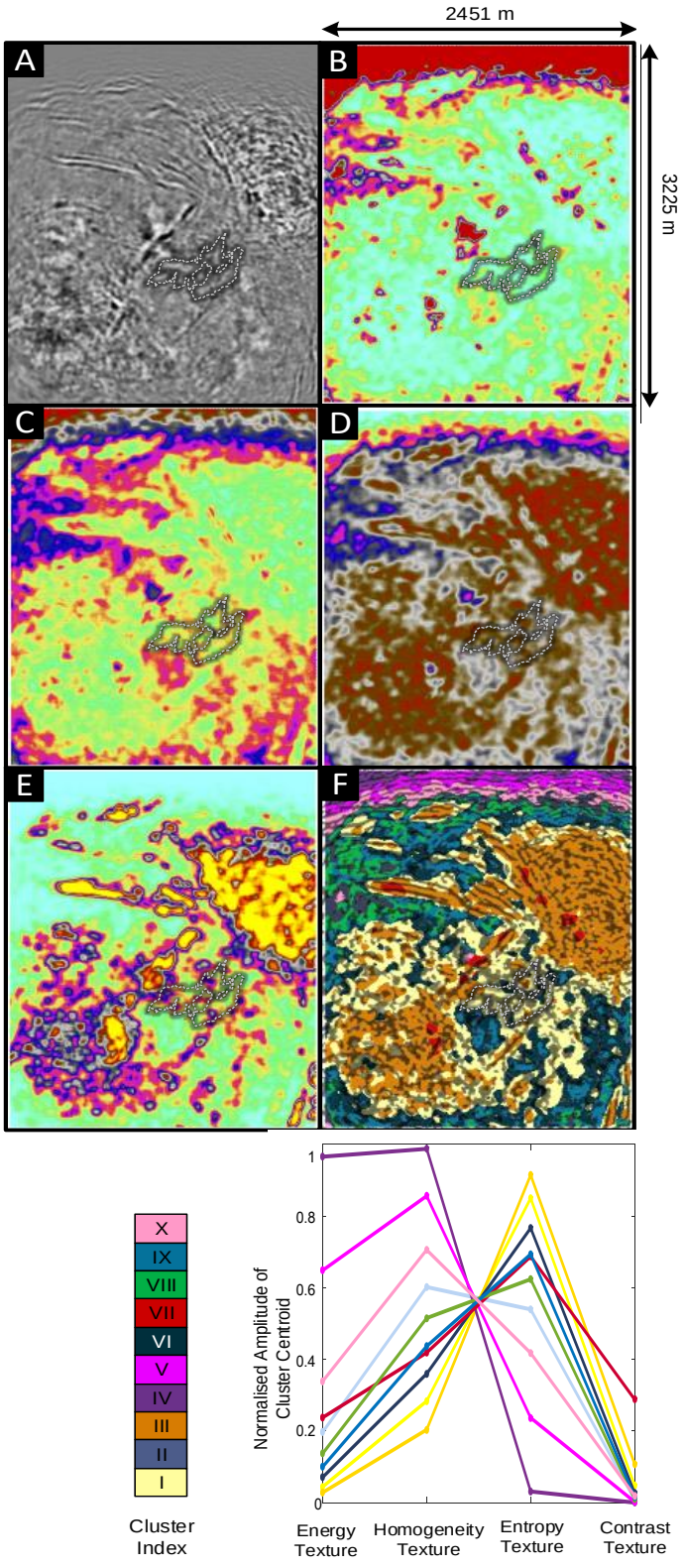

Fig. 3- 4: Reflectivity image, GLCM textural seismic attributes and textural clusters at a depth slice at 500 m below ground level for the Kevitsa site; Finland. The image includes: A) Seismic reflectivity. B) energy texture, C) homogeneity texture, D) entropy texture, E) contrast texture, and cluster indexes. The dotted white line shows the contour of 0.15% Ni concentration. F)

the seismic textural domains overlaid by the seismic attribute cosine of phase. The relationship between seismic texture of each of the ten clusters at the Kevitsa site is provided.

In Fig. 3- 4, the interior of the 0.15% Ni shell is dominantly Cluster I (yellow). Little of Cluster II (grey blue) or Cluster III (orange) is associated with the ore shell at the 500 m below ground level depth slice. There are also near linear bounding zones of Clusters III (orange) and VII (red) to the north-west and south-east of 0.15% Ni shell. The ore shell also appears to be bounded by Clusters IX (Turquoise) to the south-west. The general observation from the above is that cluster distribution at the 500 m depth slice provides geometric control over distribution of Ni. The textural domaining simplifies this complex 3D seismic volume, in which phases of emplacement of Cu, Ni, and PGE ore may crosscut major stratigraphic dips (Malehmir et al. 2012). An important conclusion is that while no cluster uniquely matches the Ni shell, there are geometric associations with clusters surrounding the ore shell but rarely crossing into it. A volume rendered image in the supplementary information (Fig. 3- 7) illustrates how Cluster III (orange) appears to wrap around the 0.15% Ni concentration volume. It is the overall association between distributions of mineralization, barren host rock and seismic texture that present enticing direction for seismic reflection. Textural domaining is mapping volumetric distributions of seismic reflectivity likely to be linked with macroscopic geological processes that were not previously considered.

Fig. 3- 5 provides a larger volumetric representation of seismic texture domains at Kevitsa. Here the “bowl” shape of the rock mass that hosts the Kevitsa deposit is traced out by Clusters I (yellow) and Cluster III (orange). A density log is included on the image and shows a sharp increase in density midway down the hole, associated with a transition from Cluster III (orange) to Cluster I (yellow) dominated rocks.

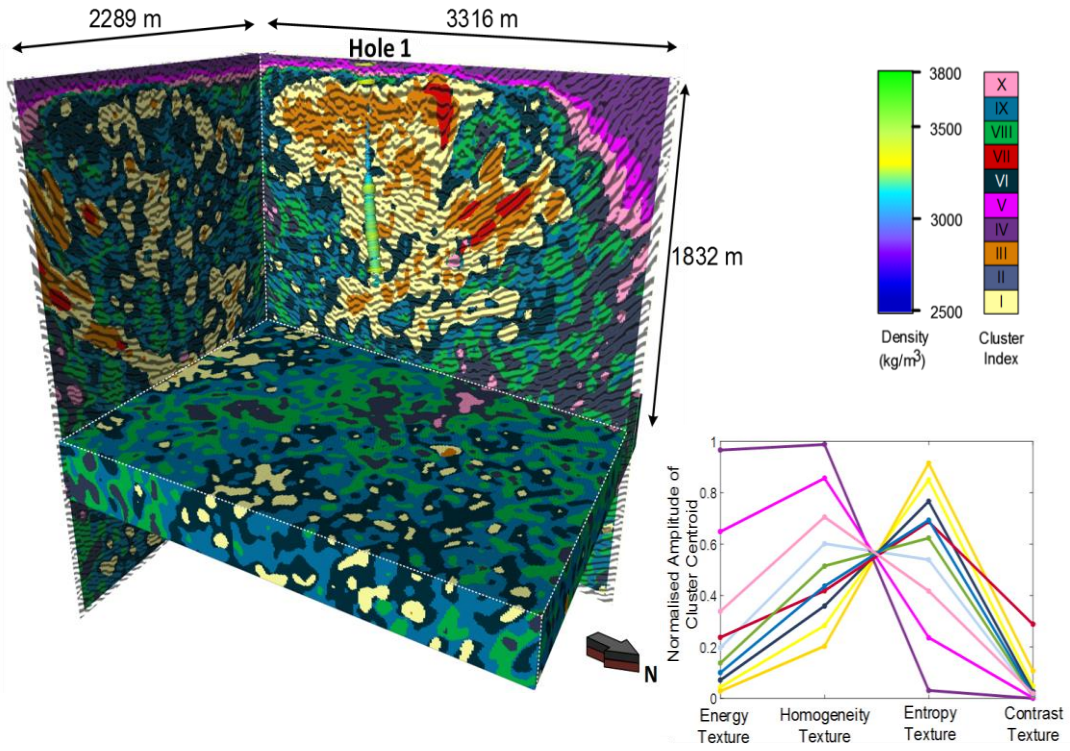

Fig. 3- 5: A cutaway 3D image of the Kevitsa seismic textural domains with an accompanying 10-cluster reference diagram. Overlying the data is a density well log from Hole 1. Several observations can be made in relation to the distribution of each cluster. Clusters IV, V and X represent anomalous textures at the fringes of quality imaging. Textural domaining provides volumetric information from which anomalous or zones of interest are quickly

3.3.3 Example 3: Seismic texture and cooperative inversion

Seismic textural domaining can assist large-scale rock-mass characterisation. It may also serve a different function. It may provide a framework for cooperative inversion intended to significantly improve the value of much lower-resolution electromagnetic or potential fields methods (See Fig. 3- 8 in the section Supplementary information).

For this application large subvolumes or textural domains with common seismic textures may be assigned conductivity based on output of unconstrained inversion or via some form of transfer function. These concepts were first explored and fully described by (Le et al. 2016), who use classic geometric seismic attributes (e.g., polar dip) in their comprehensive guide to cooperative inversion. The Nevada seismic data accompanied by close to 200 full tensor MT measurements acquired on a 3D grid. Specifications and technical details of the seismic and MT surveys for the Nevada data

are presented in Semiautomatic and Automatic Cooperative Inversion of Seismic and Magnetotelluric Data. Surveys in Geophysics (Le et al. 2016).

The cooperative inversion process has potentially to be automated because the conductivity distribution from initial unconstrained inversion of MT data is directly transferred to a single value in each subvolume as defined by the seven textural clusters (see section 3.13.2 MT inversion and Cooperative inversion). Construction of the initial or seed conductivity model triggers the final round of constrained MT inversion which we run on a Cray XC40 supercomputer system. Because the seed model that feeds the final inversion has the gross conductivities from unconstrained inversion superimposed on the detailed geometries inherited from the seismic texture domains, the final inverted conductivity distribution gains significant improvement in resolution. It is also encouraging that an exceedingly low RMS error of less than 2% is achieved by this method for a data set with some 200 full-tensor MT measurements as input.

Fig. 3- 6 compares simplified seismic texture clusters (see Fig. 3- 6A) with unconstrained MT inversion (Fig. 3- 5B) and the outcomes of seismic texture guided cooperative inversion (Fig. 3- 5C), for the Nevada data set. The planar cut-surface in Fig. 3- 6 is set at 400 m below ground level.

After cooperative inversion, the relationship between Cluster VII (yellow) and high conductivities in cover becomes clear. The depths and geometry of conductive cover match with that expected from both seismic and drilling. The detailed conductivity distribution revealed after cooperative inversion elevates the value of the MT survey (Le et al. 2016). The geometry of the major fault and detailed cover thickness become clear in the conductivity distribution.

The geometry of seismic texture Cluster VII (yellow) is sufficient to guide the MT inversion outcome towards detailed shallow three-dimensional conductive channel features in basement. These run south east towards the major fault. While there are scattered hints of these features in the outcome of the unconstrained MT inversion, they are not interpretable and only come into focus after cooperative inversion is applied.

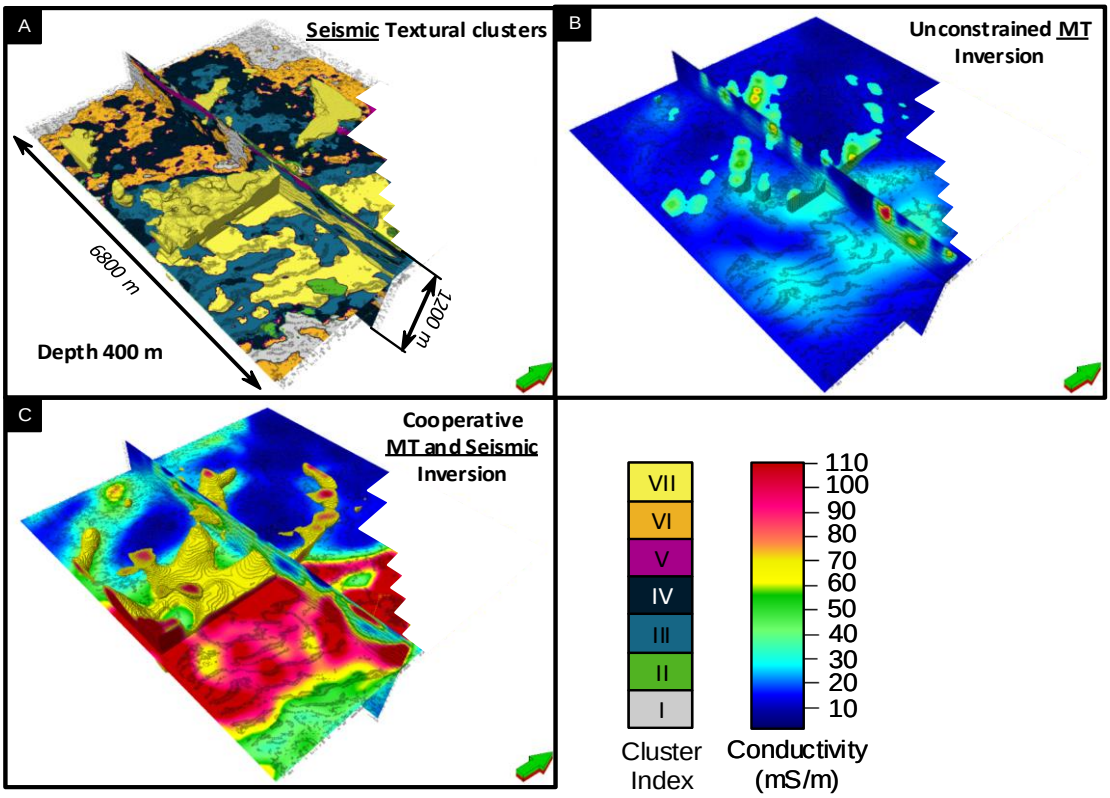

Fig. 3- 6: Volume rendered images of textural domains and conductivity distribution from cooperative inversion of co-located seismic and MT data from Nevada, USA. The Figure contains (A) a 3D representation of textural domains, (B) the resulting conductivity distribution from unconstrained MT inversion and (C) the conductivity distribution after the implementation of cooperative inversion assisted by seismic textural domaining.

3.4 Discussion

Subtle changes in seismic texture cannot be systematically mapped by the human interpreter within seismic reflectivity images. Rigorous multivariate statistical clustering or similar methods are needed. We have presented methods for partitioning a reflectivity volume into discrete textural domains. Under ideal circumstances, our seismic texture domains (i.e., the clusters) will link with rock mass with mappable geological or geotechnical character.

Modern seismic reflection methods are rapidly converging to consistent high quality true relatively amplitude processing. However, it should be recognised that recovery of 3D seismic reflectivity from raw field records (e.g., pre-stack shot records) may not always generate a precise representation of true subsurface relative reflectivity distribution. In this case it is possible for some clusters to map to artefacts or

inadequacies inherited from seismic processing or acquisition. Further we acknowledge the importance of choosing a meaningful number of clusters for k-means analysis. If a large number of clusters are chosen to represent a seismic reflectivity volume, then it is likely that sets of clusters will be texturally gradational and in this case, it may be difficult for any single cluster to map the boundaries of a distinct rock mass. Certainly, internal clustering validation measures provide the baseline quantitative method to determine the natural or optimal number of clusters for k-means analysis.

The "best" circumstance for mapping seismic texture domains to a distinct rock mass is when the nature of reflectivity persists and repeats throughout a volume of rock. For example, a persistent chaotic, high-contrast reflectivity domain will be readily mapped against a chaotic but low-contrast domain by seismic textural domains in circumstances where it's highly improbably that this type of subtle but quantifiable change in seismic texture can be mapped by an interpreter.

An opposite and unlikely extreme would exist if all rock volumes were uniform (or varied slowly) in velocity and density. In this case the cluster representing each volume can only represent the absence of reflectivity. In this end member scenario, where large rock volumes are completely uniform textural domaining can only map out differences in seismic texture along dividing boundaries. Fortunately, perfectly uniform rock volumes are exceedingly rare in nature.

Textural domaining provides one representation of the seismic reflective data and its necessary to reference interpretation back to the original reflectivity image. It's also helpful to map textural domains over other seismic attributes like cosine of phase. In Fig. 3- 6, this was achieved directly by superimposing the cosine of phase attribute onto textural clusters. Here we directly observe the geometry of reflections relative to clusters and can intuitively assess how k-means analysis has statistically partitioned textually similar domains within the seismic volume.

Ultra-high resolution seismic (Mueller, Woelz, and Kalmring 2013, Klokov, Treviño, and Meckel 2017) and deep learning (LeCun, Bengio, and Hinton 2015) algorithms are on our doorstep and processes like those represented in Fig. 3- 1 will likely drive new outcomes that can be automated by high-level code (Strecker and Uden 2002, Orozco-del-Castillo et al. 2017, Amtmann et al. 2017). In the near future it should be

possible to apply processes like seismic textural domaining across multiple 3D seismic surveys to trace geologically environments or even mineralization throughout entire geological provinces.

3.5 Conclusion

Seismic reflection methods are often essential for subsurface exploration (e.g., hydrocarbon, mineral, water, geothermal) and earth science research. We have provided new techniques and examples for extracting geological meaning from reflectivity data based on seismic texture. A set of grey level co-occurrence matrix textural seismic attributes is combined with k-means analysis for classifying the 3D seismic volume into seismic domains with common texture. Images of textural domains are accompanied by a seismic texture reference diagram. Selection of the optimum number of attributes is assisted by internal clustering validation measures. The combination of seismic textural domaining with the seismic texture reference diagram is unique and can reveal subtle variations in subsurface rock mass character. Under some circumstances the seismic texture clusters may directly recover the volumetric distribution of geologically similar rock mass.

The method is tested on high-resolution 3D land seismic reflectivity data sets from Nevada, USA and Kevitsa, Finland. We have chosen examples from hard-rock terrains where seismic reflection data is poorly endowed with continuous distinct reflections. The value of our methods becomes clear in these challenging terrains where exceedingly subtle variations in acoustic impedance distribution can be revealed as texturally distinct domains. For the Nevada example, we are able to highlight shallow channels and zones within fault transitions that are texturally distinct. We also demonstrate how textural domaining may feed into and improve cooperative inversion. For the example from Finland we show relationships between Ni Concentration at the polymetallic Kevitsa mine site and distribution of seismic texture domains.

Textural domaining provides significant steps towards mapping volumetric distributions of seismic reflectivity linked with macroscopic geological environments and processes. Seismic texture domaining and accompanying reference diagrams provide new insight into the subsurface and will hopefully acts as a catalyst for related methods of extracting geological meaning from increasingly cost effective, information rich, high-resolution 3D seismic reflectivity images.

3.6 Acknowledgments

This work has been supported by the Deep Exploration Technologies Cooperative Research Centre (DET CRC) whose activities are funded by the Australian Government's Cooperative Research Centre Program. This is DET CRC Document 2017/1013. Cuong V. A. Le would like to acknowledge the Australian government who has provided him an Australian Awards Scholarship. We would like to acknowledge and thank Barrick Gold for use of their comprehensive geophysical datasets from Nevada. We thank both First Quantum (former data owner) and Boliden (new data owner, 2017) for access to the Kevitsa seismic data from Finland. This work was supported by resources provided by the Pawsey Supercomputing Centre with funding from the Australian Government and the Government of Western Australia. We would like to thank Gary Egbert, Anna Kelbert and Naser Meqbel for permitting access to the 3D MT inversion code ModEM3D. We appreciate dGB Earth Science for providing the OpendTect software and Schumberger for providing access to their Petrel software. We are also grateful to Lee Sampson from Barrick Gold Corporation, and Chris Wijns from First Quantum for considerable assistance with the data sets and geological context at Nevada and Finland respectively.

3.7 References

Alférez, Germán H, Jocksan Rodríguez, Benjamin Clausen, and Lance Pompe. 2015. "Interpreting the Geochemistry of Southern California Granitic Rocks using Machine Learning." Proceedings on the International Conference on Artificial Intelligence (ICAI).

Amtmann, Johannes, Christoph Georg Eichkitz, Denise Hofer, and Marcellus Gregor Schreilechner. 2017. "Clustering of seismic attributes for automatic seismic interpretation—first tests on synthetic geological models." First Break 35 (5):65-69.

Chopra, Satinder, and Vladimir Alexeev. 2006. "Applications of texture attribute analysis to 3D seismic data." The Leading Edge 25 (8):934-940.

Chopra, Satinder, and Kurt J. Marfurt. 2007. Seismic attributes for prospect identification and reservoir characteriztion. Edited by Stephen J. Hill, SEG Geophysical Development Series No. 11. United States of America: Tulsa, Okla. (8801 South Yale St., Tulsa OK 74137-3175) : Society of Exploration Geophysicists

Cline, Jean S., Albert H. Hofstra, John L. Muntean, Richard M. Tosdal, and Kenneth A. Hickey. 2005. "Carlin-Type Gold Deposits in Nevada: Critical Geologic Characteristics and Viable Models." Economic Geology 100th anniversary volume:451-484.

Davies, David L., and Donald W. Bouldin. 1979. "A Cluster Separation Measure." IEEE Transactions on Pattern Analysis and Machine Intelligence.

deGroot-Hedlin, C., and S. Constable. 1990. "Occam's inversion to generate smooth, two-dimensional models from magnetotelluric data." Geophysics 55 (12):1613-1624. doi: 10.1190/1.1442813.

dGB Earth Sciences. 2015. "OpendTect dGB Plugins User Documentation version 4.6." Last Modified 02/05/2016. http://opendtect.org/relman/4.6.0/unpacked/4.6.0/doc/User/dgb/chapter2.3_attributes_with_steering.htm.

Di Giuseppe, Maria Giulia, Antonio Troiano, Claudia Troise, and Giuseppe De Natale. 2014. "k-Means clustering as tool for multivariate geophysical data analysis. An application to shallow fault zone imaging." Journal of Applied Geophysics 101:108-115.

Di, Haibin, and Dengliang Gao. 2017. "Nonlinear gray-level co-occurrence matrix texture analysis for improved seismic facies interpretation." Interpretation 5 (3):SJ31-SJ40.

Egbert, Gary D., and Anna Kelbert. 2012. "Computational recipes for electromagnetic inverse problems." Geophysical Journal International 189 (1):251-267. doi: 10.1111/j.1365-246X.2011.05347.x.

Foged, N, Pernille Aabye Marker, AV Christansen, Peter Bauer-Gottwein, F Jørgensen, A-S Høyer, and Esben Auken. 2014. "Large-scale 3-D modeling by integration of resistivity models and borehole data through inversion." Hydrology and Earth System Sciences 18 (11):4349-4362.

Gabàs, A, A Macau, B Benjumea, P Queralt, J Ledo, S Figueras, and A Marcuello. 2016. "Joint Audio-Magnetotelluric and Passive Seismic Imaging of the Cerdanya Basin." Surveys in Geophysics 37 (5):897-921.

Gao, Dengliang. 2003. "Volume texture extraction for 3D seismic visualization and interpretation." Geophysics 68 (4):1294-1302.

Grochau, Marcos Hexsel, Pedro Monteiro Benac, Leonardo de Magalhães Alvim, Rui Cesar Sansonowski, Paulo Roberto da Motta Pires, and Florine Villaudy. 2014. "Brazilian carbonate reservoir: A successful seismic time-lapse monitoring study." The Leading Edge 33 (2):164-170.

Hall-Beyer, M. 2007. "GLCM Texture Tutorial." http://www.fp.ucalgary.ca/mhallbey/tutorial.htm.

Haralick, R. M., K. Shanmugam, and I. Dinstein. 1973. "Textural Features for Image Classification." IEEE Transactions on Systems, Man, and Cybernetics SMC-3 (6):610-621. doi: 10.1109/TSMC.1973.4309314.

Harrison, Christopher B., and Milovan Urosevic. 2012. "Seismic processing, inversion, and AVO for gold exploration — Case study from Western Australia." GEOPHYSICS 77 (5):WC235-WC243. doi: 10.1190/geo2011-0506.1.

Hillis, R., D. Giles, S. Van Der Wielen, A. Baensch, J. Cleverley, A. Fabris, S. Halley, B. Harris, S. Hill, P. Kanck, A. Kepic, S. Soe, G. Stewart, and Y. Uvarova. 2014. "Coiled Tubing Drilling and Real-Time Sensing: Enabling Prospecting Drilling in the 21st Century?" In Building exploration capability for the 21st century, edited by Karen D. Kelley and Howard C. Golden, 243-259. Society of Economic Geologists, Inc.

Jones, Ian F, and Ian Davison. 2014. "Seismic imaging in and around salt bodies." Interpretation 2 (4):SL1-SL20.

Kelbert, Anna, Naser Meqbel, Gary D Egbert, and Kush Tandon. 2014. "ModEM: A modular system for inversion of electromagnetic geophysical data." Computers & Geosciences 66:40-53.

Klokov, Alexander, Ramón H Treviño, and Timothy A Meckel. 2017. "Diffraction imaging for seal evaluation using ultra high resolution 3D seismic data." Marine and Petroleum Geology 82:85-96.

Koivisto, Emilia, Alireza Malehmir, Pekka Heikkinen, Suvi Heinonen, and Ilmo Kukkonen. 2012. "2D reflection seismic investigations at the Kevitsa Ni-Cu-PGE deposit, northern Finland." Geophysics 77.

Le, Cuong V. A., Brett D. Harris, and Andrew M. Pethick. 2016. "Magnetotelluric inversion, carbonaceous phyllites and an ore zone: Kevitsa; Finland." ASEG-PESA 2016, Adelaide, Australia.

Le, Cuong V. A., Brett D. Harris, Andrew M. Pethick, Eric M. Takam Takougang, and Brendan Howe. 2016. "Semiautomatic and Automatic Cooperative Inversion of Seismic and Magnetotelluric Data." Surveys in Geophysics 37 (5):845-896. doi: 10.1007/s10712-016-9377-z.

LeCun, Yann, Yoshua Bengio, and Geoffrey Hinton. 2015. "Deep learning." Nature 521 (7553):436-444.

Lindsten, Fredrik, Henrik Ohlsson, and Lennart Ljung. 2011. "Just relax and come clustering!: A convexification of k-means clustering."

Liner, Christopher L. 2004. Elements of 3D seismology. Vol. 1: PennWell Books.

Lines, Larry R, Alton K Schultz, and Sven Treitel. 1988. "Cooperative inversion of geophysical data." Geophysics 53 (1):8-20.

Liu, Yanchi, Zhongmou Li, Hui Xiong, Xuedong Gao, and Junjie Wu. 2010. "Understanding of internal clustering validation measures." Data Mining (ICDM), 2010 IEEE 10th International Conference on.

Malehmir, Alireza, Christopher Juhlin, Chris Wijns, Milovan Urosevic, Petri Valasti, and Emilia Koivisto. 2012. "3D reflection seismic imaging for open-pit mine planning and deep exploration in the Kevitsa Ni-Cu-PGE deposit, northern Finland." Geophysics 77.

Malehmir, Alireza, Emilia Koivisto, Musa Manzi, Saeid Cheraghi, Raymond J Durrheim, Gilles Bellefleur, Chris Wijns, Kim AA Hein, and Nick King. 2014. "A review of reflection seismic investigations in three major metallogenic regions: the Kevitsa Ni–Cu–PGE district (Finland), Witwatersrand goldfields (South Africa), and the Bathurst Mining Camp (Canada)." Ore Geology Reviews 56:423-441.

MathWorks. 2014a. "MATLAB." Accessed 12 January 2017. https://au.mathworks.com/help/images/gray-level-co-occurrence-matrix-glcm.html.

MathWorks. 2014b. "MATLAB." http://au.mathworks.com/help/stats/k-means-clustering.html.

Microsoft. 2017. "Bing Maps showing the locations of Nevada USA and Kevitsa Finland." Accessed March 9th 2017. https://www.bing.com/maps.

Moorkamp, Max. 2017. "Integrating Electromagnetic Data with Other Geophysical Observations for Enhanced Imaging of the Earth: A Tutorial and Review." Surveys in Geophysics:1-28.

Mueller, Christof, Susanne Woelz, and Sven Kalmring. 2013. "High-Resolution 3D Marine Seismic Investigation of Hedeby Harbour, Germany." International Journal of Nautical Archaeology 42 (2):326-336.

Muntean, John L., Jean S. Cline, Adam C. Simon, and Anthony A. Longo. 2011. "Magmatic–hydrothermal origin of Nevada's Carlin-type gold deposits." Nature geoscience.

Orozco-del-Castillo, MG, M Cárdenas-Soto, C Ortiz-Alemán, C Couder-Castañeda, J Urrutia-Fucugauchi, and A Trujillo-Alcántara. 2017. "A texture-based region growing algorithm for volume extraction in seismic data." Geophysical Prospecting 65 (1):97-105.

Roberts, A. 2001. "Curvature attributes and their application to 3D interpreted horizons." first break 19 (2):85-100.

Roden, Rocky, Thomas Smith, and Deborah Sacrey. 2015. "Geologic pattern recognition from seismic attributes: Principal component analysis and self-organizing maps." Interpretation 3 (4):SAE59-SAE83. doi: 10.1190/INT-2015-0037.1.

Salisbury, Matthew H, Craig W Harvey, and Larry Matthews. 2003. "The acoustic properties of ores and host rocks in hardrock terranes." Hardrock seismic exploration: SEG:9-19.

Samarasinghe, Sandhya. 2006. Neural Networks for Applied Sciences and Engineering From Fundamentals to Complex Pattern Recognition: Auerbach Publications.

Shen, Judong, Shing I Chang, E Stanley Lee, Youping Deng, and Susan J Brown. 2005. "Determination of cluster number in clustering microarray data." Applied Mathematics and Computation 169 (2):1172-1185.

Strecker, Uwe, and Richard Uden. 2002. "Data mining of 3D poststack seismic attribute volumes using Kohonen self-organizing maps." The Leading Edge 21 (10):1032-1037.

Takam Takougang, Eric, Brett Harris, Anton Kepic, and Cuong V. A. Le. 2015. "Cooperative joint inversion of 3D seismic and magnetotelluric data: With application in a mineral province." Geophysics 80:1-13. doi: 10.1190/GEO2014-0252.1.

Tingdahl, Kristofer M, and Matthijs De Rooij. 2005. "Semi-automatic detection of faults in 3D seismic data." Geophysical Prospecting 53 (4):533-542.

Tingdahl, Kristofer M. 2003. "Improving seismic chimney detection using directional attributes." In Soft computing and intelligent data analysis in oil exploration, edited by M. Nikravesh, F. Aminzadeh and L.A. Zadeh, 157-173. Elsevier Science Publishers, Amsterdam.

Tingdahl, Kristofer M., and Paul F. M. De Groot. 2003. "Post-stack dip and Azimuth Processing." Journal of Seismic Exploration 12:113-126.

Yenugu, Malleswar, Kurt J Marfurt, and Shane Matson. 2010. "Seismic texture analysis for reservoir prediction and characterization." The Leading Edge 29 (9):1116-1121.

Yilmaz, Ö 2001a. "Structural Inversion." In Seismic Data Analysis: Processing, Inversion, and Interpretation of Seismic Data, edited by Stephen M. Doherty, 1591-1597. United States of America: Tulsa, OK : Society of Exploration Geophysicists.

Yilmaz, Ozdogan. 2001b. Seismic Data Analysis: Processing, Inversion, and Interpretation of Seismic Data. Edited by Stephen M. Doherty. United States of America: Society of Exploration Geophysicists.

Zhao, Tao, Vikram Jayaram, Atish Roy, and Kurt J. Marfurt. 2015. "A comparison of classification techniques for seismic facies recognition." Interpretation.

Every reasonable effort has been made to acknowledge the owners of copyright material. I would be pleased to hear from any copyright owner who has been omitted or incorrectly acknowledged.

3.8 Methods

We have developed a method for domaining any seismic reflectivity volume based on seismic texture. A set of grey level co-occurrence matrix (GLCM) textural seismic attributes (Chopra and Marfurt 2007, Haralick, Shanmugam, and Dinstein 1973, Gao 2003, Chopra and Alexeev 2006) is combined with k-means analysis (Di Giuseppe et al. 2014, Gabàs et al. 2016, Alférez et al. 2015, Le et al. 2016, Zhao et al. 2015, Shen et al. 2005, Foged et al. 2014) for classifying any 3D seismic volume into domains with common texture.

New volume rendered images of textural domains are accompanied by a seismic texture reference diagram. The seismic texture reference diagram provides the set of mean values of the seismic texture attributes and these mean values characterise each cluster. Put simply, the reference diagram provides the textural character for each cluster or domain. Our first example from Nevada provided the seven-cluster texture reference diagram with the means of the four GCLM seismic texture attributes for Nevada reflectivity volume shown in Fig. 3- 2. Selection of the optimum number of attributes is also assisted by internal clustering validation measures (Liu et al. 2010) (Davies and Bouldin 1979).

The method requires a sequence of steps culminating in the generation of (i) a 3D volume that is composed of a finite set of domains with common seismic textures, and (ii) an accompanying seismic texture reference diagram. By textural “domaining” we mean the process of subdividing the reflectivity volume into a number of domains that are texturally similar. Core steps for seismic texture domaining are:

i. computation of a “dip-steering” cube from the seismic reflectivity volume (Tingdahl and Groot 2003, Tingdahl 2003, dGB Earth Sciences 2015),
ii. conversion of seismic reflectivity data to a grey-level co-occurrence matrix (GLCM) (Hall-Beyer 2007, Haralick, Shanmugam, and Dinstein 1973),
iii. computation of textural attributes from the GLCM (Chopra and Marfurt 2007, Haralick, Shanmugam, and Dinstein 1973, Gao 2003, Chopra and Alexeev 2006),

iv. k-means cluster analysis (Di Giuseppe et al. 2014, Gabàs et al. 2016, Alférez et al. 2015, Le et al. 2016, Zhao et al. 2015, Shen et al. 2005, Foged et al. 2014) to recover domains with common seismic texture,
v. computation of internal clustering validation measures,
vi. computation of the seismic texture reference diagram, and
vii. volume rendering and comparison of seismic texture, seismic reflectivity and textural clusters

Below we detail each step, working from dip steering, to computational requirements for GLCM textural attributes and k-means cluster analysis.

3.9 Dip Steering, Textural Seismic Attributes, and Cluster Analysis

The four textural attributes, energy texture, entropy, homogeneity, and contrast (Chopra and Marfurt 2007, Haralick, Shanmugam, and Dinstein 1973, Gao 2003, Chopra and Alexeev 2006) are used as input to k-means clustering. The textural attributes are computed in a small 3D sliding calculation window that glides through the full seismic volume.

We have applied "dip steering" for calculation of textural attributes within the OpendTect software (Tingdahl and Groot 2003, Tingdahl 2003) (dGB Earth Sciences 2015). The dip-steering cube is used to ensure that the attribute calculation window follows the seismic dip. For dip steering, seismic dip and azimuth are calculated at every sample position based on analysis of reflectivity in a sliding 3D window. Dip steering enhances the quality of attributes or picking horizons (dGB Earth Sciences 2015, Roberts 2001, Tingdahl and De Rooij 2005).

Seismic amplitudes in the 3D sliding calculation window can be considered as grey-scale levels or grey levels of pixels (i.e., pixel intensity). Such data can be converted to a 2D GLCM reflecting the relative frequency of concurrence of pairs of pixels with specific values in a specified spatial relationship within the 3D calculation window (Chopra and Marfurt 2007, dGB Earth Sciences 2015, MathWorks 2014a).

Each of the seismic textural attributes is calculated from the GLCM (Hall-Beyer 2007, Haralick, Shanmugam, and Dinstein 1973). The GLCM provides a statistical characterisation of seismic data within the calculation window. Once the GLCM is computed for the sliding 3D calculation window (Chopra and Marfurt 2007, dGB Earth Sciences 2015, Hall-Beyer 2007) the attributes, energy texture, entropy, contrast

and homogeneity, are computed. The mathematical expression for each textural attribute are written in the work, Seismic attributes for prospect identification and reservoir characterization (Chopra and Marfurt 2007) and are provided below:

$$\text{Energy} = \sqrt{\sum_{i,j=0}^{N-1} P_{i,j}^2} \qquad (3.1)$$

$$\text{Entropy} = \sum_{i,j=0}^{N-1} P_{i,j}\left(-\ln\left(P_{i,j}\right)\right) \qquad (3.2)$$

$$\text{Contrast} = \sum_{i,j=0}^{N-1} P_{i,j}(i-j)^2 \qquad (3.3)$$

$$\text{Homogeneity} = \sum_{i,j=0}^{N-1} \frac{P_{i,j}}{1+(i-j)^2} \qquad (3.4)$$

where $P_{i,j}$ is the ith row and jth column of the GLCM matrix P.

Each textural attribute is sensitive to a different aspect of seismic texture. The energy texture seismic attribute highlights zones of high textural stability within each calculation window. It is independent of amplitude and is suited to highlighting continuity. Energy texture should not be confused with any of the standard energy attributes. Entropy is a measure of the level of randomness in the calculation window. Homogeneity expresses a type of smoothness in reflectivity and contrast emphasises differences in amplitude.

Yenugu, Marfurt, and Matson (2010) systematically reviewed textural attributes, tracing the history of Grey Level Co-occurrence Matrix(Haralick, Shanmugam, and Dinstein 1973) to modern applications in seismic reflectivity, especially for hydrocarbon reservoir characterisation (Gao 2003, Chopra and Alexeev 2006, Chopra and Marfurt 2007).

A 3D sliding calculation window is needed to compute 3D seismic attributes. In the time domain, the window consists of three parameters: (i) the time gate, (ii) the inline step out, and (iii) the crossline step out. In the depth domain, the time gate is replaced by a depth gate. In our examples, the depth gate will be set to approximately 16 m and the step outs for inline and crossline traces close to 40 m, which includes about 25 traces in the sliding calculation window. We systematically tested larger calculation windows for computing textural attributes but found the loss in detail rapidly became unacceptable, which is entirely consistent with statements made by Chopra, S. and Marfurt, K. J. (2017) (Chopra and Marfurt 2007) in their book on seismic attributes.

After computation of the four dip-steered textural attributes, the next action is to partition or domain the full seismic volume into domains with statistically similar seismic texture. This was done by cluster analysis. A cluster or class can be described by a set of mean values of the input seismic attributes. Each cluster represents one of a finite set of characteristic seismic textures. In our approach the four seismic texture attributes, energy, homogeneity, entropy and contrast are scaled from 0 to 1 as suggested by Samarasinghe, S. (2006) (Samarasinghe 2006) according to:

$$a_{newi} = \frac{a_i - a_{min}}{a_{max} - a_{min}} \qquad (3.5)$$

where a_i is an observation of an attribute value a. Here a_{min} and a_{max} are minimum and maximum values of the attribute a, respectively and anewi is the scaled value of a_i.

The k-means algorithm is a powerful clustering technique. It is well-tested and readily implemented for many geophysical research applications (Di Giuseppe et al. 2014, Gabàs et al. 2016, Alférez et al. 2015, Le et al. 2016, Zhao et al. 2015, Shen et al. 2005, Foged et al. 2014). Lindsten, Ohlsson, and Ljung (2011) noted that the core idea behind the k-means clustering technique was first suggested by Hugo Steinhaus in 1957. The approach "minimises the sum, over all clusters, of the within-cluster sums of point-to-cluster-centroid distances"(MathWorks 2014b). The method is defined in the equations below which are reproduced from Shen, J., Chang, S. I., Lee, E. S., Deng, Y. and Brown, S. J. (2005), and Lindsten, F., Ohlsson, H. and Ljung, L. (2011) (Lindsten, Ohlsson, and Ljung 2011, Shen et al. 2005):

$$E = \sum_{i=1}^{k} \sum_{j=1}^{n_i} d(x_{ij}, m_i) \qquad (3.6)$$

$$d(x_{ij}, m_i) = (x_{ij} - m_i)(x_{ij} - m_i)^T \qquad (3.7)$$

Here E is a cost function (Shen et al. 2005) and is the sum of square-errors for all observations in the data; x_{ij} is the jth observation in the ith cluster and m_i is the center value or mean of the cluster. The value i, within n_i is the total number of observations in each cluster i, and k is the number of clusters. Note that the number of clusters have to be defined a priori. Minimisation of the cost function E can produce k cluster centroids from the space, which are formed by all the observations (x). A summary of the steps needed for the k-means approach are:

Step 1: Select the number of clusters (user defined).

Step 2: Randomly place k points into the volume of the seismic attributes that are clustered. These k points express initial cluster centroids.

Step 3: Allocate each observation to the cluster that has the closest centroid.

Step 4: When each cluster has its observations from its initial cluster centroid, redefine the positions of the cluster centroid by calculating a mean value of its observations. Then, continue to recompute other cluster centroids.

Step 5: When k new cluster centroids are calculated, repeat Step 3 and Step 4 until the centroids do not change anymore.

The selection of the number of clusters for k-means algorithm is considered for the success of seismic interpretation in building seismic texture domains. We have employed two algorithms, as implemented in the MATLAB code, evalclusters.m, to evaluate the optimum number of clusters. These are based on high intra-cluster and low inter-cluster similarity and are also known as internal clustering validation measures (Liu et al. 2010).

Specifically, we have employed the Davies-Bouldin and Calinski-Harabsz validation measures (Davies and Bouldin 1979). The Calinski-Harabasz criterion evaluates the cluster quality based on the ratio of values between and within cluster sums of variance squares (Liu et al. 2010) . The larger the ratio the better the clusters are defined.

On the other hand, the Davies-Bouldin criterion is based on the ratio of within-cluster and between-cluster distances with the “best” clustering solution having a small Davis-Bouldin index. Since this criterion is a ratio between coherency within clusters and distance between clusters (Davies and Bouldin 1979), this number tends to be minimised with relatively few clusters.

Calculating these criteria for high numbers of clusters can become computationally intensive. For the Nevada field example, it took several days to return a value with a standard core I7 Intel ® Xeon ® CPU E5-1650 at speed 3.2 GHz for 11 k-means clusters using the four textural seismic attributes derived from the Nevada reflectivity volume. Certainly, modern supercomputing can make short work of such problems and indeed we use a high-end petascale Cray XC40 supercomputer system for

integrating textural domains into cooperative inversion (see Section Example 3: Seismic texture and cooperative inversion).

3.10 Data Availability

Methods required to compute textural attributes are supplied in this manuscript. The Nevada data are supplied and owned by Barrick Gold Corporation. Restrictions apply to the availability of these data, which were used under license for the current study. The Kevitsa data has previously been made available through the Frank Arnott Award. Request for access should be made via www.frankarnottaward.com or directed to Boliden Kevitsa. The Authors are happy to provide contacts within Barrick Gold or Boliden if required.

3.11 Author contributions

C.V.A.L ran 3D unconstrained/cooperative inversion. C.V.A.L has processed seismic and MT data. All authors interpreted the geophysics results. All the authors constructed and wrote the paper and B.D.H is the most important one.

3.12 Competing financial interests

The authors declare no financial interests

3.13 Supplementary information

3.13.1 Sites:

Seismic texture dominating has been completed on high-resolution seismic data sets from Nevada USA and Kevitsa, Finland. The first example has been provided by Barrick Gold Corporation and uses a high-resolution seismic data set spanning more 40 square kilometres. The data set is acquired in the famous Carlin-style gold district of Nevada USA. The second example, from Finland, includes a 3D high-resolution seismic reflectivity data set collected over the active Kevitsa polymetallic mine (Koivisto et al. 2012, Malehmir et al. 2012, Malehmir et al. 2014). The locations of both sites are provided in Fig. 3- 1.

3.13.1.1 Nevada, USA

The Nevada site is characterised by thick highly variable cover sequences that range from less than 100 m to more than 500 m below surface across a major fault. The Nevada site and data are fully described in the published Journal papers: (i) Cooperative Joint Inversion of 3D Seismic and Magnetotelluric Data: With

Application in a Mineral Province (Takam Takougang et al. 2015), and (ii) Semiautomatic and Automatic Cooperative Inversion of Seismic and Magnetotelluric data (Le et al. 2016). A first-order challenge at the Nevada site is characterising and differentiating thick cover sequences from geologically older prospective basement rock. Hillis et al. (2014) emphasises the importance of developing new technologies suited to exploring for Tier 1 mineral deposits under deep barren cover and the Nevada example is particularly salient in this respect.

Data quality for the Nevada 3D seismic is high with inline and crossline spacings of about 17 m and a depth sampling for seismic traces of about 0.61 m. The full reflectivity image consists of 378 inlines × 410 crosslines (155,769 traces with a total of 467462769 samples). The Nevada 3D seismic survey is also spanned by a 3D tensor MT survey making it an ideal test site for cooperative inversion.

3.13.1.2 Kevitsa, Finland.

The Kevitsa seismic survey in Finland was completed in a hard-rock environment over, what is now, an active mine. The geology from Kevitsa in Finland is strongly 3D and in places the polymetallic ore zone is crosscut by prevailing seismic dip. The Kevitsa deposit is expected to contain 240 million tons (Malehmir et al. 2012) (using a nickel cut-off grade of 0.1%). The hosting intrusion varies from gabbro to dunite composition, with distinct magmatic pulses likely to be responsible for these different phases. The mineralised zone resides in what is dominantly olivine pyroxenite(Malehmir et al. 2012). The main mineralisation, which relates to the disseminated sulfide Ni-Cu-PGE deposit, is believed to be both lithological and to some extent structurally controlled (Malehmir et al. 2014). Sub-horizontal seismic reflectors throughout the resource area have previously been ascribed to internal layering marked by changes in composition resulting from the distinct magmatic pulses (Malehmir et al. 2012). An interesting aspect of this site is the high electrically modestly conductive mineralised zone (i.e., Nickel, Copper and Platinum Group Elements). These are set within the high-resistivity Pyroxenite host rock (Koivisto et al. 2012, Le, Harris, and Pethick 2016). Fig. 3- 7 provides a volume 3D rendered image of the Kevitsa seismic texture Cluster III (orange) and the main 0.15 Ni shell. Note that in this view Cluster III appears to wrap around the mineralized zone.

3.13.2 MT inversion and Cooperative inversion

MT Inversion of field measurements to subsurface conductivity distribution requires iteratively adjusting a numerical model of subsurface conductivity distribution in a way that decreases the residual difference between the field and modelled data (deGroot-Hedlin and Constable 1990, Egbert and Kelbert 2012). For MT inversion we have used the ModEM3D code (Egbert and Kelbert 2012, Kelbert et al. 2014) within the Cooperative Inversion framework outlined in Le et al. (2016).

Cooperative inversion is the beneficial transference of information from one geophysical technique to another to improve the recovery of subsurface rock properties (Moorkamp 2017). The new seismic texture domains may provide volumetric links to macroscopic rock volumes with characteristic electrical properties and so may can be well suited to cooperative inversion.

A flow schematic of processes needed for seismic texture domaining and cooperative inversion of magnetotelluric and seismic data is provided in Fig. 3- 8. The technique for creating the prior conductivity model is called “geometric mapping” (Le et al. 2016). It uses the distribution of a seismic texture domains to divide the complete seismic volume into smaller subvolumes. Each subvolume is subsequently allocated on electrical resistivity, based on analysis of distribution of resistivity extracted from unconstrained inversion of the halfspace prior model at 100 Ohm.m (Le et al. 2016). Once each seismic domain is statistically assigned a conductivity, this conductivity distribution feeds a final 3D MT inversion, which is run with the ModEM3D code run on a petascale Cray XC40 supercomputer (see Fig. 3- 6).

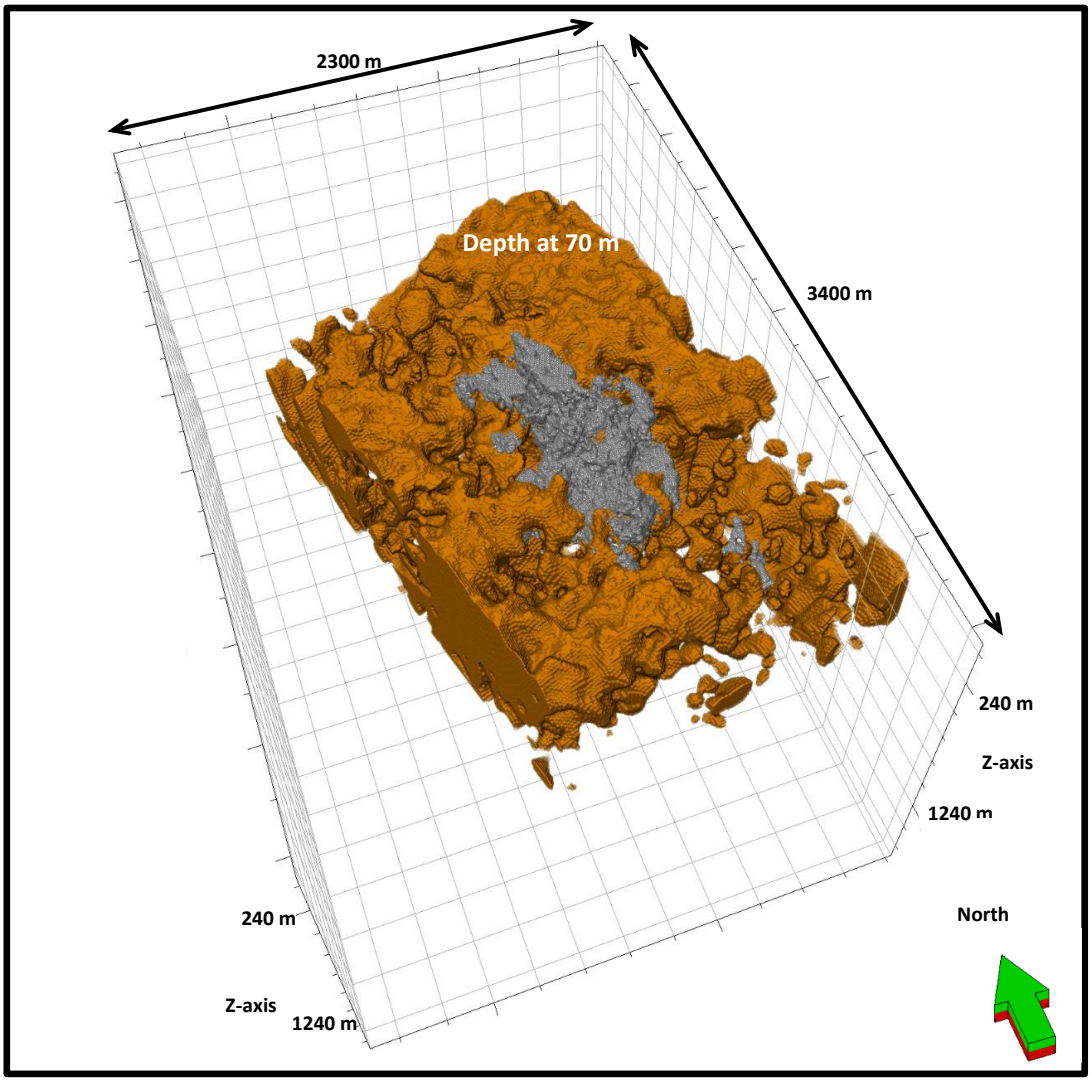

Fig. 3- 7: A 3D volume rendering the Kevitsa Seismic Texture Cluster III (orange) and the 0.15 % Ni concentration shell (metallic grey). Cluster III appears to wrap around the mineralization with little overlap into the high nickel concentration shell

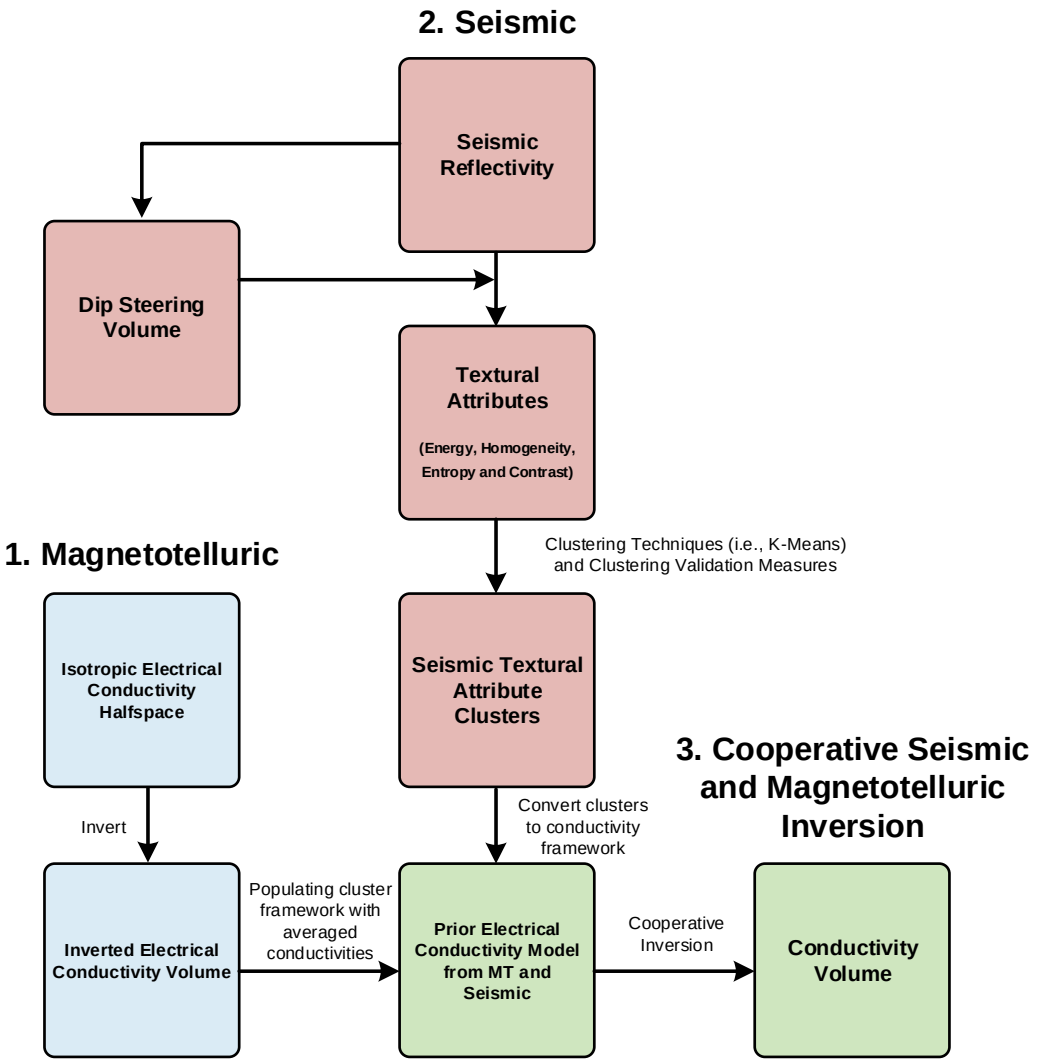

Fig. 3- 8: A schematic for seismic texture domaining combined with cooperative inversion of magnetotelluric and seismic data

CHAPTER 4. CONCLUSIONS

I have developed new strategies and concepts to enhance cooperative inversion of co-located seismic and magnetotelluric (MT) data. They focus on building prior model conductivity and co-variance coefficient distributions for input to inversion. I show that if these two parameters are suitably fed into MT inversion then there is potential to achieve a higher resolution final conductivity distribution.

I have also developed and utilised a new method for charactering seismic texture. Here the seismic reflectivity volume is divided into a discrete number of characteristic seismic textures. This new type of seismic texture is also used to build a framework for cooperative inversion. I provide the methods and main outcomes from this research in Chapter 3. The methods I have developed are tested on large co-located seismic and magnetotelluric data sets from Nevada USA and Kevista Finland. The main outcomes are summarised below.

Chapter 2: Automatic and Semiautomatic cooperative inversion

Given an appropriately processed seismic volume and MT data after QC, cooperative inversion can in principle be automated and I indicate how this may be achieved in chapter 2. A novel aspect of my research is the integration of seismic attributes into cooperative inversion. In particular, I show how geometric attributes like seismic polar dip angle can be incorporated into several inversion strategies. I have described two methods for populating a model framework with conductivities. They are (i) direct mapping via a transfer function and (ii) structural mapping which uses various statistical methods to feed conductivities from an initial round of unconstrained inversion into the seismic framework.

Direct mapping links a value of conductivity directly to the seismic attribute by a pre-defined relationship. In the Nevada example I explore direct mapping of an average polar dip angle to a conductivity. Although the method is simple and certainly not universally applicable, it provided a surprisingly detailed conductivity distribution for the Nevada data set that reveals faults and basement depressions that were not resolved by conventional inversion. The good result for the Nevada data set was largely because of

the association between dip with the large-scale division between basement and cover rocks.

For cooperative inversion with "structural mapping", the framework is recovered from the seismic data. For the next round of inversion each sub-volume within the seismic framework is assigned the average value of conductivity from the unconstrained inversion conductivity within that volume. The resulting conductivity distribution was broadly consistent with the seismic reflectivity, conductivity from wireline logs, geochemical data and lithology information.

For semiautomatic cooperative inversion, key seismic horizons were picked and these helped form the sub-volumes that were later populated based on statistical analysis of distribution of seismic attributes and conductivity from unconstrained inversion. These semiautomatic cooperative inversion strategies, which include distribution of lower covariance coefficients across key boundaries, were demonstrated to generate rapid changes in conductivity across these boundaries that were consistent with expected changes from wireline logs and geochemistry data. Of particular note was the improved resolution of conductive features proximal to a large fault.

Chapter 3: Seismic texture for rock volume classification and cooperative inversion

From analysis of various seismic attributes and combinations of attributes within cooperative inversion, a representation of seismic texture (i.e. the distribution of seismic reflectivity) can be the breakthrough needed to recover an indication of rock mass distribution in hard rock settings. I developed a method where k-means cluster analysis was applied to four Grey Level Co-occurrence Matrix (GLCM) textural attributes. The textural attributes I choose were (i) energy texture, (ii) homogeneity texture, (iii) entropy texture and (iv) contrast texture. The outcome of the k-means analysis was a discrete set of clusters representing a combination of seismic textural attributes. For the Nevada seismic data the k-means analysis was used to generate seven clusters and for the Kevitsa reflectivity data images containing 10 clusters were generated. Each image was accompanied by a reference diagram that showed how each cluster linked back to a distribution of the four GLCM textural seismic attributes. For the Nevada data set one cluster (i.e. seismic texture cluster VII in chapter 3) only occurred in cover and appeared to be highly effective in mapping out basement depressions which were suspected of containing higher conductivity rocks. The seismic texture distribution was then integrated

into one of the cooperative inversion strategies with the outcome being a low RMS error (less than 2%) and highly detailed distribution of conductivity that that was consistent with detailed shapes of cover and basement rock for Nevada.

I have presented many pathways and new ideas connected with cooperative inversion of seismic and MT data and I hope that my techniques are sufficiently well described and practical so that others are able to implement them. Cooperative and Joint inversion is an exciting area of research and in combination with modern supercomputing it could revolutionise geophysical investigations of the subsurface in the future.

APPENDIX A: MAGNETOTELLURIC INVERSION, CARBONACEOUS PHYLLITES AND AN ORE ZONE: KEVITSA; FINLAND.

Cuong V. A. Le
DET CRC, Curtin University
ARRC/CSIRO Building, H Block,
Level 4, 26 Dick Perry Avenue,
Kensington
v.le3@postgrad.curtin.edu.au

Brett D. Harris
DET CRC, Curtin University
ARRC/CSIRO Building, H Block,
Level 4, 26 Dick Perry Avenue,
Kensington
B.Harris@curtin.edu.au

Andrew M. Pethick
DET CRC, Curtin University
ARRC/CSIRO Building, H Block,
Level 4, 26 Dick Perry Avenue,
Kensington
andrew.pethick@curtin.edu.au

SUMMARY

We invert seven densely sampled magnetotelluric transects at the Kevitsa Ni-Cu-PGE (platinum group elements) deposit in Finland. The geology at the deposit presents at least two high electrical conductivity rock types within a resistive host. We consider the extent to which highly conductive phyllite and an ore zone can be separated through inversion of magnetotelluric data. Multiple inversions were completed with 312 magnetotelluric (MT) stations. It was possible to generate a three-dimensional conductivity volume from the 2D MT derived conductivities sections via volumetric interpolation. We compare the resulting 3D conductivity volume with co-located 2D and 3D seismic data. Comparisons show that an impression of the Ni-Cu-PGE ore-body could be observed in both seismic reflection and conductivity volumes. We discuss methods for constraining MT inversions and the impact they may have in separating proximal but highly conductive units. The inversions were complete as a precursor to full 3D cooperative inversion of the seismic and magnetotelluric data at this site.

Key words: Magnetotelluric, inversion, conductivity.

INTRODUCTION

Electromagnetic methods are able to detect ore bodies when highly electrically conductive minerals are present (Howe et al. 2014). Kevitsa deposit in northern Finland is a large Ni-Cu deposit hosted within a mafic to ultramafic intrusion (Malehmir et al. 2012). A magnetotelluric (MT) survey consisting of 312 stations over seven lines was co-located with both 2D and 3D seismic surveys. Higher frequency information in the electromagnetic wave field is rapidly attenuated with depth. The result is that the resolution of electromagnetic methods such as MT decreases with depth. For this reason it may be difficult to recover sharp contrasts in electrical conductivity as depth increases. Non-uniqueness and equivalence can also limit the

methods ability to recover true subsurface conductivity. A particular challenging and important application of MT inversion is the delineation of deep conductive ore bodies. However where such orebodies are proximal to carbonations shales (conductive sheet like bodies) discrete definition of the ore bodies' geometry is even greater. We will consider the exactly this situation.

The MT method detects the naturally occurring electromagnetic fields and calculates a frequency-dependent electrical impedance tensor (**Z)** (Simpson and Bahr 2005) which contains the transverse electric (TE) and transverse magnetic (TM) modes**.** The apparent effective resistivity can be extracted from the tensor and in turn can validate the quality of MT data over the survey region (Berdichevsky and Dmitriev 2008)**.** The apparent resistivity and phase data extracted from the tensor are typically plotted against log period prior to inversion for the data quality control (QC).

Unconstrained MT inversion typically creates minimal (smooth) structures due to the fact that smoothness conditions dominate every cell in the resistivity model (i.e., Occam inversion) (deGroot-Hedlin and Constable, 1990). This smoothness is not realistic in regions where sharp boundaries exist between two distinct units of electrical resistivity. Sharp Occam like that of deGroot-Hedlin et al., 2004 have the potential to produces sharp conductivity contrast in the subsurface. Cooperative approaches such as Zhou et al. (2014) and Takam Takougang et al. (2015), apply smoothness weights at boundaries derived from prior information such as geology or 3D seismic reflections images.

The Kevitsa deposit is expected to contain 240 million tons (using a nickel cut-off grade of 0.1%) grading 0.30% nickel and 0.41% copper (Malehmir et al. 2012). The hosting intrusion varies from gabbro to dunite composition, with evidence of distinct magmatic pulses responsible for these different phases. The mineralised zone resides in what is dominantly olivine pyroxenite (Appendix A- 1). Mineralisation is largely disseminated and rarely more than a few percent sulphide, with pyrrhotite often the dominant conductive mineral (Chris Wijns, pers. comm. 2016). Horizontal seismic reflectors throughout the resource area have previously been ascribed to internal layering marked by changes in composition resulting from the distinct magmatic pulses (Malehmir et al. 2012).

METHOD AND RESULTS

Method

The ModEM2D code developed by Egbert and Kelbert (2012) was applied in our inversions. ModEM2D's objective function minimises both data misfit and smoothness parameters, as given by (Egbert and Kelbert, 2012) :

$$\Phi(m,d) = (d - f(m))^T C_d^{-1}(d - f(m)) + \nu(m - m_0)^T C_m^{-1}(m - m_0) \quad (1)$$

where,

m – earth conductivity model parameter; d – field data; C_d – covariance of data errors,

f(m) – forward modelling operator; m_o – the initial model; ν – Lagrange multiplier

Cm – smoothing operator

The Lagrange multiplier, ν , balances the trade-off between the misfit and smoothness requirements. C_m, the model covariance or regularisation term, is known as a smoothing operator (Siripunvaraporn and Egbert 2000). It dictates sharpness or smoothness between the geo-electrical cells.

Results

A detailed quality control (QC) process was completed prior to inversion. Every tensor MT sounding was reviewed and erroneous data removed. The QC process was applied to 312 MT stations over 7 lines. In the end a set of 312 MT records, as shown in Appendix A- 2, were used for inversion. The final dataset consisted of 29 periods ranging between 0.001 and 1 s. The depth of investigation is estimated by the electromagnetic skin depth equation. It provides a rough guide of investigation depths for each recorded period that is used within the inversion workflow. Assuming a representative resistivity in the order of 25 Ω•m and MT periods in the range of 0.001 to 1 s, the skin depth suggests an approximate investigation depth range between 80 m and 2500 m (i.e., skin depth, $\delta = 503\sqrt{\rho \cdot T}$, where ρ is electrical resistivity in Ω·m and T is period in s).

TM mode apparent conductivities are shown in Appendix A- 2 for periods, 0.0002 s, 0.01 s, 0.1 s, and 0.67 s. Complex 3D geo-electrical structures are identified by many highly conductive and resistive zones. Interpretation of multiple 2D lines could be misleading because of the 3D geo-electrical setting at Kevitsa (see geological map in Appendix A- 1). For this reason, we compare inversion with modEM2D and

modEM3D. For both cases, we assume that no drillhole or other information is available. In this respect our example is truly baseline and may represent the raw deep greenfields exploration scenario where unconstrained inversion is a necessary start point. Inversions were performed on the Pawsey Centre Magnus Cray XC30 supercomputer.

2D inversion uses a 100 Ohm·m half space prior model. The dataset includes both off-diagonal tensor impedances components (i.e., TE and TM modes). Note that the error floors for the off-diagonal elements (Zxy and Zyx) are set to 10% of the root mean square of absolute of their complex multiplication. The root mean square (RMS) misfit reduces to approximately 3 for all MT transects (see Appendix A- 3). Considering the size (i.e. 312 stations) and complexity of the data set we achieve RMS less than 3 for this setting is difficult.

2D and 3D seismic data are overlain by 2D MT derived conductivity distributions as shown in Appendix A- 4. A well log showing nickel percentage is overlaid on the seismic and conductivity sections for comparison. The zone of higher nickel content (which includes higher pyrrhotite as well) correlates with the high conductivity zone seen in the 2D MT overlay. However, separation of the orebody from conductive carbonaceous phyllite is far from clear. According to the profile E4 (Appendix A- 4), high conductivity stripes indicate the existence of many carbonaceous phyllite units as seen in the geology map (Appendix A- 1). Also, the profile E5 could "sense" both the position of the higher sulphide zone (i.e., see nickel content) as elevated conductivity and carbonaceous phyllite (see geology map). Both correspond with zones of high conductivity. Delineating between the ore body and carbonaceous phyllite at depth is still under investigation but 3D cooperative inversion is expected to yield interesting results. Meanwhile, low conductive zones seen in the resulting MT conductivity volume correspond to the mapped volcanic or gabbro rocks (See E4 and E5 in Appendix A- 4). In the 3D view (Appendix A- 4) two zones appear to show correlation between the seismic reflection and MT conductivity images. These include a higher conductivity zone possibly related to the ore body that seems to match a high reflectivity zone. The ore body was not explicitly delineated in the seismic, but the MT could offer additional information when placed in the seismic structural context. Cooperative inversion strategies for seismic and MT data are being developed in the hope of that these discrete and highly conductivity zones can be accurately defined.

CONCLUSIONS

Inversion was completed on seven magnetotelluric transects completed over the Kevitsa Ni-Cu-PGE deposit in Finland. The magnetotelluric data was inverted in 2D and a 3D interpolated conductivity volume was generated. The conductivity volume is also compared with 2D and 3D seismic data. Generally there is a fair correlation between boundaries in the seismic image and MT derived electrical conductivity distribution. One of the challenges in this survey area is to differentiate a high conductivity ore body from thin high conductive carbonaceous phyllites using only unconstrained 2D and 3D inversion. Both unconstrained 2D and 3D inversion appeared to extend a conductive zone to the locations of the ore body. However as expected it was difficult to separate the different highly conductive units and we are encouraged to apply full cooperative inversion strategies at this site as the next phase of research.

ACKNOWLEDGMENTS

The work has been supported by the Deep Exploration Technologies Cooperative Research Centre whose activities are funded by the Australian Government's Cooperative Research Centre Programme. This is DET CRC Document 2016/784. We also acknowledge and thank First Quantum and in particular Chris Wijns for use of their comprehensive geophysical datasets. We also thank Schlumberger for providing the useful software. This work was supported by resources provided by the Pawsey Supercomputing Centre with funding from the Australian Government and the Government of Western Australia.

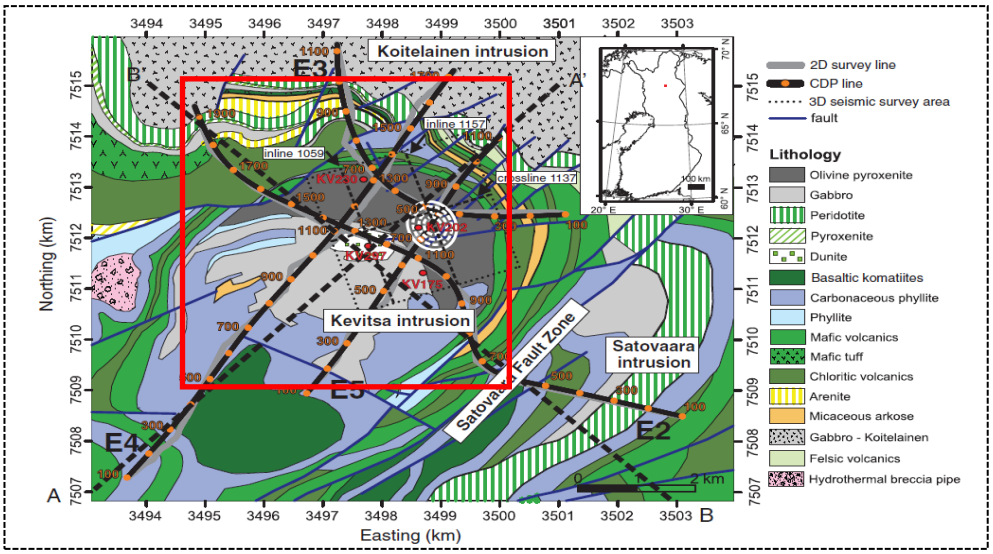

Appendix A- 1: Geological map of the Kevitsa Ni-Cu-PGE deposit. The location of the 3D survey area (black dotted box), four seismic 2D profiles (black lines) and 2D MT

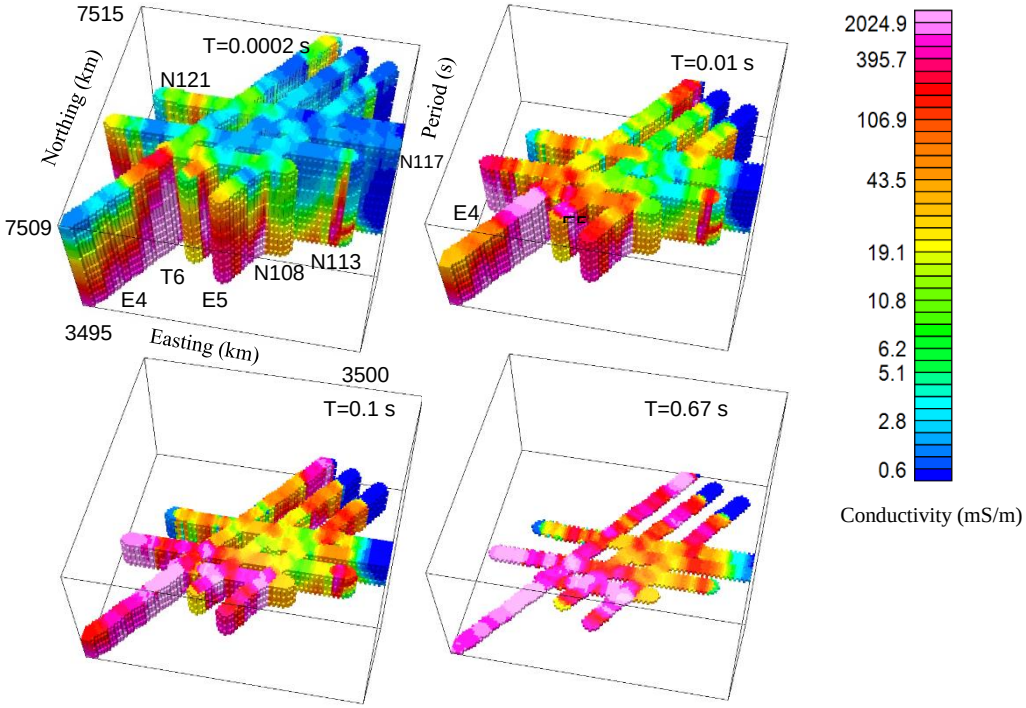

Appendix A- 2: Observed apparent conductivity of the transverse magnetic MT mode at varying source periods (i.e., 0.0002 s, 0.01 s, 0.1 s, and 0.67 s). The Kevitsa resource contains complex 3D geo-electrical structures

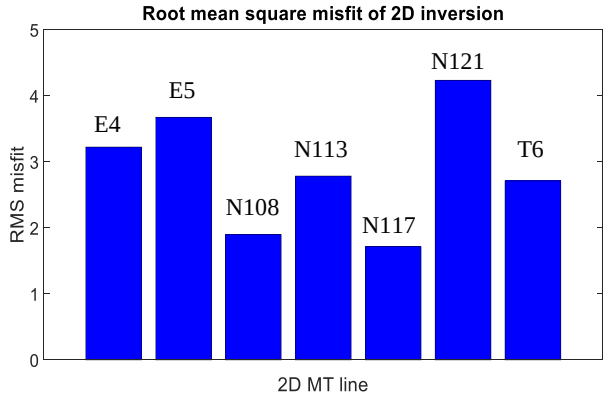

Appendix A- 3: Root mean square misfit of 2D inversion for seven 2D MT lines

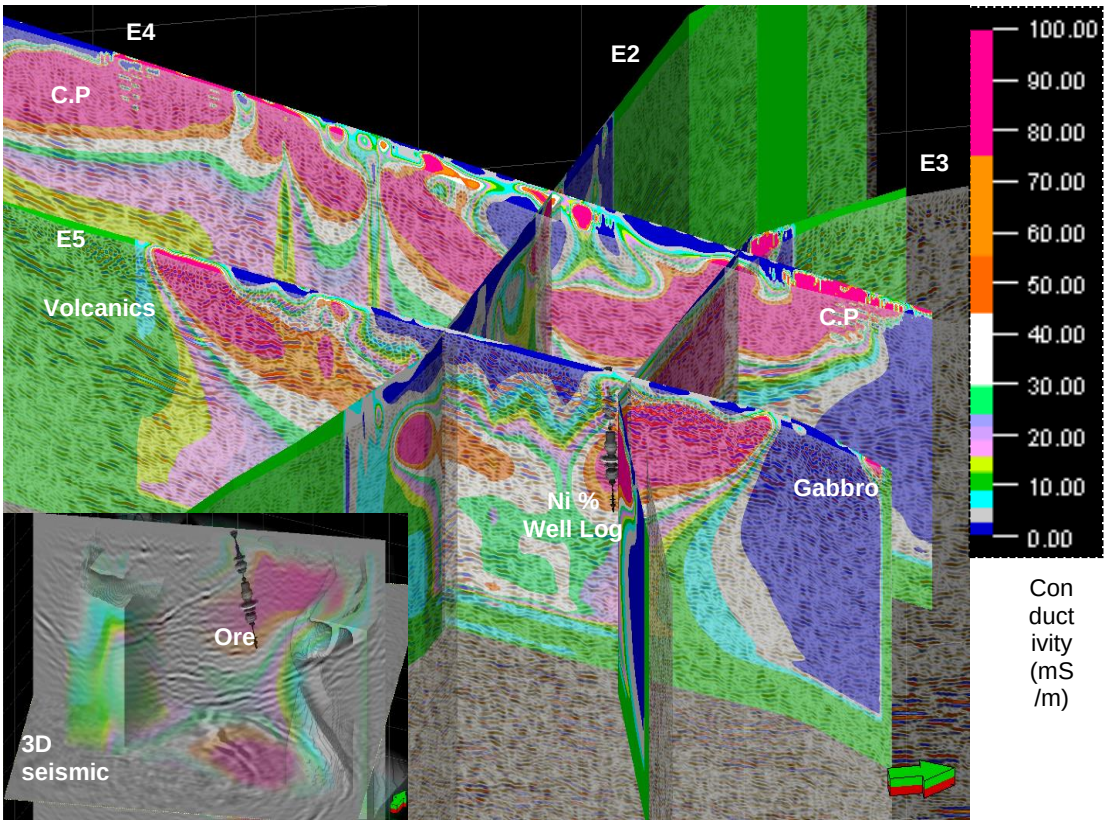

Appendix A- 4: 2D and 3D seismic data overlaid by 2D MT derived conductivity distribution. The well log shows nickel percentage. The ore body broadly correlates with a high nickel content / high conductivity zone seen in the 2D MT overlay. However, the conductivity distribution is complicated by carbonaceous phyllite (C.P) units (see Appendix A- 1). Note: (i) high conductivity zones may relate with carbonaceous phyllite or conductive part of the ore body but tend to be highly smeared; (ii) low conductivity zones tend to correlate with volcanic or gabbro rocks; (iii) some rapid transitions in conductivity correspond with seismic boundaries

References

Berdichevsky, Mark N, and Vladimir I Dmitriev. 2008. *Models and methods of Magnetotellurics*: Springer.

Egbert, Gary D., and Anna Kelbert. 2012. "Computational recipes for electromagnetic inverse problems." *Geophysical Journal International* 189 (1):251-267. doi: 10.1111/j.1365-246X.2011.05347.x.

Howe, Brendan D., Bill Doerner, Jared Townsend, and Pamela Patraskovic. 2014. "Three-dimensional magnetotelluric inversion and petrophysical interpretation of the Turquoise Ridge gold deposit, Nevada, USA." SEG Technical Program Expanded Abstracts 2014.

Malehmir, Alireza, Christopher Juhlin, Chris Wijns, Milovan Urosevic, Petri Valasti, and Emilia Koivisto. 2012. "3D reflection seismic imaging for open-pit mine planning and deep exploration in the Kevitsa Ni-Cu-PGE deposit, northern Finland." *Geophysics* 77.

Simpson, Fiona, and Karsten Bahr. 2005. *Practical Magnetotellurics*. Cambridge University Press.

Siripunvaraporn, Weerachai, and Gary Egbert. 2000. "An efficient data-subspace inversion method for 2-D magnetotelluric data." *Geophysics* 65 (3):791-803. doi: 10.1190/1.1444778.

Takam Takougang, Eric, Brett Harris, Anton Kepic, and Cuong V. A. Le. 2015. "Cooperative joint inversion of 3D seismic and magnetotelluric data: With application in a mineral province." *Geophysics* 80:1-13. doi: 10.1190/GEO2014-0252.1.

Zhou, J., A. Revil, M. Karaoulis, D. Hale, J. Doetsch, and S. Cuttler. 2014. "Image-guided inversion of electrical resistivity data." *Geophysical Journal International*. doi: 10.1093/gji/ggu001.

APPENDIX B: COOPERATIVE INVERSION BY MT AND SEISMIC TEXTURAL CLUSTERS

This appendix briefly overviews and extends some of the work from Chapter 3. Cluster indices derived from k-means clustering of the seismic textures are used to form the initial framework for cooperative MT and seismic inversion. Several different methods are trialled over both the Nevada and Kevitsa test sites.

B.1. Nevada

1. Methodology

The cooperative inversion of seismic and MT data uses volumes of seismic clusters (see Section 3.3.3) to build the frame work for the conductivity prior model. The full cooperative inversion workflow is described in Section 3.12.2 and Fig. 3-8.

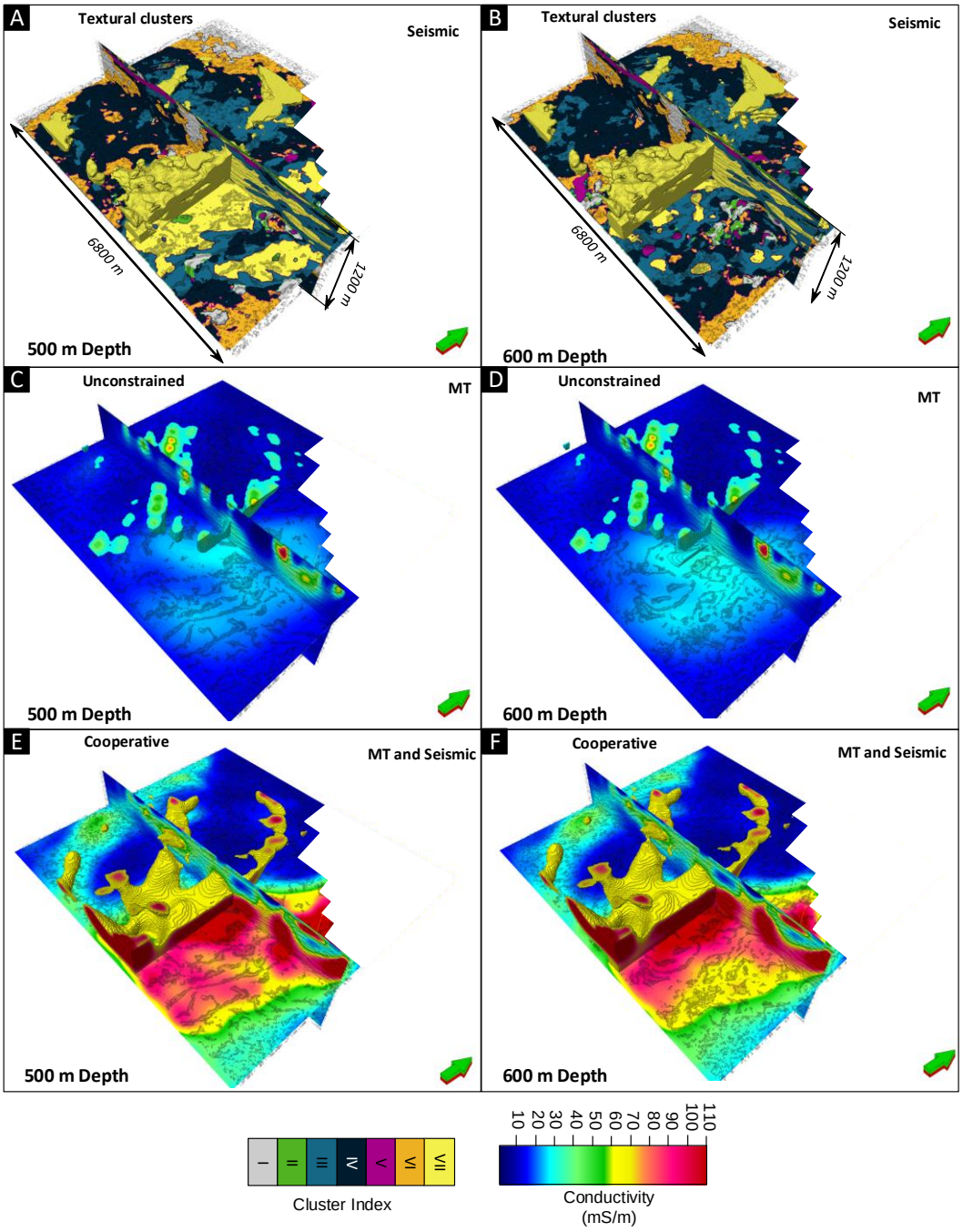

Appendix B- 1: The 3D representation of the A & B) texture cluster indexes, C & D) uncontrained inversion conductivity, and E & F) cooperative inversion using both the seismic and MT data at the Nevada site. A depth slice at 500m (left) and 600 m (right) below the surface is included for comparison

B.2. Kevitsa Case Study

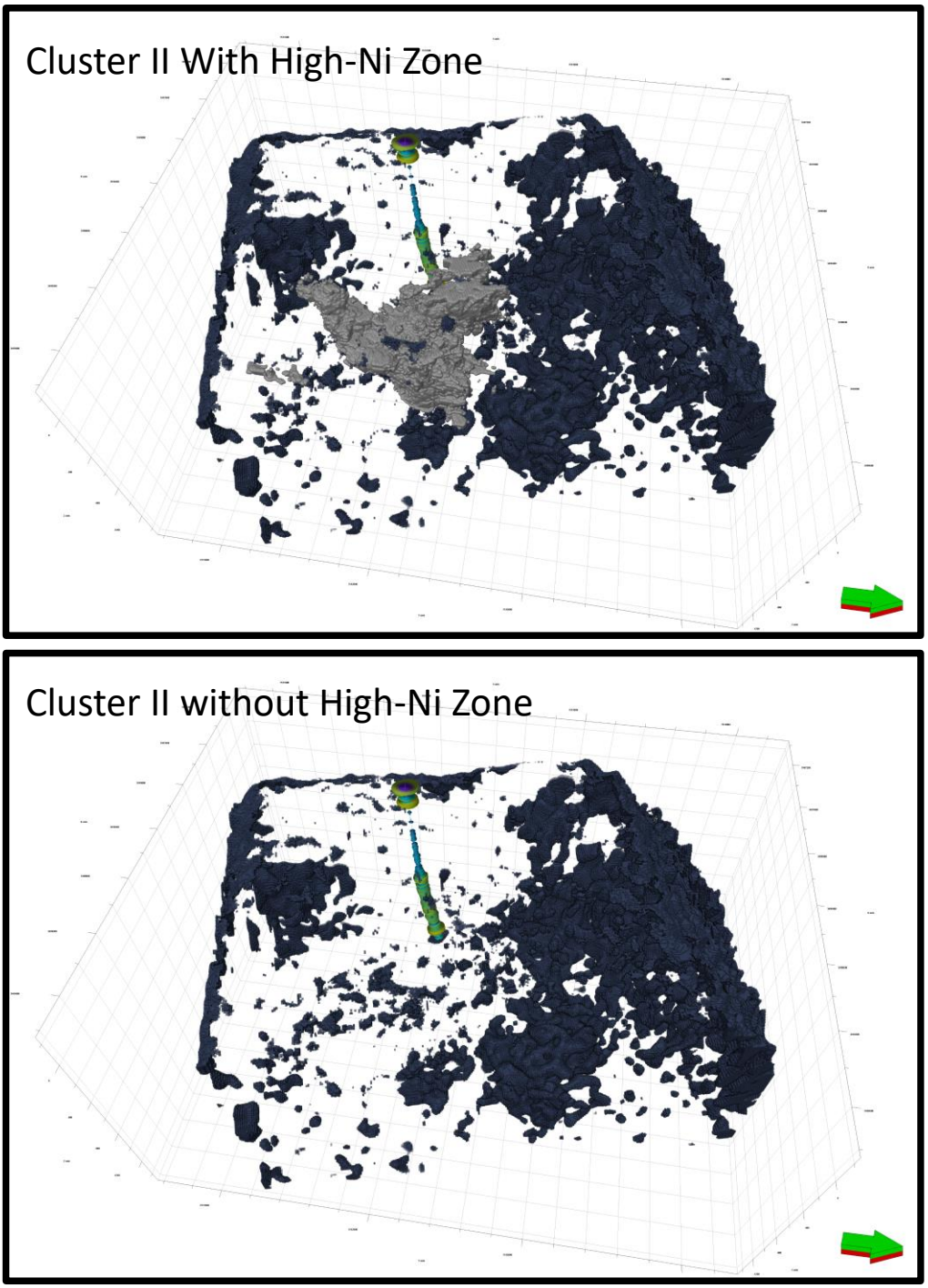

Appendix B- 2: 3D representations (volume rendering) of cluster II index within the Kevitsa site. Note that cluster II does not contribute much on the framework of the High Ni concentration zone (>0.15%)

Cooperative Inversion Methodology

To cooperatively invert seismic and magnetotelluric data a new workflow was developed. The co-located seismic survey had smaller extents than the MT survey. Therefore, there was no seismic information to form the framework over the full MT survey area. To obtain this missing structural information, a geological interpretation was used.

This workflow used information derived from the geological interpretation of well-logs and core. The interpretation was made by Koivisto et al. (2012) and First Quantum. This interpretation was then converted into a 3D model using the Geomodeller software package (Appendix B- 3). The final cooperative inversion workflow integrated this newly created 3D model into the framework that lacked seismic information. The methodology then followed the same steps as the Nevada cooperative inversion case study (see Chapter 3). The full method is shown in Appendix B- 4.

The results of the seismic textural cluster analysis, unconstrained MT inversion, and the MT and seismic cooperative inversion are shown in Appendix B- 5.

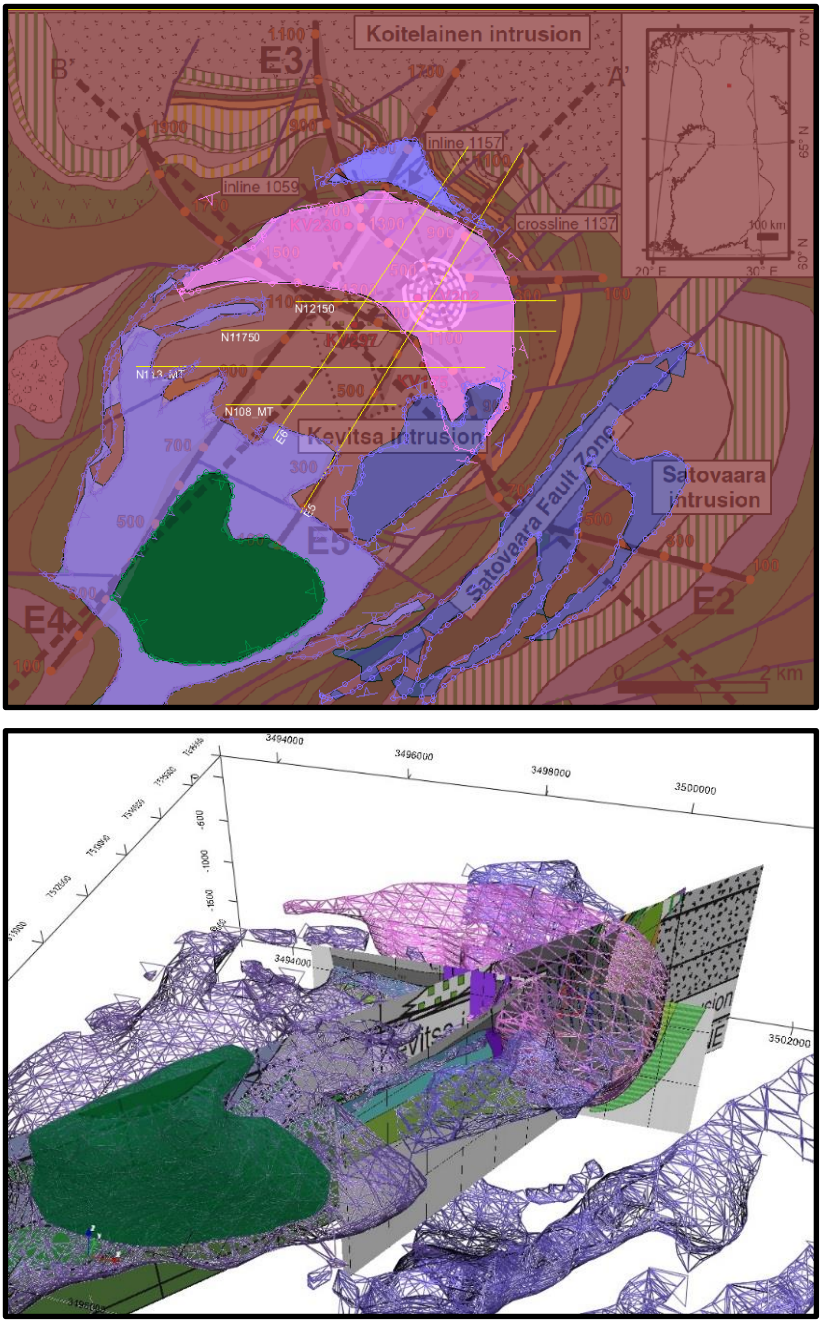

Appendix B- 3: (Top) Surface geology plan section (Koivisto et al. 2012). The highlighted sections in purple show the location of carbonaceous phyllite, the pink section highlights the location of olivine Pyroxinite and the green shows the location of basaltic Koma. (Bottom) I have built the 3D wireframe geological model in the software Geomodeller. The location of seven MT lines are highlighted (yellow lines). The cooperative inversion of seismic and MT data uses information derived from the clusters of textural atributes (see Section 3.4.2) and are incorporated within the olivine pyroxenite (the pink zone). The conductive zone is related to the carbonaceous phylite and is defined within the prior inversion model. The distance between the parallel MT lines are approximately 700 m. Examples for MT inversions are illustrated in the Appendices 3-5.

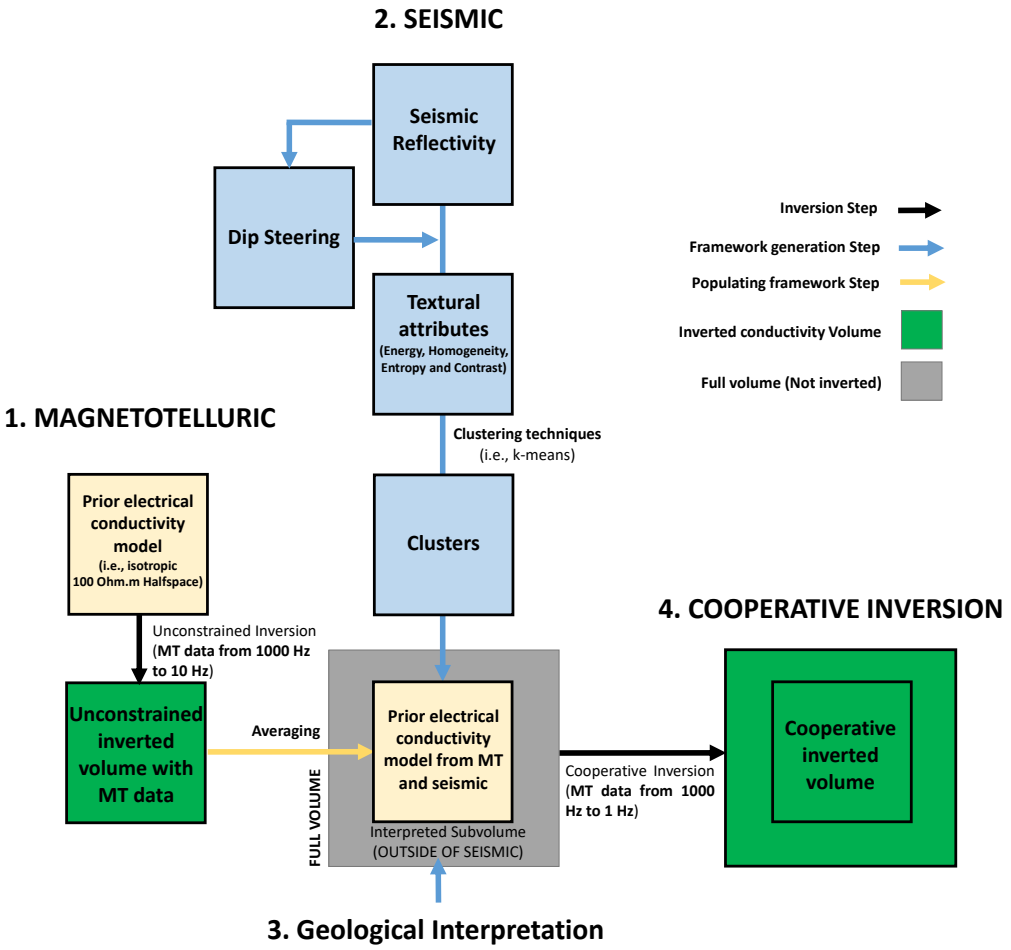

Appendix B- 4: A schematic of the workflow used to cooperatively invert the magnetotelluric and seismic data from Kevitsa

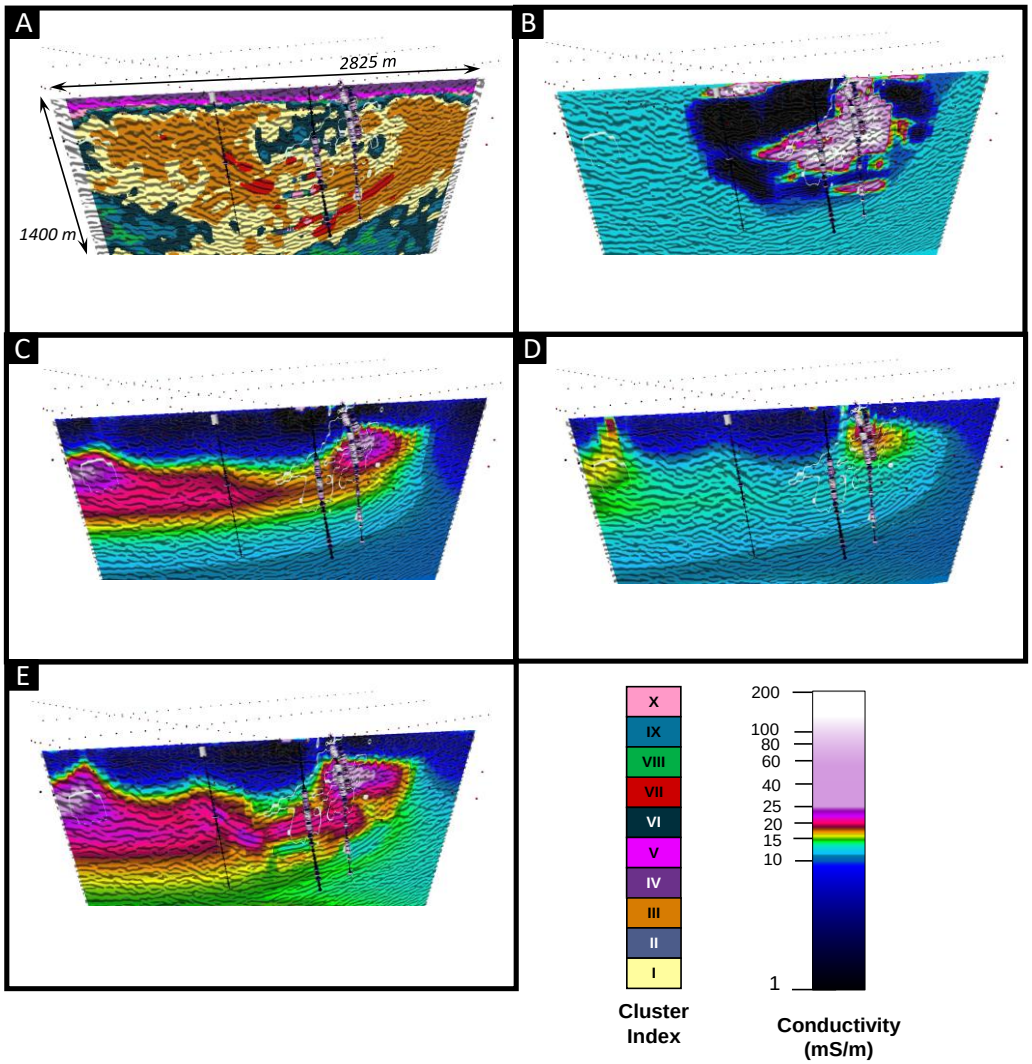

Appendix B- 5: 2D representations of seismic attributes (A), interpolated conductivity from wire logs within the olivine pyroxenite as host rock (B), unconstrained inversion conductivity with the MT period from 1000Hz to 10Hz (C), unconstrained inversion conductivity with the MT period from 1000Hz to 1Hz and halfspace prior model 100 Ohm.m (D), and the cooperative inversion using analysis of cluster of seismic attributes with the steps mentioned in Fig. B-4 for the Kevitsa site (E). Several conductivity log are represented to highlight the contour of Ni concentration (>0.15%). All the inverted conductivity results show the existence of the high Ni zone. However, the cooperative inversion using the background of (C) and structure of clusters of seismic textures shows the best match with the seismic structures and broadly correlate with the interpolated conductivity from wire logs

References

Koivisto, Emilia, Alireza Malehmir, Pekka Heikkinen, Suvi Heinonen, and Ilmo Kukkonen. 2012. "2D reflection seismic investigations at the Kevitsa Ni-Cu-PGE deposit, northern Finland." *Geophysics* 77.

APPENDIX C: COPYRIGHT CONSENT

Permission to Republish 1

The title: Semiautomatic and automatic cooperative inversion of Seismic and magnetotelluric data

Authors: Cuong V. A. Le, Brett D. Harris, Andrew M. Pethick, Eric M. Takam Takougang, and Brendan Howe

Journal: Surveys in Geophysics

Publication date: 13/7/2016

Link: http://link.springer.com/article/10.1007/s10712-016-9377-z

Type: Open Access

Copyright Clearance Center RightsLink®

Home | Create Account | Help

Title: Semiautomatic and Automatic Cooperative Inversion of Seismic and Magnetotelluric Data

Author: Cuong V. A. Le

Publication: Surveys in Geophysics

Publisher: Springer

Date: Jan 1, 2016

Copyright © 2016, The Author(s)

LOGIN

If you're a copyright.com user, you can login to RightsLink using your copyright.com credentials. Already **a RightsLink user** or want to learn more?

Permissions Request

This is an open access article distributed under the terms of the Creative Commons Attribution License, which permits unrestricted use, distribution, and reproduction in any medium, provided the original work is properly cited.

Springer and BioMed Central offer a reprint service for those who require professionally produced copies of articles published under Creative Commons Attribution (CC BY) licenses. To obtain a quotation, please email reprints@springeropen.com with the article details, quantity(ies) and delivery destination. Minimum order 25 copies.

CLOSE WINDOW

Copyright © 2017 Copyright Clearance Center, Inc. All Rights Reserved. Privacy statement. Terms and Conditions.
Comments? We would like to hear from you. E-mail us at customercare@copyright.com

Permission to Republish 2:

The title: Magnetotelluric inversion, carbonaceous phyllites and an ore zone: Kevitsa; Finland

Authors: C.V.A. Le, B. Harris, A. Pethick

Event name: ASEG-PESA-AIG 2016

Session: Minerals 6.D Distal Footprints (6) Case Studies

Publication date: 2016

Place: Adelaide, Australia

Email Communication:

Dear Sir/Madam (Asking permission for use in PhD thesis)
Plevin & Associates Pty Ltd <events@plevin.com.au>
Fri 1/27/2017 11:00 AM
Hi Cuong,

This is OK - copyright resides with the authors and/or their employing or funding institutions.

Regards,

Phil Plevin

EVENT MANAGEMENT

Plevin and Associates Pty Ltd
PO Box 54
BURNSIDE 5066
South Australia

Tel. Nat. (08) 8379 8222
Tel. Int. +61 8 8379 8222
Fax. Nat. (08) 8379 8177
Fax. Int. +61 8 8379 8177
Email: events@plevin.com.au

Van Anh Cuong Le
Thu 1/26/2017 10:28 PM
To: asegpesaaig2016@plevin.com.au
Dear Sir/ Madam,

I am Cuong Van Anh Le, PhD Student in Curtin University, Perth, Australia. I would send this email for asking your permission to use my extended abstract in my PhD thesis.

The title: Magnetotelluric inversion, carbonaceous phyllites and an ore zone: Kevitsa; Finland

Authors: C.V.A. Le, B. Harris, A. Pethick

Event name: ASEG-PESA-AIG 2016
Session: Minerals 6.D Distal Footprints (6) Case Studies
Publication date: 2016
Place: Adelaide

Thank you very much.
Yours Sincerely,
Cuong Van Anh Le
PhD Student
Curtin University, Perth, Australia